2020-09-15

Coordinated Ambient/Dedicated Radio Frequency Protocol Design for Wireless Powered Communication Networks

Kwan, Jonathan C.

UNIVERSITY OF CALGARY

Coordinated Ambient/Dedicated Radio Frequency Protocol Design for Wireless Powered Communication Networks

by

Jonathan C. Kwan

A THESIS

SUBMITTED TO THE FACULTY OF GRADUATE STUDIES

IN PARTIAL FULFILMENT OF THE REQUIREMENTS FOR THE

DEGREE OF DOCTOR OF PHILOSOPHY

GRADUATE PROGRAM IN ELECTRICAL AND COMPUTER ENGINEERING

CALGARY, ALBERTA

SEPTEMBER, 2020

Abstract

Harvesting energy from radio frequency (RF) sources to wirelessly power electronic devices have been of tremendous interest in both academia and industry in recent years. This thesis tackles the problem of maximizing the sum-throughput while ensuring fairness in a multiple source, multiple sensor environment; where the sensors reliably harvest energy from ambient sources when dedicated sources are unavailable. This thesis proposes a new protocol called the coordinated ambient/dedicated (CA/D) protocol, which has backscatter-enabled combination sensors optimized to harvest energy from intended RF energy sources when available (referred to as dedicated mode) and fall back to harvesting energy from unintended sources when only unintended sources are available (called ambient mode). It is shown that the CA/D protocol, in dedicated mode, delivers up to approximately 296% increase in sum-throughput compared to the reference state-of-the-art time-switching (TS) RF energy harvesting protocol in a dynamic environment. Further, the proposed CA/D protocol increases the Jain's fairness index from J = 0.76 under the TS protocol to up to 0.90 and 0.80 with and without sensors operating in backscatter mode, respectively. When operating in ambient mode, the proposed CA/D protocol is integrated with two new machine learning techniques, the linear forecaster with near-time linear regression-based enhancer (LFNTLRE) algorithm and an artificial neural network with environment detection (ANN-ED), to determine the optimum EH schedule. These machine learning algorithms can reliably operate in environments where there is unpredictable availability of unintended sources and ongoing changes in channel conditions between the sensors and the unintended sources. Numerical results show that sensors using the ANN-ED and LFNTLRE algorithms can successfully sense up to 99.5% and 99.6% of the data, respectively; very close to the 100% sensing achieved by an ideal sensor. Sensors using the ANN-ED and LFNTLRE algorithms achieve an

accuracy rate of up to 99% and 100%, respectively, as well. These findings on the proposed CA/D protocol are significant, necessitating the protocol's adoption in sensors deployed in the future wireless networks.

Acknowledgements

"Worthy are you, our Lord and God, to receive glory and honor and power, for you created all things, and by your will they existed and were created." (Revelation 4:11)

I would like to start off by thanking Jesus Christ, my personal Lord and Savior, to whom belongs all honor, glory, and praise.

Secondly, I would like to express my sincere gratitude to Dr. Abraham Fapojuwo. His dedication and passion to academic and research excellence has challenged me to achieve something I never expected to achieve. His selflessness in mentoring, kindness in understanding, patience in listening, knowledge in teaching, integrity in character, and above all, his friendship has made a lasting impact both in my academic career and growth as a person.

Thirdly, I would like to thank the examination committee, Dr. Abu Sesay, Dr. Rushi Vyas, Dr. Rohana Ambagaspitiya, and Dr. Lin Cai for their time and effort in improving this thesis. Special thanks to Jesse Chaulk for advising me on parts of my research with his expertise in machine learning.

My parents Albert and Grace Kwan have also been very encouraging throughout this research period. Without their full support in my studies, I definitely could not have finished my program.

I express my deepest appreciation from the bottom of my heart to my girlfriend Ami Yan and the community at Power to Change for journeying with me throughout my graduate studies career.

Dr. Hai Wang and the rest of my current and past colleagues at the Wireless Networking Research Laboratory has brought me great joy since I began my Master of Science degree in 2014.

Their friendship is what gets me excited to come into the office every morning and they have been a source of great inspiration through my coursework as well as research.

I would like to thank all the professors and administration staff in the Department of Electrical and Computer Engineering who has wrote me references for scholarships, given me opportunities to teach a course or to be a teaching assistant for their course, and processed my constant stream of paperwork throughout the year.

Lastly, I would like to thank the Natural Sciences and Engineering Research Council of Canada, Government of Alberta (Alberta Innovates and Province of Alberta Scholarship Programs), and the University of Calgary for the financial support.

To my parents Albert and Grace

Table of Contents

List of Tables

List of Figures and Illustrations

List of Abbreviations

Abbreviation	Definition
ANN	Artificial neural network
BABF	Blind adaptive beamforming
bps/Hz	bits/second/hertz
CA/D	Coordinated ambient/dedicated
CRN	Cognitive radio network
DPP	Determinantal point process
ED	Environment detection
EH	Energy harvesting
H-AP	Hybrid access point
HPPP	Homogeneous Poisson point process
HSU	Harvest-store-use
HUS	Harvest-use-store
ISM	Industrial, scientific, and medical
LFNTLRE	Linear forecaster with near-time linear regression-based enhancer
MIMO	Multiple input, multiple output
MISO	Multiple input, single output
MOO	Multi-objective optimization
MRC	Maximal ratio combining
MS2-BABF	Multi-source, multi-sensor blind adaptive beamforming
MS-BABF	Multi-sensor blind adaptive beamforming
NOMA	Non-orthogonal multiple access
ReLU	Rectified linear unit
RF	Radio frequency
RMSprop	Root mean square propagation
SISO	Single input, single output
SNR	Signal-to-noise ratio
SOO	Single-objective optimization
SSPCA	Sleep-wake scheduling and power control algorithm
ST	Sum-throughput
STF	Sum-throughput and fairness
STFIP	Sum-throughput and fairness index product
TDMA	Time domain multiple access
TS	Time-switching
WPCN	Wireless powered communication network

List of Symbols

Symbol	Definition
T_p	Accurately predicted wake up time
$\hat{b}$	Artificial neural network bias vector
$\hat{\delta}$	Artificial neural network intermediate back propagation output errors vector
$\hat{a}$	Artificial neural network intermediate feed forward input values vector
$\hat{z}$	Artificial neural network intermediate feed forward output values vector
L	Artificial neural network layer
Z	Artificial neural network training data set size
$\overline{E_{HR}}$	Average energy harvesting rate
$\bar{E}$	Average of all known capacitor energy levels for all sensors at the beginning of the sessions
$\bar{T}_w$	Average of all known successful wake up times for all sensors
P_{UL}	Average transmit power of sensor
$\hat{w}$	Beamforming weight vector or artificial neural network weight vector
Δ_{B}	Beginning of the session Δ
O	Big-O notation for algorithm complexity
ψ	Body shadowing loss margin
S_R	Capacitor energy depletion ratio
E	Capacitor energy level
ϵ	Convergence tolerance or small value to prevent division by zero
R_{sum}	Data rate summation for all sensors
D	Depth of the near-time trends
d	Distance
BB_{DL}	Downlink bandwidth bias
BR_{DL}	Downlink bandwidth ratio
h	Downlink channel power gain
R_{DL}	Downlink data rate
$R_{DL,sum}$	Downlink data rate summation for all sensors
E_{DL}	Energy harvested for the downlink data decoding
E_{UL}	Energy harvested for the uplink data transmission
E_S	Energy required for sensor to sense data once
E_C	Energy required for sensor to wake up and check the capacitor energy level
$\hat{y}_R$	Entire history of all accurate environment detections, rural
$\hat{y}_U$	Entire history of all accurate environment detections, urban

$\hat{T}_p$	Entire history of all accurately predicted wake up times
$\hat{E}$	Entire history of capacitor energy levels at the beginning of the sessions
RMS_b	Exponential weighted moving average of gradients, biases
RMS_w	Exponential weighted moving average of gradients, weights
$\hat{T}_w$	Full history of all successful last wake up times for all sensors
a	Gamma parameter a
b	Gamma parameter b
E_H	Harvested energy
Δ	Iteration index or ambient session counter
J	Jain's fairness index
H	Learning rate
S_{max}	Maximum number of times a sensor can sense data in one session
$T_{p,max}$	Maximum value in the array $\hat{T}_p$
Ω	Nakagami-*m* average power parameter
m	Nakagami-*m* fading parameter
x_E	Normalized capacitor energy level
y_T	Normalized known accurately predicted wake up time
x_T	Normalized last successful wake up time
Q	Number of antennas on a hybrid access point
N	Number of hybrid access points
K	Number of sensors
PL_{ref}	Path loss in dB at the reference distance d_{ref}
p_f	Perturbation factor
$\hat{p}$	Perturbation vector
I	Perturbation vector quantity
η	Portion of harvested energy used for data transmission or decoding by each sensor
φ	Power loss exponent
λ	Power splitting ratio
α	Proportion of time RF source spends in transmitting energy
P_R	Received power at sensor
$P_{R,B}$	Received power at the H-AP from the sensor operating in backscatter mode
d_{ref}	Reference distance
s	Scaling term related to the sensor scattering efficiency
$\bar{E}_{T,D}$	Sensor average energy harvesting acceleration or deceleration

$\bar{E}_D$	Sensor average energy harvesting rate in the considered D
ς	Sensor energy harvesting efficiency
$x_{E_{T,D}}$	Sensor normalized average energy harvesting acceleration
E_{res}	Sensor reserve energy
τ	Sensor time slot
τ_{EH}	Sensor time slot for energy harvesting
τ_{DL}	Sensor time slot to decode data
τ_{UL}	Sensor time to upload data
$\tau_{UL,B}$	Sensor time to upload data in backscatter mode
T_w	Sensor wake up time
Γ	Signal to noise ratio gap from Shannon channel capacity
β	Small-scale fading power gain
$\sigma_{\hat{E}}$	Standard deviation for all known capacitor energy levels for all sensors at the beginning of the sessions
$\sigma_{\hat{T}_w}$	Standard deviation for all known successful wake up times for all sensors
r_d	The difference between antenna reflection coefficients
k_B	The number of sensors currently operating in backscatter mode
σ^2	Thermal noise power
T	Time block
Z	Time ratio
$T_{t,k}$	Total elapsed time since a reference start time of zero
P_C	Transmit power of cell phone tower
P_A	Transmit power of H-AP
BB_{UL}	Uplink bandwidth bias
BR_{UL}	Uplink bandwidth ratio
g	Uplink channel power gain
P_{UL}	Uplink data rate
$R_{DL,sum}$	Uplink data rate summation for all sensors

CHAPTER 1: INTRODUCTION

1.1. Background

The study of wireless powered communication networks (WPCNs) using radio frequency (RF) energy harvesting (EH) has been of tremendous interest in both academia and industry in the past few years [1], [2]. These sensors are popular with consumers and health care professionals to measure bodily vital statistics such as physical activity, body temperature, and heart rate. As technology continues to improve, on-body sensors continue to become increasingly affordable, smaller in size, powerful in hardware, and better in power efficiency. For example, Texas Instruments' CC1312 wireless microcontroller unit only uses 0.85µA during standby, 30.8µA while idling, and 808µA when active [3]. Furthermore, the CC1312's radio power consumption is only 5.8mA in active mode.

However, the requirement for a battery that needs to be recharged or replaced on a constant basis prohibits sensor deployment in applications where this is not feasible, such as sensors implanted in the human body. Therefore, RF EH for powering on-/in-body sensors is a growing area of research interest as a promising solution [4]. Energy sources that have potential for EH include natural (e.g., wind), mechanical (e.g., vibrations), thermal (e.g., friction), solar (e.g., the sun), and radio frequency (RF) (e.g., Wi-Fi access points, cellular base stations, TV stations) [5].

This thesis focuses on RF EH because it does not depend on nature and the sensor's form factor does not need to be significantly increased to accommodate the EH circuitry compared to other EH methods like solar or wind. Also, RF signals enable power delivery at larger distances, thus better than magnetic induction schemes used for near-field power transmission. A WPCN comprises portable data-capable wireless devices such as sensors housing an RF circuit for energy harvesting [6] and dedicated RF EH source devices like hybrid access points (H-APs). RF EH is

desirable compared to other sources for its relative ease of implementation for sensors on applications like the human body.

Hardware design and protocols are both major components of RF EH research. Hardware design covers elements such as circuit design [7], [8] and antenna design [9], [10]. Protocols, strategies, and techniques such as timing optimization, system scheduling, and beamforming have their figures of merit measured by wireless network performance and sensor operation ability. This thesis focuses solely on protocols, strategies, and techniques. Hardware design is not within the scope of this thesis.

This thesis aims to improve the WPCN performance and sensor operation ability; specifically, a system with one or more RF sources and multiple on- and/or in-body sensors. Currently, there are two major streams in RF energy harvesting. The first is using pure unintended or ambient RF energy sources that already exist in the environment, such as cell phone signals radiated by cell phone towers in the licensed frequency bands and Wi-Fi access points in the unlicensed frequency bands. However, in order to effectively harvest unintended RF energy, one must know the amount of available unintended RF energy that can be used for EH. The second is using dedicated or intended RF energy sources operating in the unlicensed industrial, scientific, and medical (ISM) frequency bands, such as a smartphone or dedicated transmitter like the Powercast TX91501-3W-ID [11]. However, in order to effectively harvest RF energy from both unintended and intended sources in the real world, a proper wireless protocol must be implemented to ensure optimal performance and functionality of all devices in the system.

Metrics of WPCN performance include sum-throughput and fairness. Sensor operation ability can be measured by dropout rate in dedicated mode, how effective it is in preventing itself from running out of energy unexpectedly in ambient mode (e.g, battery outage and miss count),

and ensuring it has sufficient energy to sense as much data as possible whenever needed in ambient mode (e.g., hit count and accuracy rate). A sensor drops out when the data throughput falls below a required data throughput threshold, usually due to the doubly near far problem [12]. The doubly near far problem is where large data transmission time is unfairly allocated to nodes that can harvest more energy, causing nodes that cannot harvest as much energy to also receive less data transmission time, therefore achieving a lower data throughput.

1.2. Problem Statement

The research in this thesis centers on the two major streams in RF EH systems, addressing three main problems.

- *Problem #1 (Chapter 3): How to design a WPCN with RF EH sensors that maximizes the sum-throughput and sensor operation ability by integrating time-switching, power splitting, and backscatter communication techniques with a dedicated RF energy source?* Problem #1 can be further broken down to three subproblems that arise from currently existing RF EH protocols for WPCNs in literature. The first subproblem, peculiar to WPCNs with dedicated RF sources, is the lack of downlink data decoding [13], [14]. Second, existing RF EH protocols rely on mathematically and computationally complex methods of combining a time-switching and power splitting receiver that do not allow direct communication between the transmitter and energy harvesting receivers [15], [16]. The third subproblem, applicable to WPCNs assisted by backscatter communication, is the lack of appropriate methods for integrating backscatter communication without blocking some receivers in the network from functioning. Chapter 3 tackles these three subproblems to address Problem #1.

- *Problem #2 (Chapters 4 and 5)*: *What methods can be used to utilize one or more H-APs in the same WPCN with blind adaptive beamforming at each H-AP to maximize the sum throughput, fairness, and operation ability of the sensors proposed in Problem #1?* Problem #2 can be made into three subproblems with respect to the current state-of-the-art. The first subproblem is WPCNs with multiple intended sources lack power splitting downlink data decoding phase [5], [17]. Second, existing beamforming techniques, particularly blind adaptive beamforming, are not designed to work with WPCNs with multiple intended sources and multiple sensors [18], [19], [20]. The third subproblem is the lack of an appropriate method to interface the backscatter communication-enabled combination sensors with one or more beamforming H-APs [17], [19], [21]. Solving these three problems are challenging but results in increased WPCN performance found in Chapters 4 and 5.
- *Problem #3 (Chapter 6)*: *How can smart decision-making strategies be implemented to improve the data sensing success of EH sensors when dedicated RF transmitters are out of range, and thus, increase the EH sensors' operation ability?* Problem #3 can be divided into two subproblems to solve. The first subproblem is RF EH sensors are either optimized to harvest energy from intended sources [13], [22], [23] or unintended sources [24], [25], [26], [27] but not both. Second, existing ambient RF EH techniques, strategies, and/or heuristics [24], [25], [26], [27], [28], [29] are insufficient to allow sensors to reliably operate in an environment where there are unpredictable availability of unintended sources and/or ongoing changes in channel conditions between the sensors and unintended sources [18]. Therefore, a new protocol optimized to harvest energy from and communicate with H-APs when available, reliably sense data when only unintended sources are available, and

seamlessly transition between the two different types of sources is needed. When only unintended sources are available, the protocol needs to maximize the use of limited harvested energy by optimizing the wake up and sleep schedule. Solving these two subproblems is challenging because the proposed solution will need to ensure sensors can reliably operate in an environment where there are ongoing changes in channel conditions and unknown availability of unintended sources. Chapter 6 has the solution to the two subproblems, which will result in RF EH sensors that maintain consistent functionality whether or not they are within range of an H-AP.

1.3. Thesis Motivation and Objectives

1.3.1. Thesis Motivation

The main motivation to solve the three problems addressed in this thesis is to improve the performance of a wireless powered communication network in the real world for future generation sensors powered with harvested RF energy. The creation and optimization of a protocol that can be used in wireless communications that improves the WPCN performance is needed.

The performance of a WPCN in a dynamic environment can be improved by jointly considering both the H-AP side and sensors side. Integrating novel techniques such as backscatter communication, multi-source, multi-sensor blind adaptive beamforming, and smart decision-making strategies using machine learning are necessary to support this motivation.

1.3.2. Thesis Objectives

The following research objectives are defined to solve the three research problems described in this thesis:

- *Thesis Objective #1 (Chapter 3): Formulate and solve optimization problems whose objective is to maximize the sum-throughput of wireless sensor networks with radio*

frequency energy harvesting and backscatter communication. This chapter will first need to propose three time-division based RF EH protocols that optimize the sum-throughput of a WPCN. Second, this chapter will need to formulate and solve a two-way RF EH and data transmission optimization problem using two time division based RF EH protocols. Third, a computation-efficient algorithm will need to be proposed to work in conjunction with a third backscatter enabled time division based RF EH protocol to increase the sum-throughput of a WPCN. Lastly, the impact of various parameters such as distance between sensor(s) and the H-AP, as well as the H-AP transmission power on the sum-throughput of the WPCN, will need to be investigated.

- *Thesis Objective #2 (Chapters 4 and 5): Formulate and solve a multi-objective joint optimization problem where both the sum-throughput and fairness of a radio frequency energy harvesting WPCN are maximized using multiple beamforming hybrid access points and backscatter communication-enabled combination sensors.* In Chapters 4 and 5, an RF EH and two-way data transmission multi-objective optimization problem needs to be formulated and solved. This optimization problem will consider, in a joint manner, one or more blind adaptive beamforming H-APs and power splitting hybrid or backscatter communication-enabled combination sensors. Second, the multi-source, multi-sensor blind adaptive beamforming with combination sensors (MS2-BABF/combo) protocol will need to be proposed. The MS2-BABF/combo protocol will be a low complexity algorithm that integrates the combination sensors with the multiple source, multiple sensor blind adaptive beamforming algorithm. The MS2-BABF/combo algorithm should not require explicit channel state information estimation and supports multiple sources and multiple sensors. Lastly, the impact of various parameters such as the number of antennas and H-APs on the

sum-throughput, throughput fairness, sum-throughput and fairness tradeoff, and sensor dropout rate of a WPCN will have to be investigated.

- *Thesis Objective #3 (Chapter 6): Design a coordinated ambient/dedicated (CA/D) protocol where backscatter-enabled combination sensors are optimized to harvest energy from intended RF sources when available and fall back to harvesting energy from unintended sources when only unintended sources are available*. First, this chapter will propose a coordinated ambient/dedicated (CA/D) RF EH protocol for backscatter-enabled combination sensors that can intelligently switch between harvesting energy from one or more beamforming H-APs when within range and harvesting from unintended sources when such H-APs are out of range. Second, two separate techniques – the linear forecaster with near-time linear regression-based enhancer (LFNTLRE) and artificial neural network with environment detection (ANN-ED) – will be proposed to determine the optimum sensor data collection. Two separate techniques will be proposed because they will have different sensor hardware and network design requirements, and either can be better than the other depending on how it is used. Lastly, the LFNTLRE and artificial neural networks-based machine learning algorithms' performance, measured by its accuracy rate and quantity of data collected, in environments where the unintended sources' locations are Ginibre-distributed [30] with channels modeled by Nakagami-*m* fading will need to be investigated.

1.4. Summary of Thesis Contributions

This thesis contributes protocols for unintended and intended RF energy harvesting designed to maximize the wireless network performance and sensor operation ability of an RF EH system

with multiple RF sources and sensors. The specific contributions are further described in the following paragraphs, as they correspond to the content of each contribution chapter.

In Chapter 3, optimization problems whose objective is to maximize the sum-throughput of wireless sensor networks with RF EH and backscatter communication are formulated and solved. The chapter proposes and analyzes three protocols for maximizing the sum-throughput; namely, the time-division with downlink data decoding protocol, hybrid power splitting/data decoding protocol, and backscatter-enabled combination protocol. The time-division protocol optimizes a WPCN with a two-way communication link between the sensors and a hybrid access point. The hybrid protocol optimizes a WPCN with a power splitting downlink data decoding phase. The backscattered-enabled combination protocol optimizes a WPCN with a power splitting downlink data decoding phase and backscatter communication enabled sensors. Numerical results show that the hybrid and combination protocols deliver up to 15.0% and 31.3% increase in sum-throughput, respectively, compared to the reference time-switching RF EH protocol in a dynamic environment.

In Chapter 4, a joint-optimization problem whose objective is to maximize the sum-throughput of a WPCN with RF EH and backscatter communication using a beamforming hybrid access point is formulated and solved. A new multi-sensor blind adaptive beamforming with combination protocol (MS-BABF/combo) is proposed and analyzed. A second joint-optimization problem whose objective is to maximize both the sum-throughput and fairness of a WPCN with RF EH is also formulated and solved. An algorithm based on the multi-source blind adaptive beamforming with hybrid protocol that maximizes the sum-throughput and fairness (MS-BABF/hybrid-STF) is proposed and analyzed. Numerical results show that the jointly optimized MS-BABF/combo protocol delivers up to 48.8% and 26.4% increase in sum-throughput compared to a single input, single output configuration and the MS-BABF with time-switching (MS-BABF/TS) protocol,

respectively, in a dynamic environment. The MS-BABF/combo protocol considerably decreased the sensor dropout rate compared to the MS-BABF/TS protocol from 1.0% to 0.43% at 7.5m as well. The jointly optimized MS-BABF/hybrid-STF protocol achieves a 36.7% increase in fairness compared to a single input, single output configuration in a dynamic environment and delivers an average of 19.1% fairness gain when the number of sensors is varied from 2 to 8 compared to a similar protocol that optimizes only the sum-throughput of a WPCN instead.

In Chapter 5, a multi-objective joint optimization problem where both the sum-throughput and fairness of an RF EH WPCN are maximized using multiple beamforming H-APs and backscatter communication-enabled combination sensors is formulated and solved. The chapter proposes the MS2-BABF/combo protocol. The protocol is analyzed to determine its performance with metrics including WPCN sum-throughput, fairness in the achievable rates by sensors, sum-throughput and fairness tradeoff, and sensor dropout rate. Numerical results show that the MS2-BABF/combo protocol delivered up to approximately 296% increase in sum-throughput compared to the reference time-switching RF energy harvesting protocol in a dynamic environment, achieved a dropout rate of 0% instead of 28.5% by the reference TS protocol at 10mW H-AP transmission power, and increased Jain's fairness index from $J = 0.76$ to up to 0.90 and 0.80 with and without sensors operating in backscatter mode, respectively.

In Chapter 6, a coordinated ambient/dedicated (CA/D) protocol where backscatter-enabled combination sensors are optimized to harvest energy from intended RF sources when available and fall back to harvesting energy from unintended sources when only unintended sources are available is introduced. The CA/D protocol can use either of the two new machine learning techniques proposed, the LFNTLRE algorithm and ANN-ED, to determine the optimum EH schedule. These machine learning algorithms can reliably operate in environments where there is

unpredictable availability of unintended sources and ongoing changes in channel conditions between the sensors and the unintended sources. Numerical results show that sensors using the ANN-ED and LFNTLRE algorithm can achieve up to 99.5% and 99.6% hit count relative to that of ideal sensors, respectively, compared to 100% by an ideal sensor. Sensors using the ANN and LFNTLRE algorithm have an accuracy percentage of up to 99% and 100%, respectively, as well.

Table 1.1. Summary of Main Contributions of Thesis

Contribution	Chapter/Section	Corresponding Publication(s)
1. Formulation and solutions to a two-way RF EH and data transmission optimization problem using three time division-based RF EH protocols, where the combination protocol is backscatter-enabled	3.3	[31]
2. Formulation and solutions to an RF EH and two-way data transmission joint optimization problem that considers a beamforming H-AP using the combination protocol	4.3	[32]
3. Formulation and solution to a RF EH and two-way data transmission multi-objective joint optimization problem that considers a beamforming H-AP using the time-switching/power splitting hybrid protocol	4.4	[33]

4. Formulation and solution to an RF EH and two-way data transmission multi-objective optimization problem that considers in a joint manner multiple blind adaptive beamforming H-APs and power splitting with backscatter communication-enabled combination sensors	5.3, 5.4	[34]
5. A CA/D RF EH protocol for backscatter-enabled combination sensors that intelligently switches between harvesting energy from one or more intended sources such as the beamforming H-APs when within range and harvesting from unintended sources when the H-APs are out of range	6.3	[35]
6. The LFNTLRE algorithm for determining the optimum time to wake up to attempt data sensing	6.4	[35]
7. The ANN-ED algorithm for determining the optimum time to wake up to attempt data sensing	6.4, 6.5	[35], [36]

1.5. Thesis Outline

The remainder of this thesis is organized as follows: Chapter 2 is a review of the current research work in the area of RF EH systems. The similarities and differences between the work presented in this thesis and those in literature are also discussed in Chapter 2. In Chapter 3, three protocols for maximizing the sum-throughput; namely, the time-division with downlink data

decoding protocol, hybrid power splitting/data decoding protocol, and backscatter-enabled combination protocol, are proposed and analyzed. Chapter 4 introduces the new MS-BABF/combo and MS-BABF/hybrid-STF protocols with performance simulation results. Chapter 5 contains the MS2-BABF/combo protocol. The MS2-BABF/combo protocol is analyzed in Chapter 5 to determine its performance with metrics including WPCN sum-throughput, fairness in the achievable rates by sensors, sum-throughput and fairness tradeoff, and sensor dropout rate. In Chapter 6, the CA/D protocol is proposed, where backscatter-enabled combination sensors are optimized to harvest energy from intended RF sources when available. The CA/D protocol will fall back to harvesting energy from unintended sources using either of the two new machine learning techniques when only unintended sources are available. Finally, the major contributions of this thesis, engineering significance of thesis findings, and recommendations for future work are presented in Chapter 7.

CHAPTER 2: LITERATURE REVIEW

2.1. Introduction

Radio frequency (RF) energy harvesting (EH) has been of tremendous research interest in the past few years as a promising approach to power portable wireless devices hence eliminating batteries that require periodical charging and/or replacement. From the literature review, RF EH protocols and techniques aim to improve two main areas: wireless network performance and sensor operation ability. Therefore, this chapter contains a critical assessment of existing literature. A section that compares the work in this thesis with existing work can be found in this chapter as well.

2.2. Critical Assessment of Existing Literature

2.2.1. Wireless Network Performance

Wireless network performance includes data throughput and network fairness, which are all important metrics in evaluating whether nodes in a network receive an adequate quality of service. Data throughput considers the rate achieved by each individual node, whereas network fairness is a measure of the variance in the rates achieved by the multiple nodes in a network, for example, a network utilizing an RF EH protocol is fair when the variance of the rates achieved by the nodes is close to zero. Protocols that optimize the sum-throughput only are generally unfair [13], hence the need to achieve an improved balance in the data throughput and fairness tradeoff. In order to increase data throughput and network fairness, the trade-off between sum-throughput and network (or system) fairness in a WPCN consisting of one hybrid access point (H-AP) and multiple nodes was investigated by proportional fairness [37]. A hybrid access point is a transceiver connected to the mains supply that can alternate between transmitting RF energy to the sensors for energy harvesting and data for data decoding as well as receiving data transmitted from

the sensors. When all nodes are located at the same distance from the H-AP, the time domain multiple access (TDMA) protocol is less complex while yielding similar performance as non-orthogonal multiple access with time-sharing (NOMA-TS) protocol. If the nodes are located at varying distances from the H-AP, NOMA-TS delivers better sum-throughput, better per user rate, and better fairness than both TDMA and NOMA with fixed decoding/adaptive power. This means the NOMA-TS protocol has better user scalability than the other compared schemes. Despite the fact there is no analysis on how NOMA-TS performs in a fast fading environment, the contributions of [37] are important in creating a WPCN with nodes that need to meet rate requirements while mitigating the doubly near far problem [12].

Proportional fairness in an RF EH wireless network was also a topic of interest [38] using the TDMA protocol. The authors found that optimal scheduling occurs when each timeslot is either used for energy harvesting or data transmission. A deterministic path loss model was used, which implies a static environment based on the placement of the EH nodes. The opportunistic policy used to overcome the doubly near far problem was evaluated using Jain's Fairness Index [39], which was raised from approximately 0.7 to close to 0.9. Although the data throughput fairness of this scheme is not as good as optimizing the common throughput [13] (optimizing the common throughput implies Jain's Fairness Index of very close to 1), it is computationally simpler with a closed form solution.

The use of a cognitive radio network (CRN) to improve spectrum and energy efficiency was investigated [40]. In the system model, energy harvesting secondary users access an idle channel to transmit data and harvests energy from an occupied channel. To improve the throughput of the energy harvesting nodes, a 2-channel sensing scheme to search for further opportunities to data transmission was implemented. However, as transmission opportunities increase, less time is

available for harvesting energy and therefore increases outage, which proposes a tradeoff between the two. Outage occurs when the energy harvesting secondary users completely run out of energy. The mathematical analysis of [40] is relatively simple, but forms a good foundation for understanding the tradeoffs between data throughput and dropout probability with respect to the channel sensing scheme. To optimize EH and data transmission between sensors, power transmitters, and an access point, Sharma *et al.* [41] evaluate a multi-agent reinforcement learning framework while [42] considers reinforcement learning with deep Q-network enhancement as well.

A WPCN with one H-AP and multiple nodes was considered [21]. Since nodes in a traditional harvest-then-transmit protocol system are required to harvest sufficient energy before transmitting data, the authors of this paper [21] integrate a backscatter mode into the energy harvesting nodes and optimizes the sum-throughput of the system to improve system sum-throughput. Backscatter communications communication is a technique where a sensor re-modulates an incoming continuous carrier wave signal to transmit data on-the-fly without storing the RF energy [43]. In this paper, backscatter and harvest-then-transmit cannot occur simultaneously in each timeslot. However, it is shown that an optimal combination exists for harvest-then-transmit and backscatter communication for each node.

Backscatter communication was also investigated [44]. Since existing energy detection techniques provide poor performance at low signal to noise ratio scenarios, this paper attempts to improve the bit error rate by calculating the distributions of two covariance-based statistics and from that design corresponding detection rules. This paper [44] shows the bit error rate is dependent on the number of samples and the covariance matrix of the received signal and the autocorrelations of the received signal can be calculated by exploiting its statistical covariance

property. From there, the ratio of these statistics can be used to improve the output detection accuracy. However, the authors model only one reader, one RF source, and one backscatter tag in the system. The scalability of the system accounting for more elements is needed to prove the feasibility of their algorithm.

The bit error rate of an RF EH system was minimized by mitigating the effects of interference [45]. This was done by jointly optimizing the sleep-waking scheduling and transmit power in a WPCN in a mixed integer non-linear programming problem, which was transformed into a convex problem through integer relaxation. A sleep-wake scheduling and power control algorithm (SSPCA) to obtain the optimal power allocation scheme using the harvest-use-store (HUS) protocol rather than the harvest-store-use (HSU) protocol was proposed. As a result, SSPCA with HUS outperformed HSU in charging efficiency and circuit power loss with eight sensor nodes, which resulted in reduced bit error rate. However, [45] should have accounted for the difference in distances between the sensor nodes and the RF EH sources, because this affects EH fairness, and thus rate fairness, which is an important performance metric when the charge state is optimized.

Using the MRC strategy in a single antenna configuration [46], the authors derived a closed form expression for harvested energy over coherent time slots in a Rayleigh fading channel with interference. The expressions for average packet loss, average packet delay, and average transmission power were also derived. It was shown that the maximal ratio combining strategy outperformed channel-blind strategies without employing maximal ratio combining as the signal-to-noise ratio decreases. By using a single antenna configuration, the same packet is transmitted in different time slots. This strategy trades reliability for data throughput and latency.

2.2.2. Sensor Operation Ability

An energy harvesting CRN evaluated by its coverage probability and energy outage probability was investigated [47]. Secondary transmitters harvest RF energy from primary transmitters in its system model. To improve reliability and spectrum and energy efficiency, an interference threshold-based transmission strategy was implemented on the secondary transmitters. There exists a relationship between the interference threshold and energy outage probability, transmission probability, coverage probability, and spatial throughput of the secondary network. The energy outage probability is a major figure of merit [47], and is defined as the probability the harvested and stored energy is insufficient for data transmission. The energy outage probability increases as the interference threshold increases, and a tradeoff exists between the secondary transmitters' harvested energy and data transmission. Coverage probability decreases as the interference threshold increases, because a higher interference threshold means less protection for the secondary transmitter. By exploiting the correlation between the harvested energy at secondary transmitters and the total interference at secondary receivers, the optimal interference threshold that maximizes the spatial throughput of the secondary network is derived to reduce the energy outage probability. In the simulations, the locations of all primary transmitters and secondary transmitters are homogeneous Poisson point process (HPPP) distributed with a given density. Although this is practical for analyzing large networks that does not have a fixed number of nodes, analysis in the context of smaller networks where there is a smaller number of fixed nodes can provide valuable insight into the performance of body area networks.

A decision-making policy that minimizes frequency band switching to maximize EH and minimize power consumption was presented [25]. The authors aim to increase EH rate from ambient (unintended) RF sources in a WPCN by using their Bayes-Upper Confidence Bound

algorithm [25]. This paper [25] suggests that if the potential of the best frequency band for RF EH can be determined algorithmically, it will lower the number of frequency band switches, which lowers the overhead, and increases the system performance. However, the selection scheme is very primitive, because the authors claim almost every factor is out of the scope of their research. These factors include energy harvesting efficiency, antenna design, and even fading model. Although this could be justified to some extent, at the very least, the authors could have cited a model from existing literature that shows how they got their simulation values in the simulated cases to give more credibility to their results.

Another statistical ambient RF EH strategy was formed in literature [24]. The premise of this sleeping and RF energy strategy is that, in general, when the node is better off sleeping when ambient RF energy is low, while waking up is necessary to harvest energy when the availability of ambient RF energy is high. Since the knowledge of the amount of ambient RF energy is not known beforehand, the ambient RF energy arrival model is described by a two-state Gilbert–Elliott Markov chain in two scenarios. The first scenario is where the transition probabilities of the Markov chain is known, while the second model is where the transition probabilities are unknown and is determined heuristically. The authors show the EH reliability of an EH node increases given the tradeoffs between sleeping and waking on the inconsistent arrival of ambient RF energy, which is important in effectively harvesting ambient RF energy. However, the modeled work is based on static parameters such as channel conditions and quantity of harvested energy.

The authors of [27] used two machine learning techniques, linear regression and decision tree, to predict the amount of available ambient RF energy for EH in different frequency bands during different times of the day. Similar to [24], the premise of its scheduling strategy is to sleep when the available ambient RF energy is low and wake up when the available ambient RF energy

is high. The authors in [27] found that the linear regression approach outperformed the decision tree method by achieving a minimum 85% accuracy.

Resource allocation by a simultaneous wireless information and power transfer two-way relaying network via time-switching and power splitting schemes was explored [48]. The joint optimization problem of time-switching/time phase and power splitting/time phase parameters for the time switching and power splitting schemes, respectively, to minimize power dropout probability was derived and solved. The authors propose the use of sub-optimal schemes by fixing certain parameters, such as the time phase ratio to a statistical optimal, to reduce implementation complexity, and show that the dropout is reduced compared to the benchmark. It can be seen that the time-switching, time phase, and power splitting ratios have a direct impact in the probability of dropout of the system. Although all parameters can be optimized in a closed form to find a global optimum, suboptimal methods yield lower computational complexity at the expense of performance. However, the analysis is only limited to two devices and one relay. For the suboptimal methods, the system can only select from one of two statistical optimum time switching/power splitting candidate values. There is no justification on why the system cannot generate more candidate values, as this can improve the performance of the sub-optimal methods.

The performance of a battery-free wireless sensor powered by purely ambient RF energy was analyzed using a stochastic geometry approach [49]. Ambient RF sources such as cell phones, access points, and base stations are distributed as a Ginibre α-determinantal point process (DPP) [30], as the DPP can capture repulsion among points (or location of the ambient RF sources in this context). Two common receiver architectures, separated and time-switching, were analyzed for its EH and uplink transmission outage probabilities with and without co-channel interference. An optimal time value in a time-switching receiver can be derived to minimize outage probability.

This paper is important for modeling WPCN with sensors powered purely by ambient RF energy. A similar paper by the same authors that analyzes the general-case network performance of a cellular network with general fading channels and a conditioning technique [50] is also available [51]. Both papers are crucial in modeling the feasibility of ambient RF EH sensors.

A blind adaptive beamforming algorithm (BABF) that mimics maximal ratio combining (MRC) diversity to improve RF EH was presented [52]. Since channel state information and channel model do not need to be explicitly estimated by using a matched filter, the authors of this paper claim the algorithm is computationally light. The algorithm was then implemented in a testbed to validate the results in a wireless information and power transfer context, and EH efficiency increased in a two to four antenna setup at up to 1.5m compared to a single antenna configuration. The algorithm in this paper [52] requires multiple iterations to converge to an optimal weight vector, which shows the unknown state of channel state information can be iteratively solved at the expense of some processing power and latency. Although the authors state the filter convergence latency is not a big issue compared to data transmission, latency is potentially a problem in real world fast fading channels, which was not accounted for in this paper. Furthermore, the BABF algorithm is only designed to support one transmitter and one receiver, which can be expanded to include multiple transmitters and multiple receivers.

The use of beamforming to increase RF EH performance was also explored [53]. The authors considered a WPCN on a time-switching protocol, where nodes harvest energy from dedicated and ambient RF energy sources in the first time slot and uses the harvested energy to transmit data to a receiver in the subsequent time slot. By using multiple antennas at both the dedicated RF energy source and at the nodes, accounting for co-channel interference, two beamforming techniques– best antenna-based beamforming and optimal beamforming vector –

were evaluated. As expected, beamforming, especially with the optimal beamforming vector technique, increased the average harvested energy. However, the authors assume up to 100 antennas in their array, which implies considerable form factor problems if implemented in a device with small form factor, such as an on-body sensor. While beamforming is a novel technique to improve RF EH performance, timing control in a time-switching protocol has a direct impact on harvested energy and data rate [13], [14], [37]. The use of half the timeslot for RF EH and the other half for data transmission in [53] will result in sub-optimal performance. Modeling the ambient source distribution using DPP [49] is probably better than the homogeneous Poisson point process distribution used by the authors [53]. Assuming 80% circuit conversion efficiency is not reasonable either; it is closer to 50% in reality [54]. Using a single massive multiple input, multiple output (MIMO) RF source to maximize the common throughput with time-division or power splitting sensors can also be found in [55].

2.3. Thesis Work in the Context of Existing Work

2.3.1. Wireless Network Performance

This thesis is similar to [13] and [14] because a sum-throughput maximization technique was used to optimize the data throughput of a wireless powered communication network in Chapter 3. This sum-throughput maximization technique is used as the basis for the three time-division protocols proposed in Chapter 3. However, the proposed protocols in Chapter 3 exploit the intrinsic nature of producing the optimum ratio between the harvested energy and timing allocation when the sum-throughput of a WPCN is maximized, which was not considered by the authors in [13] and a previously published work by this author [14]. Furthermore, the WPCNs in both [13] and [14] only features an energy harvesting phase and a sensor data uplink phase. The proposed protocols in Chapter 3 further adds a downlink data decoding phase, a power splitting

downlink data decoding phase, and/or an integrated backscatter communication phase while optimizing the sum-throughput, which was neither found in [14] nor [13]. The sum-throughput technique is implemented in a dynamic environment, where the channel power gains between the RF sources and the sensors are constantly changing, and Chapter 3 further investigates how the channel variations affect data throughput over time.

Furthermore, the sum-throughput optimization technique was reformulated in Chapter 3 into a series of new optimization problems for use with time-switching, power splitting, and backscatter communication enabled sensors in a dynamic environment. A new mathematical approach was used along with a sensor operation mode algorithm (Algorithm 3.1) to ensure optimum rate of the system with reduced computational complexity; totally different from the focus of [13] and [14].

Chapter 4 is like existing literature [13], [14] because sum-throughput maximization is used to optimize the data throughput of a WPCN. Data throughput of a WPCN was also optimized in Chapter 4 while maintaining throughput fairness between sensors. However, Chapter 4 proposes a new WPCN protocol that features an H-AP with multiple antennas for a multiple input, single output (MISO) design rather than single input, single output (SISO) as in previous works. While the form factor of H-APs makes multiple antenna configurations permissible, the physical size of on-body sensors will limit the number of antennas per sensor to one. A new joint optimization mathematical approach is used along with an algorithm (Algorithm 4.1) that optimizes parameters from both the transmitter and the sensors to ensure maximum rate of the system. Another new mathematical approach is also used along with an algorithm (Algorithm 4.2) that jointly optimizes system operating parameters at both the transmitter and the sensors to ensure maximum system throughput and throughput fairness of the WPCN; all new compared to previous works [13], [14].

Chapter 5 is like previous works [13], [14], because a sum-throughput maximization technique was used to optimize the WPCN throughput using one or more H-APs. However, the MS2-BABF/combo protocol also considers multiple blind adaptive beamforming H-APs with combination sensors, which was not found in previous works [13], [14], [20], [52], [55]. This MS2-BABF/combo protocol therefore defines the computational process for solving a series of completely new optimization problems that jointly maximizes the sum-throughput and fairness for multiple H-APs each with multiple antennas for a MISO design rather than SISO [13], [14], [20] or single H-AP MISO design [55]. These joint optimization problems are used in a low complexity algorithm (Algorithm 5.1) for all H-APs and sensors in a WPCN; totally different than those used in previous works [13], [14], [20], [52], [55].

The concept of the hybrid protocol in combining time switching with a power splitting downlink data decoding phase proposed in Chapter 3 is inspired by the work in [16]. The authors in [16] also provided a solution to optimize the sum-throughput of a WPCN. Different than [16], a direct link between the H-AP and sensor is assumed in Chapter 3 without an energy harvesting relay. In other words, the entire system model is different: The H-AP can directly communicate with sensors in the network with the solutions provided in Chapter 3 and vice versa. The combination protocol in Chapter 3 also adds a backscatter communication phase while mathematically and algorithmically optimizing the sum-throughput of the network, which was not found in [16]. Lastly, a totally different mathematical approach and algorithm design is created in Chapter 3 due to an entirely different system model, whether it is the time-switching with downlink, hybrid, or the combination protocol.

Similar to [20], Chapter 3 considers a WPCN that integrates backscatter communication with the harvest-then-transmit energy harvesting method in one of the three protocols proposed;

particularly, the combination protocol. The combination protocol contains a throughput maximization problem with bistatic backscatter communication and the harvest-then-transmit method, which has some similarities with only the indoor scenario of [20]. However, the system model and problem formulation, and thus, the problem solved in Chapter 3 is totally different than that of [20]. In [20], frequency division is used for long range outdoor communications (e.g., between the continuously transmitting high-power H-AP and primary users), while time division is used across Wi-Fi zones (e.g., between secondary users and secondary transmitters). Therefore, the optimization problem in [20] must switch between harvest-then-transmit, ambient, and backscatter to improve the throughput of each node and/or cell. In Chapter 3, a single zone short range body area network is considered using purely time division methods for data communications. As such, the single H-AP is compliant with the unlicensed industrial, scientific, and medical band standards [56], [57], and only transmit a continuous wave or data signal as required. Sensors are switched to backscatter mode in the combination protocol to improve the sum-throughput of the entire WPCN rather than individual sensors. Ambient backscatter was not considered, because considering ambient backscatter makes the protocol considerably more complex with a marginal increase in performance. The combination protocol in Chapter 3 has a power splitting downlink data decoding phase, which was not found in [20]. Lastly, Chapter 3 also focuses on two additional protocols; namely, the time-switching with downlink data decoding and hybrid protocols, which do not consider backscatter communication. These two additional protocols maximize the sum-throughput of a WPCN in a body area network; completely different than the focus of [20].

A WPCN that integrates backscatter communication with the harvest-then-transmit energy harvesting method is considered in Chapter 5 as well like [20]. However, the system model and

problem formulation, and thus, the problem solved in Chapter 5, is different. Due to the use of frequency and time division techniques at different zones of the heterogeneous WPCN [20], the optimization problem must switch between harvest-then-transmit, ambient RF EH, and backscatter communication to improve the throughput of each node and/or cell. A single zone short to medium range body area network featuring multiple beamforming intended sources jointly optimized with the backscatter communication-enabled combination protocol is investigated in Chapter 5, different than that in the heterogeneous WPCN [20].

Similar to [21], Chapter 3 also provides a solution to optimize the sum-throughput of a WPCN with backscatter communication. However, the protocol design, mathematical formulation, and algorithmic approach proposed in Chapter 3 are different than the one in [21]. The authors in [21] assume only one user can work in backscatter mode per time block, and backscatter communication cannot be succeeded by a harvest-then-transmit phase in the same time block. In Chapter 3, more than one user can work in backscatter mode per time block if the proposed algorithm determines the sum-throughput can be increased, and a harvest-then-transmit phase can succeed a backscatter phase in the same time block. Another difference is that the algorithm in [21] is limited in a way that it frequently blocks one or more sensors from transmitting within the same time block to achieve the highest sum-throughput, whereas the protocol in Chapter 3 ensures all sensors will have a chance to transmit in every time block with no blocking. The combination protocol in Chapter 3 also has a power splitting downlink data decoding phase, while the solution in [21] has no downlink data decoding phase at all. Lastly, Chapter 3 assumes a backscatter model where the data throughput is modeled on fast-fading channel conditions representative of the real world. In [21], the backscatter rate is always constant, which is not a realistic assumption.

2.3.2. Sensor Operation Ability

Algorithms 4.1 and 4.2 proposed in Chapter 4 are like the BABF algorithm [52] because they also include a computationally light beamforming algorithm that does not require explicit channel state information estimation. However, Algorithms 4.1 and 4.2 work in a multiple sensor environment, unlike BABF which only works with a single sensor. Algorithm 4.1 interfaces with the combination sensor and jointly optimizes both the weight vector and system timing values to maximize the sum-throughput rather than simply calculating the weight vector that maximizes harvested energy of one sensor. Also, Algorithm 4.1 has integrated sum-throughput joint optimization with a beamforming H-AP and sensors using the combination protocol, which is totally new compared to the existing literature [52].

Meanwhile, Algorithm 4.2 in Chapter 4 interfaces with the hybrid sensor and jointly optimizes both the weight vector and system timing values to maximize the sum-throughput and fairness as a multi-objective optimization problem. Using beamforming and system timings to jointly optimize both the sum-throughput and fairness of a WPCN is a new problem that has not been previously attempted in literature.

The multi-source, multi-sensor blind adaptive beamforming with combination sensors (MS2-BABF/combo) protocol proposed in Chapter 5 contains an element like the BABF algorithm [52] because it also includes computationally light beamforming algorithm that also does not require explicit estimation of the channel state information. However, MS2-BABF/combo works in a multiple source, multiple sensor environment, unlike current literature [52]. Existing technique simply calculate the weight vector that maximizes harvested energy of one sensor only [52]. Algorithm 5.1 interfaces with combination sensors presented in Chapter 3 and jointly optimizes

the weight vector and system timing values for multiple H-APs and sensors to maximize the sum-throughput and fairness between sensors.

The system model and problem formulation in Chapter 5 are completely different compared to literature [55]. In Chapter 5, multiple H-APs each with up to 8 antennas are considered, while [55] only considers a single H-AP, but with up to one million antennas. The massive MIMO algorithm is exponentially complex and changes the beamforming weight vector multiple times per time block, up to as many times as there are sensors, to maximize the common throughput. Chapter 5 features a linear low complexity algorithm, each H-AP with a weight vector that changes only in accordance to channel conditions. Sum-throughput and fairness between sensors are achieved by allocating different proportions of time to each H-AP instead. Lastly, Chapter 5 formulates a joint multi-objective optimization problem featuring sensors where each has integrated power splitting and backscatter communication support and considers factors like the power splitting ratio as part of the joint optimization problem, which is not found in [55].

Chapter 6 is like existing literature [24], [25], [26], [27], [28], [29] because the proposed coordinated ambient/dedicated (CA/D) RF EH protocol operating in ambient mode also uses a prediction algorithm to determine the optimum wake and sleep schedule for maximum sensor operation ability. However, the proposed CA/D RF EH protocol uses the novel linear forecaster with near-time linear regression-based enhancer approach or an artificial neural network, which is completely new compared to previous works [24], [25], [26], [27], [28], [29]. To the best of the author's knowledge, these machine learning approaches have never been used previously in the context of ambient RF EH sensors where the unintended sources' locations are Ginibre-distributed with channels modeled by Nakagami-*m* fading.

2.4. Summary

In this chapter, solutions to improve the performance of a WPCN using the harvested RF energy were surveyed. In order to improve the two major performance metrics of a WPCN, including wireless network performance and sensor operation ability, various protocols were proposed in the surveyed literature. These include protocol optimization techniques, beamforming algorithms, decision making strategies, and statistical analysis from ambient and/or dedicated RF energy sources. Based on the identified gaps in knowledge, new protocols that combines ambient and dedicated RF EH that accounts for real world channel characteristics is an open problem and a research challenge. This new protocols can combine smart decision-making strategies to select between ambient and dedicated RF sources, statistics-based heuristics for ambient RF EH-capable sensors, multiple H-AP WPCNs and beamforming techniques for dedicated RF sources, and improved timing and parameter design for energy harvesting sensors. Engaging in these topics of research can lead to improved performance and feasibility of next-generation wireless powered communication networks and RF EH sensors using both ambient and dedicated RF energy sources.

Table 2.1. Comparison of Main Features/Capabilities of Proposed Protocols with Existing Protocols in Literature

Proposed Protocol	Main Features/Capabilities of Proposed Protocol	Main Features/Capabilities of Comparable Existing Protocols
Time-Switching	Uplink and downlink data communication	Uplink data communication only [13], [14]
Hybrid	Uplink and downlink data communication with power splitting downlink phase	Uplink data communication only [13], [14], power splitting design limited to wireless relay networks [16]
Combination	Uplink and downlink data communication with power splitting downlink phase, backscatter-enabled	Uplink data communication only [13], [14], no power splitting downlink phase [20], backscatter is theoretically present but unusable [21]
MS-BABF	Blind adaptive beamforming with multi-sensor support; interfaced with time-switching, hybrid, or combination sensors	Single-source blind adaptive beamforming for a single simple energy harvesting node [52]
MS2-BABF	Blind adaptive beamforming with multi-source and multi-sensor support; interfaced with time-	Single-source blind adaptive beamforming for a single simple energy harvesting node [52]

	switching, hybrid, or combination sensors	
CA/D	Encapsulates the MS2-BABF/combo protocol in dedicated mode and automatically switches to ambient mode when required; uses machine learning techniques to determine optimal wake up schedule in ambient mode	Simple wake up and sleep scheduling for basic ambient RF EH sensors with no dedicated mode support [24], [25], [26], [27], [28], [29]

CHAPTER 3: SUM-THROUGHPUT MAXIMIZATION IN A WIRELESS ENERGY HARVESTING SENSOR NETWORK WITH BACKSCATTER COMMUNICATION[1]

3.1. Introduction

This chapter formulates and solves optimization problems whose objective is to maximize the sum-throughput of wireless sensor networks with radio frequency (RF) energy harvesting (EH) and backscatter communication. The chapter proposes and analyzes three protocols for maximizing the sum-throughput; namely, the time-division with downlink data decoding protocol, hybrid power splitting/data decoding protocol, and backscatter-enabled combination protocol. The time-division protocol optimizes a wireless powered communication network (WPCN) with a two-way communication link between the sensors and a hybrid access point (H-AP). The hybrid protocol optimizes a WPCN with a power splitting downlink data decoding phase. The backscattered-enabled combination protocol optimizes a WPCN with a power splitting downlink data decoding phase and backscatter communication enabled sensors.

3.2. System Model

3.2.1. System Architecture

The system architecture features one hybrid access point with K sensors each located at a certain radial distance d_k away, shown in Fig. 3.1. The H-AP, an intended source, can either be a low-power device such as a cell phone or a high-power device, for example, the Powercast TX91501-3W-ID transmitter [11], connected to a mains supply. The cell phone can also be configured to be a dedicated transmitter for energy harvesting. In the considered WPCN body area

[1] The content of this chapter has generated one journal paper [31]: J. C. Kwan and A. O. Fapojuwo, "Sum-Throughput Maximization in Wireless Sensor Networks With Radio Frequency Energy Harvesting and Backscatter Communication," in *IEEE Sensors Journal*, vol. 18, no. 17, pp. 7325-7339, Sept. 1, 2018.

network system, the K sensors are battery-less on-body/in-body EH sensors, where each is used for sensing a specific vital statistic such as physical movement, heart rate, or body temperature. The harvested energy by each battery-less sensor is temporarily stored in a capacitor, which will be fully discharged in the subsequent downlink or uplink data transmission phases to maximize the sum-throughput. For simplicity, we assume the capacitors are capable of charging and discharging as quickly as needed. The sensed data is then transmitted back to the H-AP, which serves as a gateway to the Internet. The H-AP subsequently uploads the sensed data to places like the doctor's office or health care service provider's database. The H-AP can also transmit data such as device configuration changes or health alerts/data query requests from the doctor's office or health care service provider to the sensors.

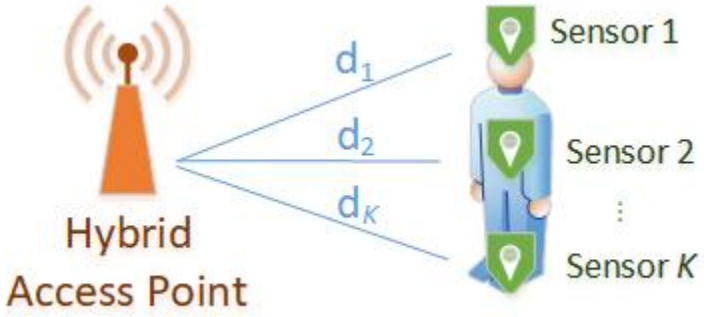

Fig. 3.1. A K sensor system with each sensor k on a human body located at radial distance $d_k, k = 1 \ldots K$ from a hybrid access point.

The H-AP has the knowledge of all the sensors in the WPCN within its coverage area, like a Wi-Fi router's knowledge of the connected devices, and thus acts as a global controller. The assumption that the H-AP has the knowledge of all sensors in the WPCN is reasonable because the sensors can make themselves known to the H-AP via a registration message piggy-backed on the first data packet transmission. Furthermore, the received power level at each sensor from the H-AP can be piggy-backed on each data packet transmission to keep the information up to date at

the H-AP without incurring additional signaling overhead. The ratio of the piggy-backed control data to sensor data depends on the size of each packet, which can be configured by the WPCN designer. Short packet lengths will have a higher control data to sensor data ratio, which is undesirable, but less data needs to be retransmitted when a retransmission is needed. Conversely, long packet lengths will have a lower control data to sensor data ratio, but more data needs to be retransmitted when a retransmission is needed. Each node in the network only receives or transmits during its allocated time slot.

3.2.2. Energy Harvesting and Data Transmission Protocol

To prevent destructive wireless interference, all protocols proposed in this chapter work on the basis of time division, where only the H-AP or one sensor can transmit at any given time slot τ. The only exception is the combination protocol, where sensors operating in the backscatter mode transmit data during the downlink energy harvesting phase by reflecting a portion of the received energy back to the H-AP.

For the system considered in an existing WPCN design [13], the entire time slot τ_{EH} is allocated to the sensor nodes to harvest energy, time slot $\tau_{DL,k}, k = 1 \dots K$ for each sensor k to decode data received from the H-AP, and time slot $\tau_{UL,k}, k = 1 \dots K$ for each sensor k to transmit data back to the H-AP. The τ_{EH} phase uses a continuous wave signal because it is the simplest and most efficient energy carrying waveform in a high frequency RF EH system [58]. It is assumed that all sensors use up all its harvested energy within the same time block T. The only exception to this is the energy harvested during the power splitting downlink data decoding phase for sensors operating in the backscatter communication mode in the combination protocol, which will be used in the subsequent time block T instead.

The first time-division based protocol proposed is the time-switching protocol with downlink data decoding (referred to as the time-switching sensor or time-switching protocol in shortened form for the rest of this chapter). The time-switching protocol is a sum-throughput optimized method that harvests energy, decodes data, and transmits data using orthogonal time slots. In the time-switching protocol, a downlink data decoding phase $\tau_{DL} = \sum_{k=1}^{K} \tau_{DL,k}$ is new compared to current works [13], [14], where time slot $\tau_{DL,k}, k = 1 \ldots K$ for each sensor k is used by the H-AP to send data (e.g. health hazards) to the sensors, as shown in Fig. 3.2.

Due to the presence of the data downlink and uplink phases, the length of the energy harvesting phase τ_{EH} is given by $\tau_{EH} = \tau_{EH,DL} + \tau_{EH,UL}$, where $\tau_{EH,DL}$ and $\tau_{EH,UL}$ are sub-time slots allocated to the sensor nodes to harvest energy for the downlink data decoding phase and uplink data transmission phase, respectively. Therefore, the optimal τ_{EH}, τ_{DL}, and τ_{UL} will need to be solved to maximize the sum-throughput of the WPCN.

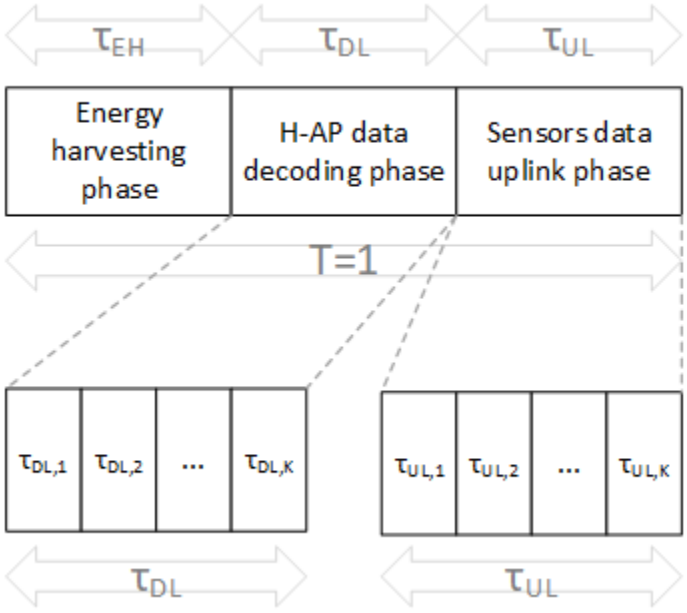

Fig. 3.2. Timing diagram comprising energy harvesting, downlink data decoding, and uplink data transmission phases.

The time-switching protocol will serve as a baseline reference for comparing the relative performance of the other two protocols proposed in this chapter, because its design is comparable to strict time-division, harvest-then-transmit protocols currently used in literature [13], [14].

The second proposed protocol is the hybrid protocol, which combines the time-switching and power splitting receiver structures. Inspired by an energy harvesting protocol applied to wireless relay networks [16], the hybrid protocol proposed in this chapter features a direct communication link between the H-AP and the sensors but with no relay. The hybrid protocol has some of its foundations in the time-switching protocol, but completely reformulated in a way such that the downlink data decoding phase τ_{DL} is also used for energy harvesting and the received power during τ_{DL} is split by a power splitting ratio λ, the proportion used for energy harvesting, and $(1-\lambda)$ for downlink data decoding, as shown in Fig. 3.3. Compared to the time-switching protocol, the length of the τ_{EH} phase changes, because some of the received power during τ_{DL} is considered as harvested energy to power the circuit inside the sensor. Therefore, the optimal τ_{EH}, τ_{DL}, and τ_{UL} will need to be solved as a totally new optimization problem accounting for the power splitting downlink data decoding phase to maximize the sum-throughput of the WPCN.

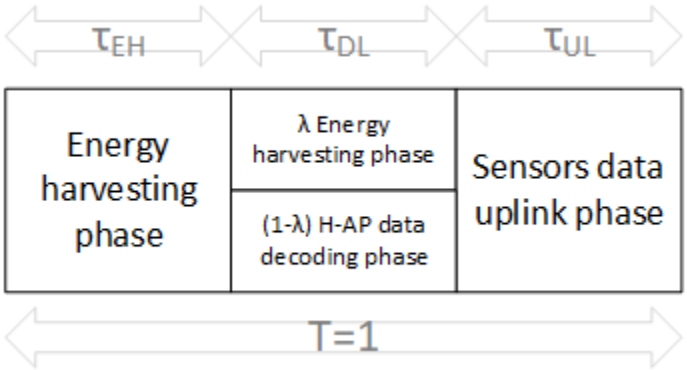

Fig. 3.3. Timing diagram comprising energy harvesting, power-splitting downlink energy harvesting and data decoding, and uplink data transmission phases.

The third proposed protocol is the combination protocol, which combines the time-switching and power splitting receiver structures with backscatter communication. The combination protocol integrates backscatter communication with the hybrid protocol without blocking other receivers in the network from functioning; different from the current state of the art [21]. Since an energy harvesting phase that generates a continuous carrier wave signal in the hybrid protocol exists during the τ_{EH} phase, utilizing that phase for backscatter communication, which was previously used exclusively for sensor energy harvesting, has the potential to increase the sum-throughput of a WPCN. Sensors that operate in backscatter mode will upload data to the H-AP during the τ_{EH} phase, harvest energy and decode data during the τ_{DL} phase, and remain off during the τ_{UL} phase, as shown in Fig. 3.4. Otherwise, sensors operating in non-backscatter mode will harvest energy during the τ_{EH} and τ_{DL} phases, decode data during the τ_{DL} phase, and transmit data during the τ_{UL} phase like the hybrid protocol.

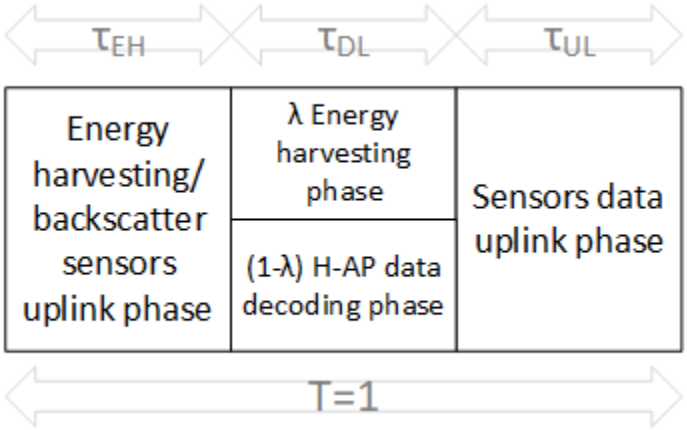

Fig. 3.4. Timing diagram comprising backscatter-enabled energy harvesting, power-splitting downlink energy harvesting and data decoding, and uplink data transmission phases.

The most challenging aspect is creating a working algorithm for the H-AP. The H-AP also acts as a global controller to determine which and how many sensors to run in backscatter mode,

which has not been done in previous literature. The algorithm needs to be run at the H-AP rather than as a distributed algorithm at each sensor, because optimizing the sum-throughput of the entire WPCN is the goal. It is not possible for the sensors to determine independently whether to enter backscatter mode or not without global knowledge of every other sensor in the WPCN to optimize the sum-throughput. The H-AP should always start from setting sensors with the lowest signal-to-noise ratio (SNR) into backscatter mode first. Moving slow (low SNR) sensors into backscatter mode is more effective and likely to increase the system sum-throughput than fast (high SNR) sensors in harvest-then-transmit mode, especially when bandwidth constraints are introduced. This is because backscatter rate is less affected by low channel gains than the harvest-then-transmit rate, represented by (3.8) and (3.10). The best way to determine how many sensors to run in backscatter mode should be determined based on whether operating the selected number of sensor(s) in backscatter mode will increase the system sum-throughput.

To compound the challenge of designing the combination protocol, sensors operating in backscatter mode will temporarily store the energy harvested during the power splitting downlink data decoding phase in its capacitor. This is no different than in other time division protocols, except for use in the subsequent time block when operating in non-backscatter mode. The energy harvested and stored from a backscatter sensor in a previous time block will need to be accounted for when optimizing the sum-throughput when the sensor operates in the non-backscatter mode in the current time block. Therefore, the combination protocol in this chapter has a correspondingly totally different mathematical approach than current literature [21].

3.2.3. Energy Harvesting Model

Both distance-dependent path loss and small-scale fading are included in the channel propagation model. Path loss assumes the log-distance path loss model with path loss exponent φ,

and small-scale fading is modeled by Rayleigh fading. The channel power gain from the H-AP to sensor k, h_k, is calculated using the following formula [59]:

$$h_k = 10^{-\frac{(PL_{ref}+\psi_k)}{10}} \left(\frac{d_k}{d_{ref}}\right)^{-\varphi} \beta_k, k = 1 \dots K, d_k > d_{ref} \quad (3.1)$$

where PL_{ref} is the path loss in dB at the reference distance d_{ref}, ψ_k is the body shadowing loss margin between the H-AP and sensor k in dB, d_k is the distance between the H-AP and sensor k, and β_k is the small-scale fading power gain between the H-AP and sensor k. Based on the assumed Rayleigh small-scale fading, β_k is exponentially distributed with unity mean. For simplicity, the chapter assumes $\psi_1 = \cdots = \psi_K = \psi$. It is also assumed that channel reciprocity holds, so the uplink channel power gain between sensor k and the H-AP, g_k, is equal to h_k, i.e. $g_k = h_k, k = 1 \dots K$. Block fading is assumed, i.e., the fading channel power gain is assumed to remain constant for an entire time block T, but varies from block to block.

3.2.4. Energy Harvesting Model

The energy harvested during $\tau_{EH,DL}$ and $\tau_{EH,UL}$ for the downlink data decoding and uplink data transmission phases, respectively, of sensor k are denoted by $E_{DL,k}$ and $E_{UL,k}$, and calculated as follows [13]:

$$E_{DL,k} = \varsigma_k P_A h_k \tau_{EH,DL}, k = 1 \dots K, \quad (3.2)$$

$$E_{UL,k} = \varsigma_k P_A h_k \tau_{EH,UL}, k = 1 \dots K, \quad (3.3)$$

where ς_k is the EH efficiency at each sensor k, $0 < \varsigma_k < 1, k = 1 \dots K$, the chapter assumes $\varsigma_1 = \cdots = \varsigma_K = \varsigma$ for simplicity, and P_A is the transmit power of the H-AP. From (3.3), the average transmit power of sensor k for the uplink data transmission phase $P_{UL,k}$ is derived as follows:

$$P_{UL,k} = \frac{\eta_k E_{UL,k}}{\tau_{UL,k}}, k = 1 \dots K, \quad (3.4)$$

where η_k is the portion of harvested energy used for data transmission or decoding by each sensor k. Also, for simplicity, the chapter assumes $\eta_1 = \cdots = \eta_K = \eta$. The $1 - \eta$ portion is used for powering the sensor circuitry.

The calculation of the average power for the downlink data decoding phase is different than the uplink data transmission phase. While the received power at sensor k from the H-AP is simply $P_A h_k$ during the downlink data decoding phase τ_{DL}, the sensor circuitry still requires power to turn on and do data decoding. This means the sensors must harvest sufficient energy beforehand to power its circuitry to obtain the optimal downlink data rate.

Given η is the portion of harvested energy used for data decoding as aforementioned and $1 - \eta$ is the portion used for powering the sensor circuitry, this implies a relationship exists between the circuit power required for data decoding and the received power of the signal that contains data [60]. This relationship results in the following equality:

$$\eta_k P_A h_k \tau_{DL,k} = (1 - \eta_k) E_{DL,k}, k = 1 \dots K. \tag{3.5}$$

Substituting $E_{DL,k}$ in (3.2) into (3.5) and rearranging (3.5), the required energy harvesting time for the downlink phase $\tau_{EH,DL}$ to decode data during the τ_{DL} phase can be calculated as follows:

$$\tau_{EH,DL} = \left(\frac{\tau_{DL,k}}{\varsigma_k}\right)\left(\frac{\eta_k}{1 - \eta_k}\right), k = 1 \dots K. \tag{3.6}$$

Substituting (3.6) back into (3.2) will show the relationship between the energy harvested for the downlink data decoding phase and the downlink decoding phase length. Given that sensors will use all energy harvested during the $\tau_{EH,DL}$ phase from the power splitting receiver for data decoding in the same phase, this shows that $\tau_{DL,k}$ will be the same for all k, $k = 1 \dots K$ when $\varsigma_1 = \cdots = \varsigma_K = \varsigma$ and $\eta_1 = \cdots = \eta_k = \eta$.

3.2.5. Backscatter Communication Model

Backscatter communication relies purely on a continuous wave signal generated by the H-AP without storing the RF energy by intentionally mismatching each sensor's antenna input impedance to generate a re-modulated reflected signal for uplink data transmission. The variation of the antenna load impedance allows the sensor to encode digital symbols into the re-modulated reflected signal to transmit information.

To prevent destructive wireless interference at the H-AP, only one sensor can transmit at a time using backscatter during the τ_{EH} phase (i.e., each sensor operating in backscatter mode occupies one orthogonal sub-time slot during the τ_{EH} phase) of the combination protocol. Equal time allocation is given to all sensors operating in backscatter mode for fairness.

The received power at the H-AP from the sensor k operating in backscatter mode $P_{R,B,k}$ can be calculated as follows [20]:

$$P_{R,B,k} = P_A g_k h_k s^2 \left(\frac{\mathrm{r}_{d,k}}{2}\right)^2 \left(\frac{4}{\pi}\right)^2 \tag{3.7}$$

where s is a scaling term related to the sensor scattering efficiency and $\mathrm{r}_{d,k}$ is the difference between antenna reflection coefficients r_0 and r_1 calculated via antenna load impedance switching according to data bits '0' and '1', respectively at sensor $k, k = 1 \ldots K$. Mathematically, $\mathrm{r}_{d,k} = |r_0 - r_1|$.

From (3.7), the uplink rate in bits/second/Hz (bps/Hz) when sensor k is in backscatter mode can be calculated using the Shannon-Hartley theorem [20], [61]:

$$R_{UL,B,k}(\tau_{UL,B}, r_{d,k}) = \tau_{UL,B} \log_2\left(1 + \frac{P_{R,B,k}}{\Gamma\sigma^2}\right), \tag{3.8}$$

where $\tau_{UL,B} = \frac{\tau_{EH}}{k_B}$, k_B is the number of sensors currently operating in backscatter mode determined by Algorithm 1, Γ is the SNR gap from Shannon channel capacity due to use of a practical modulation and coding scheme, and σ^2 is the thermal noise power. A popular practical modulation and coding scheme for backscatter communication is EPCglobal Ultra High Frequency Class 1 Generation 2 [62].

3.3. Sum-Throughput Analysis and Optimization

3.3.1. Time-Switching Protocol with Downlink Data Decoding

In the time-switching protocol with downlink data decoding based on Fig. 3.2, the sum-throughput of both the downlink and uplink will need to be maximized. The downlink data rate in bps/Hz to sensor k is expressed as:

$$R_{DL,k}\left(\tau_{EH,DL}, \tau_{DL,k}\right) = \tau_{DL,k} \log_2\left(1 + \frac{P_A h_k}{\Gamma\sigma^2}\right), \tag{3.9}$$

$R_{DL,k}(\tau_{EH,DL}, \tau_{DL,k})$ is the rate of the sensor k calculated using the Shannon-Hartley theorem [61]. The uplink data rate in bits/second/Hz (bps/Hz) of sensor k is expressed as:

$$\begin{aligned} R_{UL,k}(\tau_{EH,UL}\tau_{UL,k}) &= \tau_{UL,k} \log_2\left(1 + \frac{g_k P_{UL,k}}{\Gamma\sigma^2}\right) \\ &= \tau_{UL,k} \log_2\left(1 + \gamma_{UL,k}\frac{\tau_{EH,UL}}{\tau_{UL,k}}\right), k = 1 \dots K, \end{aligned} \tag{3.10}$$

where the second equality follows from substituting for $P_{UL,k}$ using (3.4) and (3.3), and $\gamma_{UL,k}$ is the received signal to noise ratio at the H-AP due to transmission by sensor k, given by $\gamma_{UL,k} = \frac{\varsigma_k \eta_k g_k P_A h_k}{\Gamma\sigma^2}, k = 1 \dots K$.

To maximize the sum-throughput of the time switching protocol, the following optimization problem is proposed and needs to be solved:

$$(P3.1): \quad \max_{\tau} R_{sum}(\tau), \tag{3.11a}$$

$$s.t. \quad \tau_{EH,DL} + \tau_{EH,UL} + \tau_{DL} + \tau_{UL} \leq 1, \tag{3.11b}$$

$$\tau_{EH,DL}, \tau_{EH,UL}, \tau_{DL,k}, \tau_{UL,k} \geq 0, k = 1 \dots K, \tag{3.11c}$$

$$R_{UL,k}(\tau) \geq 2R_{DL,k}(\tau), k = 1 \dots K, \tag{3.11d}$$

where $\tau = \left[\tau_{EH,DL}\ \tau_{EH,UL}\ \tau_{DL,1} \cdots \tau_{DL,K}\ \tau_{UL,1} \cdots \tau_{UL,K}\right]$, $\tau_{DL} = \sum_{k=1}^{K} \tau_{DL,k}$, $\tau_{UL} = \sum_{k=1}^{K} \tau_{UL,k}$, and $R_{sum}(\tau) = R_{DL,sum}(u) + R_{UL,sum}(v)$ where $u = \left[\tau_{EH,DL}\ \tau_{DL,1} \cdots \tau_{DL,K}\right]$, $v = \left[\tau_{EH,UL}\ \tau_{UL,1} \cdots \tau_{UL,K}\right]$, $R_{DL,sum}(u) = \sum_{k=1}^{K} R_{DL,k}(\tau_{DL,k})$, and $R_{UL,sum}(v) = \sum_{k=1}^{K} R_{UL,k}(\tau_{UL,k})$. Eqn. (3.11a) is the objective function, (3.11b) is the time scheduling constraint, (3.11c) is the non-negativity constraint for the decision variables, and (3.11d) is the bandwidth allocation constraint where the uplink sum-throughput is assumed to be at least twice as fast as the downlink data rate [63]. Eqn. (3.11d) can be modified if there are different uplink/downlink bandwidth requirements. For (*P*3.1), the objective function specified by (3.11a) is concave and its corresponding constraints are affine. Hence, (*P*3.1) is convex.

Problem (*P*3.1) can be simplified by breaking it down into two separate sub-problems and solving them individually in (*P*3.2) and (*P*3.3) as follows:

$$(P3.2): \quad \max_{u} R_{DL,sum}(u), \tag{3.12a}$$

$$s.t. \quad \tau_{EH,DL} + \tau_{DL} \leq 1, \tag{3.12b}$$

$$\tau_{EH,DL}, \tau_{DL,k} \geq 0, k = 1 \dots K. \tag{3.12c}$$

$$(P3.3): \quad \max_{v} R_{UL,sum}(v), \tag{3.13a}$$

$$s.t. \quad \tau_{EH,UL} + \tau_{UL} \leq 1, \tag{3.13b}$$

$$\tau_{EH,UL}, \tau_{UL,k} \geq 0, k = 1 \dots K, \tag{3.13c}$$

For both (P3.2) and (P3.3), the objective functions specified by (3.12a) and (3.13a) are each concave and their corresponding constraints are affine. Hence, both (P3.2) and (P3.3) are convex and can be solved using standard convex optimization techniques. Due to the constraints in (3.12b) and (3.13b) for (P3.2) and (P3.3), respectively, both will provide a solution in normalized time (i.e., $T = 1$). Note that this is an intermediate solution because adding the solutions of (P3.2) and (P3.3) together will result in a solution double the normalized time (i.e., $T = 2$), which does not satisfy the requirements for the constraint in (3.11b) in problem (P3.1). The solutions to (P3.2) and (P3.3) in normalized time allow flexibility in case there is a change in uplink/downlink bandwidth requirement, which will be discussed shortly.

To satisfy the requirement of the constraint in (3.11b) using the solutions to (P3.2) and (P3.3), two WPCN properties are exploited, described in Proposition 1 and Proposition 2.

Proposition 1: There is a direct proportionality between the sum-throughput of the uplink or downlink data decoding phase and optimum timings.

Proof: See Appendix A.

The first property is important because if optimum timing values can be multiplied by any positive real number α and result in a directly proportional change in data rate, then the optimal solution in normalized time is still an optimal solution in non-normalized time.

Proposition 2: There exists a constant optimal ratio of harvested energy to downlink or uplink data sum-throughput.

Proof: See Appendix B.

The second property is also important, since harvested energy is directly proportional to the optimum timings from (3.2) and (3.3). The optimum timings are directly proportional to the sum-throughput. Therefore, the solutions to (P3.2) and (P3.3) are actually the normalized optimal

ratios between the harvested energy and the downlink or uplink data transmission rate, and will remain constant regardless of the value of T. As it was in the first property, the optimal solution in normalized time is still the optimal solution in non-normalized time.

Based on Proposition 1 and Proposition 2, the constraint in (3.11b) can be satisfied by multiplying every $\tau_{EH,DL}, \tau_{DL,k}$ by a downlink bandwidth ratio BR_{DL} and $\tau_{EH,UL}, \tau_{UL,k}$ by an uplink bandwidth ratio BR_{UL}. BR_{DL} can be calculated by:

$$BR_{DL} = BB_{DL} \frac{R_{DL,sum}(u) + R_{UL,sum}(v)}{2R_{DL,sum}(u)}, \tag{3.14}$$

where BB_{DL} is the downlink bandwidth bias. Bandwidth bias is a parameter used to control the downlink and uplink bandwidth. Similarly, BR_{UL} can be calculated by:

$$BR_{UL} = BB_{UL} \frac{R_{DL,sum}(u) + R_{UL,sum}(v)}{2R_{UL,sum}(v)}. \tag{3.15}$$

where BB_{UL} is the uplink bandwidth bias. Eqns. (3.14) and (3.15) equalize the rate by increasing the slower rate and decreasing the faster rate to the average of the two rates when $BB_{DL} = BB_{UL} = 1$. As (3.11d) specified the uplink data rate to be at least twice as fast as the downlink data rate [63], setting $BB_{DL} = 2$ and $BB_{UL} = 1$ will satisfy (3.11d).

Multiplying all the u and v values obtained from solving problems (*P*3.2) and (*P*3.3) individually by their corresponding bandwidth ratios will not satisfy $\tau_{EH,DL} + \tau_{EH,UL} + \tau_{DL} + \tau_{UL} = T$. This can be resolved by multiplying all u and v values by a time ratio Z after multiplying them by their corresponding bandwidth ratios. Z can be calculated as follows:

$$\mathrm{Z} = \frac{T}{BR_{DL}(\tau_{EH,DL} + \tau_{DL}) + BR_{UL}(\tau_{EH,UL} + \tau_{UL})}. \tag{3.16}$$

In short, the optimal $\tau^* = \left[\tau^*_{EH,DL}\ \tau^*_{EH,UL}\ \tau^*_{DL,1} \cdots \tau^*_{DL,K}\ \tau^*_{UL,1} \cdots \tau^*_{UL,K}\right]$ values to satisfy problem (*P*3.1) using the values obtained from problems (*P*3.2) and (*P*3.3) can be calculated using the following equations:

$$\tau^*_{EH,DL} = \tau_{EH,DL} BR_{DL} \mathrm{Z}, \tag{3.17}$$

$$\tau^*_{EH,UL} = \tau_{EH,UL} BR_{UL} \mathrm{Z}, \tag{3.18}$$

$$\tau^*_{DL,k} = \tau_{DL,k} BR_{DL} \mathrm{Z}, k = 1 \dots K, \tag{3.19}$$

$$\tau^*_{UL,k} = \tau_{UL,k} BR_{UL} \mathrm{Z}, k = 1 \dots K, \tag{3.20}$$

where the solutions to problems (*P*3.2) and (P*3*.3) appear on the right-hand side of (3.17) to (3.20). The calculated optimal τ^* values result in the optimal sum-throughput solution for a WPCN operating with the time-switching protocol with downlink data decoding (*P*3.1).

3.3.2. Hybrid Time-Switching/Power Splitting Protocol

The hybrid protocol is like the time-switching protocol in the previous Section 3.3.1, except the energy received from the H-AP for the downlink data decoding phase is split by a ratio λ, the portion of the received energy from the data signal harvested for powering the sensor, and the balance $(1 - \lambda)$ is expended on downlink data decoding. Power splitting during the downlink data decoding phase of length τ_{DL} does not necessarily eliminate the energy harvesting phase of duration $\tau_{EH} = \tau_{EH,DL} + \tau_{EH,UL}$, because the energy harvested from power splitting during τ_{DL} may not be sufficient to power the sensors. However, it will reduce the length of τ_{EH} because, instead of harvesting all the required energy for each sensor to use in time block T during τ_{EH}, some of it is harvested during τ_{DL}. Therefore, the aggregate harvested energy by sensor k now becomes:

$$E_{DL,k} = \varsigma_k P_A h_k \left(\tau_{EH,DL} + \lambda \tau_{DL}\right), k = 1 \dots K. \tag{3.21}$$

From (3.6) and (3.21) and given the fact that the portion $(1-\lambda)$ of the received energy is used for regular data decoding, the required energy harvesting time for the downlink phase to decode data becomes:

$$\tau_{EH,DL} = \left(\frac{\tau_{DL,k}\,(1-\lambda)}{\varsigma_k}\right)\left(\frac{\eta_k}{1-\eta_k}\right) - \lambda\tau_{DL}, k = 1 \dots K. \tag{3.22}$$

Although it is logical to think that $\tau_{EH,DL}$ must be greater than or equal to zero since negative downlink energy harvesting time is physically unrealizable, negative $\tau_{EH,DL}$ does not necessarily imply negative total energy harvesting time τ_{EH}. The constraint $\tau_{EH} \geq 0$ must hold. Negative $\tau_{EH,DL}$ simply means the energy from power splitting downlink data decoding phase is more than required for optimal downlink data decoding. This excess energy can be used during the uplink data transmission phase later. Including the constraint $\tau_{EH} \geq 0$ along with the power splitting ratio λ in problem (P3.2) creates the convex optimization problem (P3.4):

$$(P3.4): \qquad \max_{u,\lambda} R_{DL,sum}\,(u,\lambda), \tag{3.23a}$$

$$s.t. \qquad \tau_{EH,DL} + \tau_{DL} \leq 1, \tag{3.23b}$$

$$\tau_{DL,k} \geq 0, k = 1, \dots K, \tag{3.23c}$$

$$\tau_{EH,DL} + \tau_{EH,UL} \geq 0, \tag{3.23d}$$

$$0 < \lambda < 1. \tag{3.23e}$$

The objective function $R_{DL,sum}(u,\lambda)$ is defined as $\sum_{k=1}^{K} R_{DL,k}(\tau_{EH,DL}, \tau_{DL,k}, \lambda)$, where $R_{DL,k}(\tau_{EH,DL}, \tau_{DL,k}, \lambda)$ is a modification of (3.9) to account for the portion $(1-\lambda)$ of the received energy used for regular data decoding and given by:

$$R_{DL,k}\big(\tau_{EH,DL}, \tau_{DL,k}, \lambda\big) = \tau_{DL,k}\log_2\left(1 + \frac{P_A h_k (1-\lambda)}{\Gamma\sigma^2}\right). \tag{3.24}$$

Recall $u = [\tau_{EH,DL}\ \tau_{DL,1} \cdots \tau_{DL,K}]$. Now, (3.21) and (3.22) and problem (*P*3.4) in the hybrid protocol will replace (3.2) and (3.6) and problem (*P*3.2), respectively, in the time-switching protocol. Problem (*P*3.3) remains the same. Therefore, for the hybrid protocol, problem (*P*3.1) will be solved by breaking it down into problems (*P*3.3) and (*P*3.4) and solving the two separately. The proof of concavity for problem (*P*3.4) can be found in Appendix C.

Similar to the time-switching protocol, the constraint in (3.11b) has not been satisfied after solving (*P*3.4) and (*P*3.3). This can be fixed by calculating the bandwidth ratios BR_{DL} using (3.14) and BR_{UL} via (3.15) for the hybrid protocol, and multiplying the value of each element in u by its corresponding time ratio using (3.16) with the reduced $\tau_{EH,DL}$ value calculated using (3.22). Therefore, problem (*P*3.1) applies to the hybrid protocol as it did with the time-switching protocol. The optimal τ^* values to satisfy problem (*P*3.1) using the solutions from problems (*P*3.4) and (*P*3.3) can be calculated using (3.17) to (3.20).

3.3.3. Combination Time-Switching/Power Splitting/Backscatter Protocol

The combination protocol integrates backscatter communication into the hybrid time-switching/power splitting protocol. In the combination protocol, any sensor operating in backscatter mode in a previous time block *prev* will have unused harvested energy from the power splitting during the downlink data decoding phase temporarily stored in the sensor's capacitor. This temporarily stored harvested energy will affect the received SNR at the H-AP in the current time block when the sensor is operating in non-backscatter mode. The uplink data transmission rate for sensor k in non-backscatter mode then becomes:

$$R_{UL,k}(\tau_{EH,UL}, \tau_{UL,k}) = \tau_{UL,k} \log_2 \left(1 + \frac{\varsigma_k \eta_k P_A g_k \left(h_k \tau_{EH,UL} + h_{k,prev} \lambda_{prev} \tau_{DL,prev}\right)}{\Gamma \sigma^2 \tau_{UL,k}}\right), \quad k = 1 \ldots K, \tag{3.25}$$

where $h_{k,prev}$, λ_{prev}, and $\tau_{DL,prev}$ are the channel power fading gain, power splitting ratio, and duration of downlink data decoding phase in the previous time block, respectively. Notice that (3.25) does not include the rate achieved by sensor k when operating in backscatter mode; this was calculated previously by (3.8).

Now, accounting for backscatter communication as part of the uplink sum-throughput, problem (P3.3) then becomes:

$$(P3.5): \quad \max_{v, r_{d,k}} R_{UL,sum}\left(v, r_{d,k}\right), \tag{3.26a}$$

$$s.t. \quad \tau_{EH,UL} + \tau_{UL} \leq 1, \tag{3.26b}$$

$$\tau_{EH,UL}, \tau_{UL,k} \geq 0, k = 1 \dots K, \tag{3.26c}$$

$$\tau_{UL,B} \geq 0, k = 1 \dots K, \tag{3.26d}$$

$$0 < r_{d,k} < 1. \tag{3.26e}$$

Recall $v = \left[\tau_{EH,UL}\ \tau_{UL,1} \cdots \tau_{UL,K}\right]$. The objective function $R_{UL,sum}\left(v, r_{d,k}\right)$ in (3.26a) is the aggregate uplink rate in the network under both backscatter and non-backscatter modes. Therefore, $R_{UL,sum}\left(v, r_{d,k}\right) = \sum_{k=1}^{K} R_{UL,k}(\tau_{EH,UL}, \tau_{UL,k}) + \sum_{k=1}^{K} R_{UL,B,k}(\tau_{UL,B}, r_{d,k})$. The constraints in (3.26b) and (3.26c) are identical to those in (3.13b) and (3.13c), respectively, since problem (P3.5) is an enhancement of (P3.3). Constraint (3.26d) specifies the non-negativity of the time a sensor operates in backscatter mode. Eqn. (3.26e) is the constraint on $r_{d,k}$, the difference between antenna reflection coefficients r_0 and r_1. Following the same explanation for the convexity of problem (P3.3), problem (P3.5) is also convex.

Next, problem (P3.1) is solved under the combination protocol such that problem (P3.1) is decomposed into problems (P3.4) and (P3.5). The optimal τ^* values to satisfy problem (P3.1) based on the solutions to problems (P3.4) and (P3.5) can be calculated via (3.17) to (3.20).

However, a solution to determine which and the number of sensors to run in backscatter mode, k_B such that the sum-throughput of the system is maximized remains to be determined. In other words, sensor(s) operating in backscatter mode with their rate calculated by (3.8) and sensor(s) operating in non-backscatter mode with their rate calculated by (3.25), which satisfy problem (*P*3.5), have yet to be determined. Analytical determination of k_B is non-trivial, hence we resort to a heuristic described in Algorithm 3.1, outlined as follows:

Algorithm 3.1 Sensor Operation Mode Algorithm

1. **Input:** K, P_A, BB_{DL}, BB_{UL}
2. **Output:** $\tau^*, R_{sum}(\tau^*)$
3. Solve problem (*P*3.4) to get the optimal $\tau_{DL,k}$ and λ values in normalized time for each sensor $k, k = 1 \dots K$.
4. Calculate $R_{DL,k}(\tau_{EH,DL}, \tau_{DL,k})$ in normalized time for all sensors, $k = 1 \dots K$ using (3.24).
5. Calculate the reduced optimum $\tau_{EH,DL}$ in normalized time using (3.22).
6. Solve problem (*P*3.5) to get the optimal $\tau_{UL,k}$ and $r_{d,k}$ values in normalized time for each sensor $k, k = 1 \dots K$ currently not operating in backscatter mode. (If this is the first run, no sensors are currently operating in backscatter mode.)
7. Calculate $R_{UL,k}(\tau_{EH,UL}, \tau_{UL,k})$ in normalized time for all sensors k currently not selected to be operating in backscatter mode with (3.25). (If this is the first run, no sensors are currently operating in backscatter mode.)
8. Calculate the bandwidth ratios BR_{DL}, BR_{UL} using (3.14) and (3.15), respectively.
9. Calculate the time ratio Z using (3.16).

10. Calculate all τ^* values using (3.17) to (3.20) to obtain $R_{sum}(\tau)$.

11. If there are two or more sensors remaining not currently selected for operating in backscatter mode:

Select the sensor with the lowest SNR to operate in backscatter mode.

Else

Go to Line 15.

Endif

12. Repeat Steps 3 to 10 with the backscatter sensor(s) removed from the uplink data transmission phase.

13. Calculate the rate $R_{UL,B,k}(\tau^*_{UL,B}, r^*_{d,k})$ for the kth sensor(s) operating in backscatter mode using (3.8).

14. Calculate $R_{sum}(\tau^*)$ and check if it increased.

If $R_{sum}(\tau^*)$ did NOT increase:

Change the last sensor that entered backscatter mode back to non-backscatter mode and go to Line 15. The τ^* values are the τ^* values before the last sensor entered backscatter mode.

Else If $R_{sum}(\tau^*)$ increased

Add the next lowest SNR sensor into backscatter mode and go to Line 11.

Endif

15. End

Algorithm 3.1 starts off by selecting the input parameters of number of sensors in the system K, transmit power of the H-AP P_A, and downlink and uplink bandwidth bias BB_{DL}, BB_{UL}.

Lines 3 to 10 implement the hybrid protocol. Lines 11 to 13 consider the sensors one at a time, starting from the one with the lowest SNR, to operate in backscatter mode. The algorithm will keep at least one sensor in non-backscatter mode to ensure the τ_{EH} phase will not reduce to zero. Line 14 checks if there is any improvement in the sum rate compared to the previous sensors operation mode configuration. When the sum rate of the WPCN begins to decrease, it means adding more sensors to backscatter mode will not further increase the sum-throughput of the WPCN and the global optimum solution has already been found. The algorithm will stop checking and revert to the previously calculated τ^* values for the global optimum solution.

The hybrid access point runs Algorithm 3.1 in the beginning of each iteration of length T. The physical length of each iteration is arbitrary in nature, but in practice, it should be short enough such that the channel condition is static within the length of each iteration. For simplicity, we assume $T = 1$ second. The complexity of the algorithm is $O(K)$, since Lines 3, 4, 6, 7, 13, and 14 add one additional calculation for each additional sensor. The figure of merit of Algorithm 3.1 is the sum-throughput of the WPCN using the combination protocol and will be measured against the time-switching and hybrid protocols, which will be shown in the simulation results in Section 3.4.

3.4. Simulation Results and Discussion

3.4.1. System Configuration

Unless stated otherwise, a user is assumed to be equipped with $K = 3$ sensors located at $d_1 = \cdots = d_K = d = 2$ meters away from the hybrid access point. The channel power gain values for sensor k, h_k, are generated using (3.1) to reflect factors such as movement of other objects/people around the user of interest. The rest of the assumed system parameter values are summarized in Table 3.1.

Table 3.1. Assumed System Parameter Values

Parameter	Definition	Value
PL_{ref}	Path loss at reference distance of 1m and transmitter frequency of 900MHz	30dB
ψ	Body shadowing loss margin	15dB [64]
φ	Path loss exponent	3.8 [65]
ς	EH efficiency at each sensor	0.5 [54]
η	Portion of harvested energy used for information transmission by each sensor	0.5 [60]
P_A	Hybrid access point transmission power	10mW [66] or 4000mW [56], [57]
Γ	SNR gap	1.5dB [67]
σ^2	Background noise power in 1MHz channels	-114dBm [66]
s	Tag scattering efficiency scaling	-1.1dB [20]
BB_{DL}	Downlink bandwidth bias	2 [63]
BB_{UL}	Uplink bandwidth bias	1 [63]

3.4.2. Results and Discussion

The three proposed time division based protocol were implemented and tested in a Monte Carlo simulator using MATLAB with the system parameter values listed in Table 3.1, unless otherwise stated. New h_k values are generated at the beginning of each time block T of 1 second to simulate ongoing changes in channel quality in a dynamic environment. A time block denotes one run (or iteration) of a simulation. The length of a simulation is set to 1000 runs per system

configuration (one system configuration is a specific combination of test parameters). Generally, results enter steady-state condition after 100 runs. The 1000 runs therefore represent a large sample set to assure the system is operating under steady-state condition while the simulation can be completed within a reasonable amount of time.

The time-switching protocol results in this section are not directly comparable to the ones found in literature [13] due to the use of more realistic simulation parameters in a dynamic environment [14]. The addition of a downlink data decoding phase that was not found in previous works [21], [13], [14] make the results in this chapter not directly comparable to those papers as well. Hence, the time-switching protocol will be used as a reference baseline in this chapter, because its *design* is comparable to strict time-division, harvest-then-transmit protocols currently used in literature.

First, a WPCN with $P_A = 10$mW was simulated in a dynamic environment, typical for a Bluetooth transmitter inside a cell phone [66]. The same test was run again with $P_A = 4000$mW, the maximum allowed in the unlicensed wireless spectrum [56], [57]. For an H-AP with 10mW transmission power, the average sum-throughput (averaged over the 1000 runs) in a dynamic environment for a time-switching, hybrid, and combination protocol is 2.3 bps/Hz, 2.4 bps/Hz, and 2.6 bps/Hz, respectively, as shown in Fig. 3.5. Assuming a channel width of 1MHz as in Bluetooth [66], the average sum-throughput for these respective protocols will be 2.3 Mbps, 2.4 Mbps, and 2.6 Mbps. Since data rate requirements for on-body sensors do not generally exceed 1 Mbps [68], channel width can be reduced when the H-AP transmission power is high while still meeting the necessary data rate requirements to increase spectrum efficiency. For example, a high resolution 12-bit, fast polling 10Hz 9-axis accelerometer sensor generates data at only approximately 1kbps (12 bits * 10/second * 9 axis = 1080bps). Clearly, the above average sum-throughput of the WPCN

exceeds the required data rate for transmitting the necessary data with acceptable quality in a body area network application.

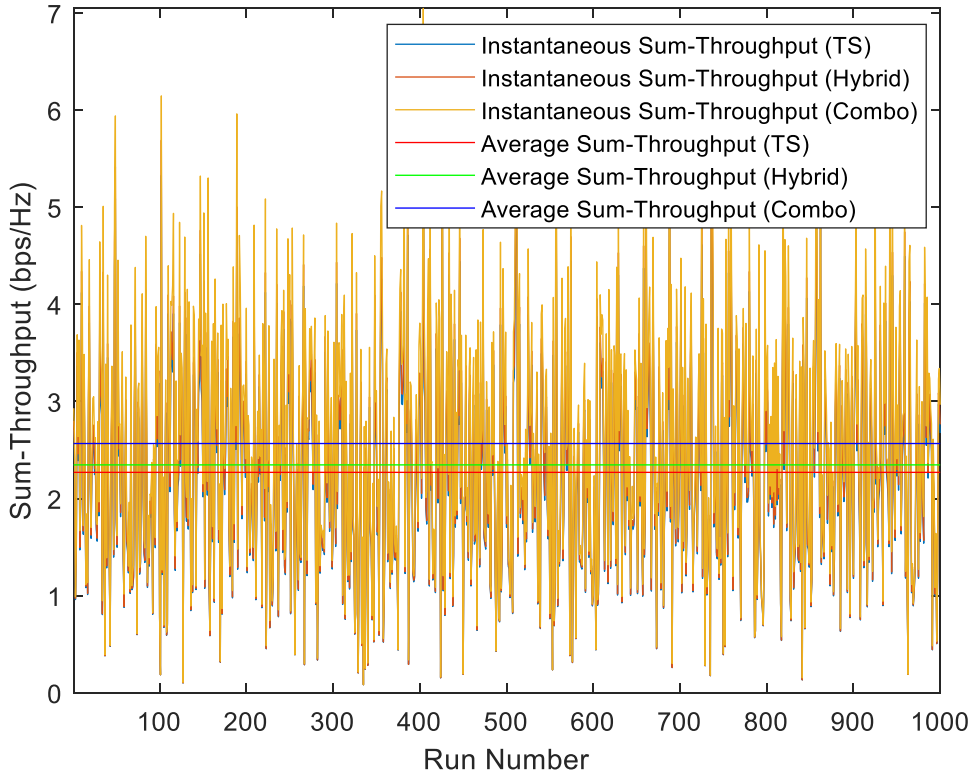

Fig. 3.5. System throughout versus run number, $P_A = 10$mW. The abbreviations in the legend are defined as follows: TS = Time-switching protocol with downlink data decoding, Hybrid = hybrid protocol, and Combo = combination protocol.

For an H-AP with 4000mW transmission power, the average sum-throughput in a dynamic environment for a time-switching, hybrid, and combination protocol is 9.4 bps/Hz, 10.4 bps/Hz, and 12.1 bps/Hz, respectively, as presented in Fig. 3.6. The hybrid and combination protocols had a 2.1% and 12.6% improvement in sum-throughput over that of the time-switching protocol, respectively, for a 10mW H-AP in Fig. 5. When a 4000mW H-AP is used (Fig. 3.6), the corresponding improvements jump to 9.9% and 27.6%. As expected, the 4000mW H-AP exhibits a higher improvement over that achieved by the 10mW H-AP. For either the 10mW or 4000mW

H-AP, it is seen that backscatter communication implemented in the combination protocol is beneficial, providing a higher average sum-throughput over that of the hybrid protocol. Similarly, the backscatter communication improvement achieved with the 4000mW H-AP is higher than that of the 10mW H-AP. For the same channel condition, higher transmit power by the H-AP implies higher received power at the sensor and hence a higher reflected power for backscatter communication, resulting in the higher backscatter rate.

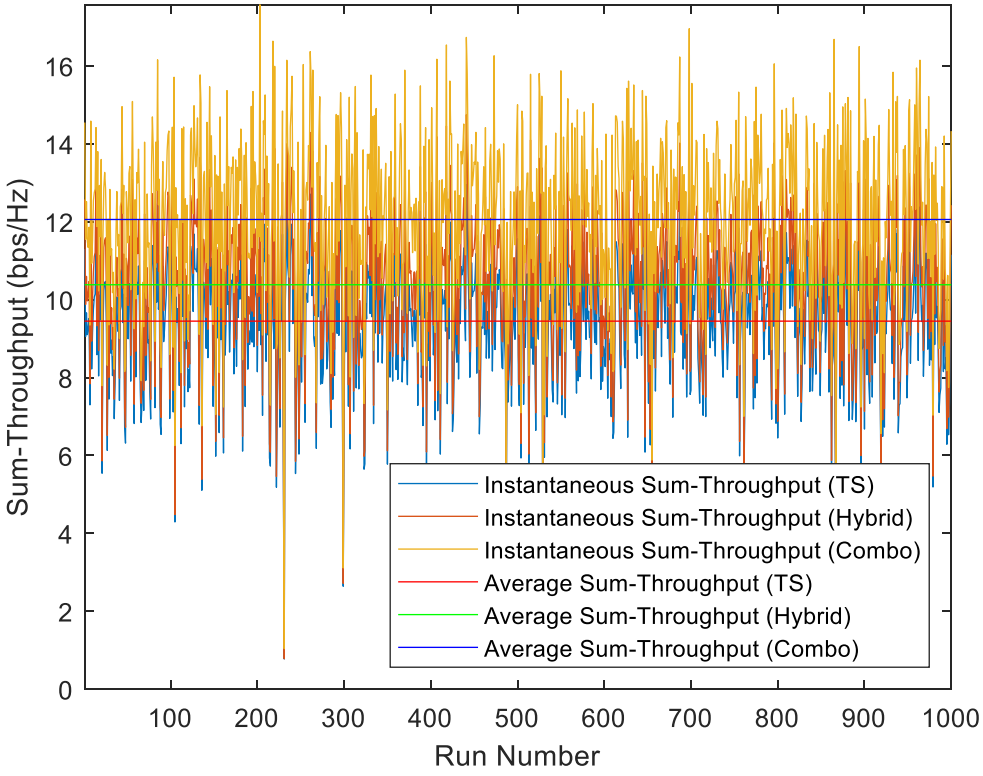

Fig. 3.6. System throughout versus run number, $P_A = 4000$mW.

For the proposed time-switching, hybrid, and combination protocols, the average sum-throughout is limited by the time allocations to the protocol operational phases in each time block and, therefore, the available harvested energy in the system. For example, in the hybrid protocol when the power received during the downlink data decoding phase is split, the SNR of the received

power used for data decoding decreases, which decreases the downlink data decoding rate. Decreasing the downlink data decoding rate implies the circuit has less power to decode the data received from the H-AP, which changes the downlink energy harvesting time, bandwidth ratio, and time ratio values. Although the hybrid protocol increases the amount of energy harvested in relation to available time by splitting the power received during the downlink data decoding phase, it still leaves the energy harvesting phase τ_{EH} unused for data decoding or transmission. By enabling backscatter communication during the energy harvesting phase, the combination protocol enables data decoding or transmission to occur during every phase of the WPCN, which resulted in a considerable increase in the average sum-throughput.

Next, the three protocols are investigated with regards to the scaling of H-AP transmission power from 10mW to 4000mW. Each data point in Fig. 3.7 represents the average of 1000 runs in the simulator. It is observed from Fig. 3.7 that, as the transmit power increases, both the hybrid and combination protocols consistently delivered better sum-throughput compared to the time-switching protocol. This is due to an increase in energy harvested with relation to available time for both the hybrid and combination protocols, and utilizing a previously unused uplink data transmission phase with the combination protocol. It should be noted that the performance of the combination protocol is always at least as good as the hybrid protocol, because Algorithm 1 will automatically revert to the hybrid protocol if it is not advantageous to utilize any sensors in backscatter mode. The results presented in Fig. 3.7 are significant because they enable the WPCN designer or operator to set the power level of the H-AP to achieve a given sum-throughput requirement.

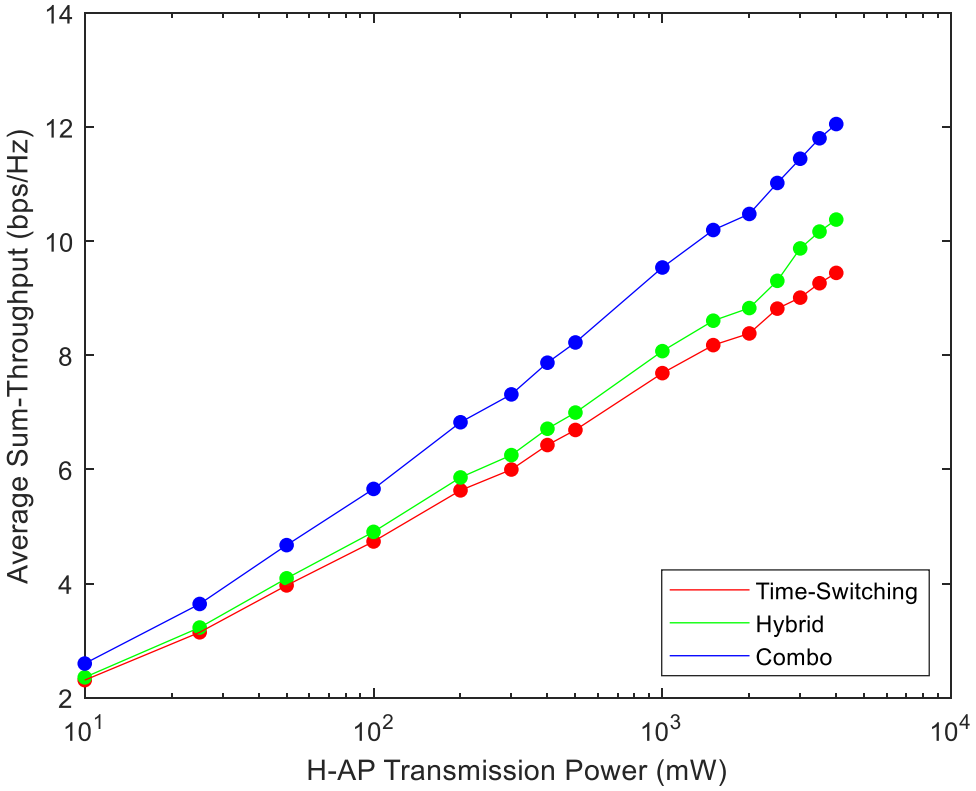

Fig. 3.7. Average sum-throughput versus H-AP transmission power. The lines interconnecting the data points are polynomial lines of best fit.

The sensitivity of the average sum-throughput to the distance between the H-AP and the sensors is presented in Figs. 3.8 and 3.9, where the distance is varied from 1.5m to 3.0m (Fig. 3.8) and from 1.5m to 6.0m (Fig. 3.9). In both Figs. 3.8 and 3.9, the average sum-throughput decreases as the separation distance increases due to a decrease in average received power. It is interesting to note that the average sum-throughput achieved by the three protocols begins to converge to the same value as the distance increases. When the distance increases, the path loss becomes the dominating factor resulting in less received power and the peculiarities of the different protocols are immaterial on the average sum-throughput.

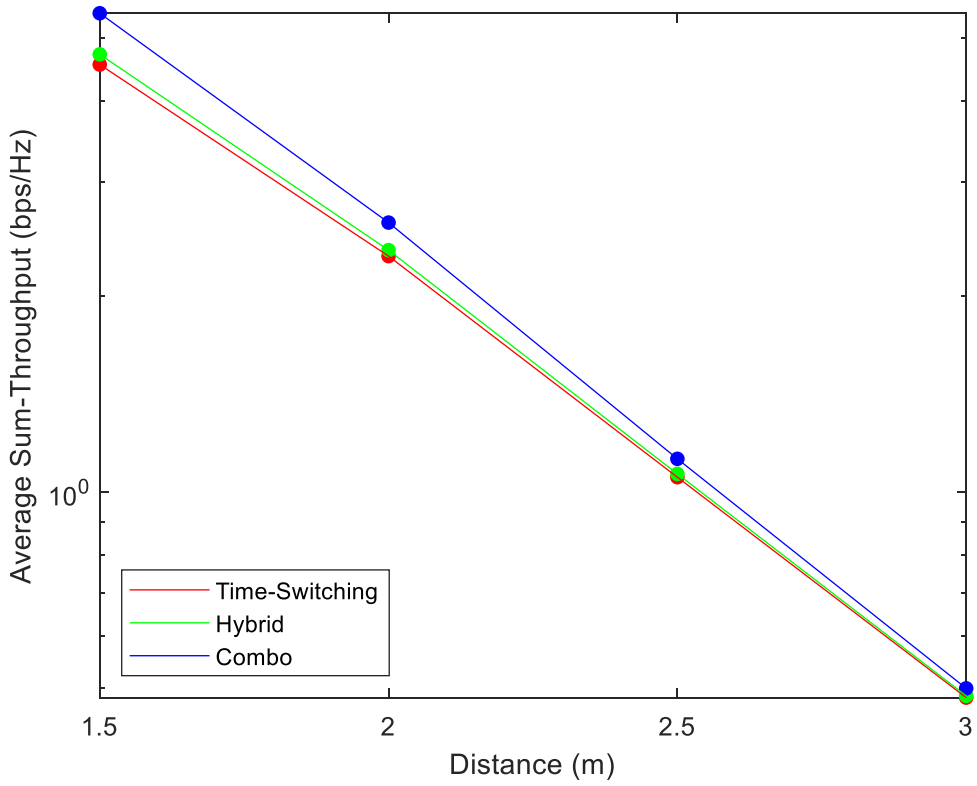

Fig. 3.8. Average sum-throughput versus distance between the H-AP and the sensors, $P_A = 10$mW.

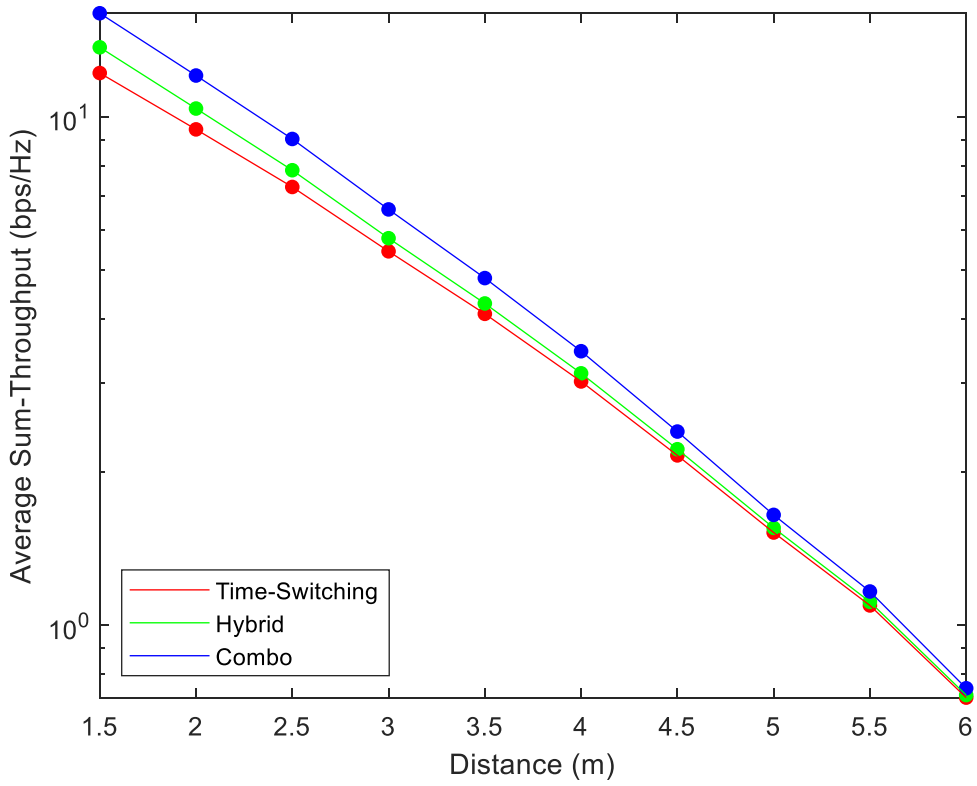

Fig. 3.9. Average sum-throughput versus distance between the H-AP and the sensors, $P_A = 4000$mW.

Lastly, the impact of the number of sensors on the average sum-throughput of all three protocols was evaluated. The results are shown in Figs. 3.10 and 3.11 for the 10mW and 4000mW H-APs, respectively, where it is seen that a high number of sensors lead to higher average sum-throughput for all three protocols.

Increasing the number of sensors increases the throughput of the WPCN because when more sensors are all actively communicating during the same time block T, the average amount of time each sensor is allocated for energy harvesting and/or data transmission reduces. When the allocated time for each sensor becomes tight, efficient time allocation in the combination protocol, where an entire phase previously not used for data communication by the hybrid protocol, becomes critical. This time allocation method resulted in a considerable performance increase attained by

the combination protocol over the time-switching and hybrid protocols, as shown in Figs. 3.10 and 3.11. It is also observed from Figs. 3.10 and 3.11 that the gain of the sum-throughput of the hybrid protocol over the time-switching protocol is not that significant as the number of sensors increases. An explanation for this behavior is the limited amount of harvested energy due to low received power. The gap between the hybrid and time-switching sum-throughput performance is larger for the 4000mW H-AP (Fig. 3.11) compared to the 10mW H-AP (Fig. 3.10) due to higher received power associated with the former case.

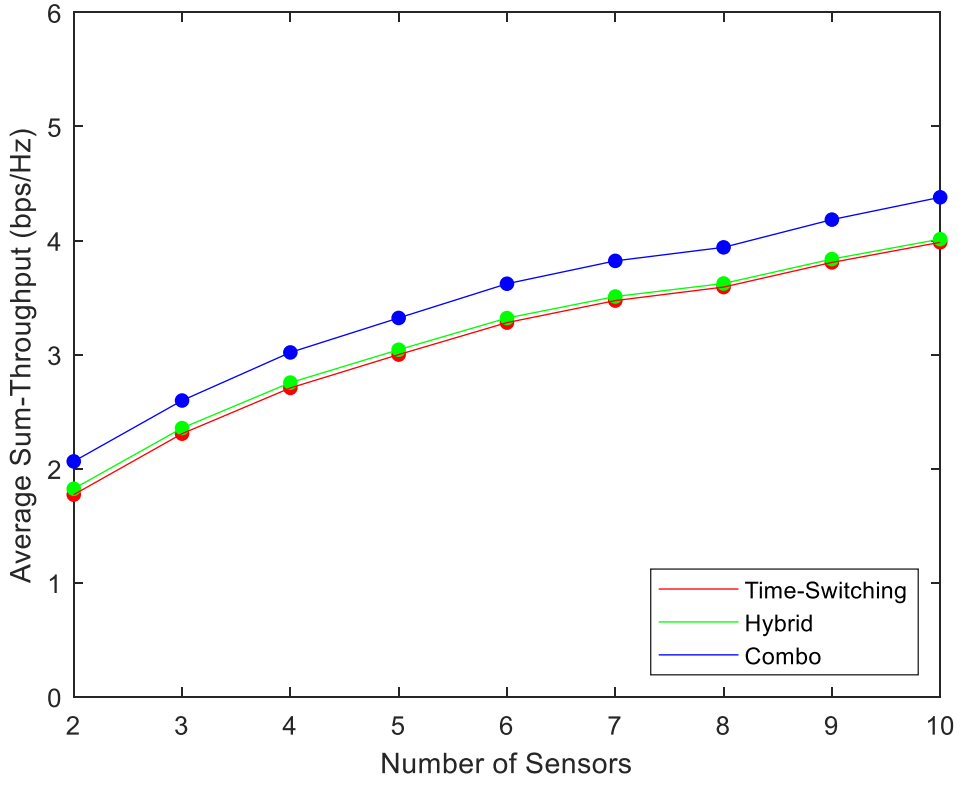

Fig. 3.10. Average sum-throughput versus number of sensors, $P_A = 10$mW.

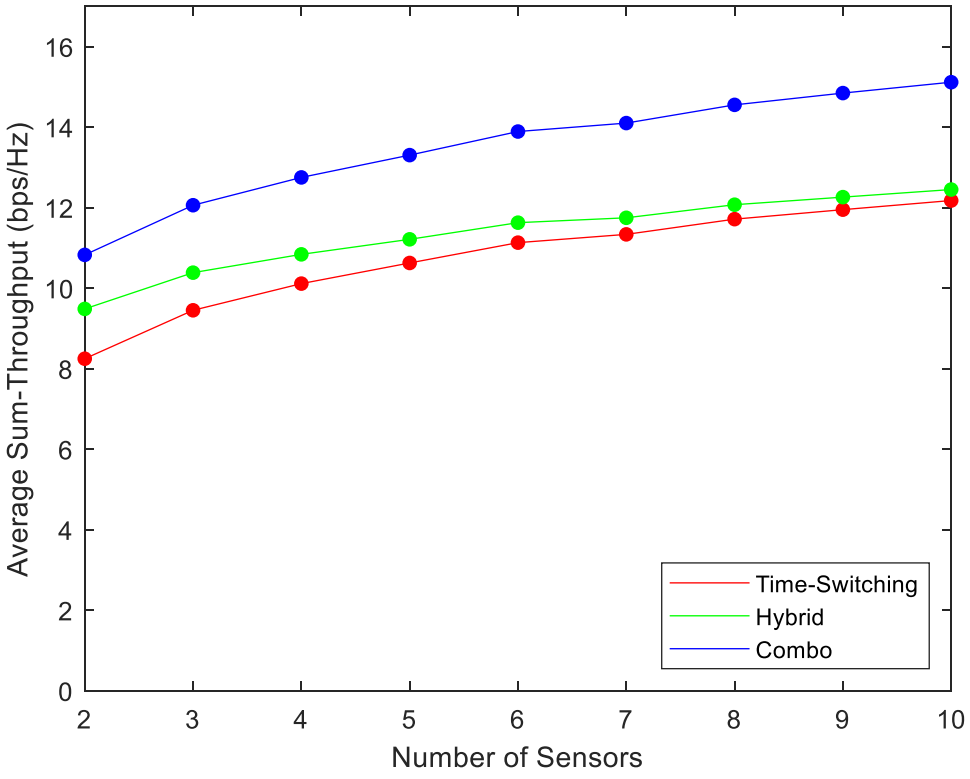

Fig. 3.11. Average sum-throughput versus number of sensors, $P_A = 4000$mW.

From the results shown in Figs. 3.5 to 3.11, the hybrid and combination protocols always outperformed the reference time-switching protocol with a maximum sum-throughput increase of 15.0% and 31.3%, respectively. The combination protocol always exceeded the performance of the hybrid protocol as well, with a maximum sum-throughput increase of 21.4%.

3.5. Summary

This chapter presented a solution for maximizing the sum-throughput of a two-way communication WPCN by optimizing the system timings for energy harvesting, downlink data decoding, and uplink data transmission using the time-switching, hybrid, and combination protocols. The combination protocol delivered the highest sum-throughput of the three, but at the expense of increased sensor hardware design complexity and higher computational power

requirements at the H-AP. The hybrid protocol holds the middle ground in sum-throughput, sensor hardware design complexity, and H-AP computational power requirements. The time-switching protocol with downlink data decoding is the simplest of the three protocols in sensor hardware design and has the lowest H-AP computational power requirements, but also has the lowest sum-throughput in relative to the other two protocols.

CHAPTER 4: SUM-THROUGHPUT AND FAIRNESS OPTIMIZATION OF A WIRELESS ENERGY HARVESTING SENSOR NETWORK WITH BACKSCATTER COMMUNICATION AND BEAMFORMING[2]

4.1. Introduction

This chapter formulates and solves a joint-optimization problem whose objective is to maximize the sum-throughput of a wireless powered communication network (WPCN) with radio frequency (RF) energy harvesting (EH) and backscatter communication using a beamforming hybrid access point. A new multi-sensor blind adaptive beamforming (BABF) with combination protocol (MS-BABF/combo) is proposed and analyzed. A second joint-optimization problem whose objective is to maximize both the sum-throughput and fairness is formulated and solved. An algorithm based on the multi-source BABF with hybrid protocol that maximizes the sum-throughput and fairness (MS-BABF/hybrid-STF) is also proposed and analyzed.

4.2. System Model

4.2.1. System Architecture

A body area WPCN is considered. The system architecture comprises one hybrid access point (H-AP) with Q antennas, where $Q > 1$, and K sensors, where sensor $k, k = 1 \ldots K$ is located at a certain radial distance d_k away; similar to what was described in Figure 3.1 in the previous chapter. In Fig. 3.1, $Q = 1$.

---

[2] The content of this chapter has generated two conference papers:
[32] J. C. Kwan and A. O. Fapojuwo, "Optimized Wireless Energy Harvesting Sensor Network with Backscatter Communication and Beamforming," *2019 IEEE 90th Vehicular Technology Conference (VTC2019-Fall)*, Honolulu, HI, USA, 2019, pp. 1-6.
[33] J. C. Kwan and A. O. Fapojuwo, "Sum-Throughput and Fairness Optimization of a Wireless Energy Harvesting Sensor Network," *2019 IEEE 90th Vehicular Technology Conference (VTC2019-Fall)*, Honolulu, HI, USA, 2019, pp. 1-6.

The hybrid protocol combines the time-switching and power splitting receiver structure proposed in Chapter 3. The combination protocol was introduced in Chapter 3 as well.

4.2.2. Channel Propagation Model

The propagation channel is modeled by path loss, shadowing, and small-scale fading. The log-distance path loss model is assumed with path loss exponent φ and small-scale fading modeled by Nakagami-*m* fading with fading depth parameter m and average power parameter Ω. Nakagami-*m* fading is used in this chapter and in the remaining chapters of this thesis compared to Rayleigh fading in Chapter 3, because Nakagami-*m* is a can be easily used for H-APs with $Q > 1$ [69], [70]. In Chapter 3, Q is always equal to 1. Randomness of shadow fading is not considered for analytic simplicity. Instead, shadow fading is modeled by a fixed body shadowing loss margin. The channel power gain between sensor k and the H-AP's antenna $q, q = 1 \dots Q$, $h_{k,q}$, is calculated using the following formula [59]:

$$h_{k,q} = 10^{-\frac{(PL_{ref}+\psi_k)}{10}} \left(\frac{d_k}{d_{ref}}\right)^{-\varphi} \beta_{k,q}, k = 1 \dots K, q = 1 \dots Q, d_k > d_{ref}, \qquad (4.1)$$

where PL_{ref} is the path loss in dB at the reference distance d_{ref}, ψ_k is the body shadowing loss margin between the H-AP and sensor k in dB, d_k is the distance between the H-AP and sensor k, and $\beta_{k.q}$ is the small-scale fading power gain between the sensor k and the H-AP's antenna q. Based on the assumed Nakagami-*m* small-scale fading, $\beta_{k,q}$ is Gamma distributed with the shape parameter $a = m$ and the scale parameter $b = \Omega/m$ [59]. For simplicity, the chapter assumes $\psi_{1,1} = \cdots = \psi_{K,Q} = \psi$ and channel reciprocity holds., so that the uplink channel power gain between sensor k and the H-AP's antenna q, $g_{k,q}$, is equal to $h_{k,q}$, i.e. $g_{k,q} = h_{k,q}, k = 1 \dots K, q =$

$1 \ldots Q$. The fading channel power gain is assumed to remain constant for an entire time block T, but varies from block to block.

4.2.3. Multi-Sensor Blind Adaptive Beamforming

For an H-AP with $Q \geq 2$ antennas, a multi-sensor blind adaptive beamforming (MS-BABF) with combination protocol is used to circumvent the computational burden of explicit estimation of the channel state information and increase the received power at the sensors. The MS-BABF with combination protocol jointly optimizes the beamforming weight vector $\hat{w}$, and system timings τ to maximize the sum-throughput of a multiple sensor WPCN. The algorithm, referred to as the MS-BABF with combination (MS-BABF/combo) protocol hereafter, is found in Section 4.3.

The MS-BABF/combo algorithm generates weight vector $\hat{w}$ of size Q in each time block T. $\hat{w}$ is heuristically determined and is selected from an iteratively calculated set of weight vectors $\hat{w}_i, i = 1 \ldots I$, where I is the perturbation vector quantity, calculated as follows [52]:

$$\hat{w}_i^{[\Delta]} = \sqrt{Q} \frac{\hat{w}_{best}^{[\Delta-1]} + p_f \hat{p}_i}{\left\| \hat{w}_{best}^{[\Delta-1]} + p_f \hat{p}_\imath \right\|}, \tag{4.2}$$

where Δ is the MS-BABF iteration index, $\hat{w}_{best}^{[\Delta-1]}$ is the best weight vector from the previous iteration, p_f is the perturbation factor, and $\hat{p}_i$ is the ith perturbation vector of dimension Q, $i = 1 \ldots I$. I is the quantity of perturbation vectors per iteration. When $\Delta = 1$, $\hat{w}_{best}^{[0]}$ is randomly selected. This chapter adopts the BABF algorithm [52] with the combination protocol in a multiple sensor environment.

4.3. Sum-Throughput Analysis and Optimization

Sum-throughput is the total of all the throughput rates achieved by all the K sensors. The downlink data rate in bits/second/Hz (bps/Hz) achieved by sensor k is expressed as:

$$R_{DL,k}\left(\tau_{EH,DL}, \tau_{DL,k}, \widehat{w}, \lambda\right) = \tau_{DL,k} \log_2\left(1 + \frac{P_{R,k}(1-\lambda)}{\Gamma\sigma^2}\right), \tag{4.3}$$

where $\tau_{EH,DL}$ is the portion of time allocated to the sensor nodes to harvest energy for the downlink data decoding phase, $R_{DL,k}(\tau_{EH,DL}, \tau_{DL,k}, \widehat{w}, \lambda)$ is calculated using the Shannon-Hartley theorem [61], λ is the power splitting ratio, $P_{R,k}$ is the received power at sensor $k, k = 1 \dots K$ given by $P_{R,k} = \left\|\widehat{w}^T \hat{h}_k\right\| P_A$, $\widehat{w}^T$ is the transpose of the MS-BABF complex weight vector, $\hat{h}_k = \left[h_{k,1} \dots h_{k,Q}\right]^T, k = 1 \dots K$, P_A is the transmit power of the H-AP, Γ is the signal to noise ratio (SNR) gap from Shannon channel capacity due to use of a practical modulation and coding scheme, and σ^2 is the thermal noise power.

The uplink data rate in bps/Hz of sensor k operating in non-backscatter mode is expressed as:

$$R_{UL,k}\left(\tau_{EH,UL}, \tau_{UL,k}, \widehat{w}\right) = \tau_{UL,k} \log_2\left(1 + \varsigma_k \eta_k P_A \left\|\widehat{w}^T \hat{g}_k\right\| \frac{\left(\left\|\widehat{w}^T \hat{h}_k\right\| \tau_{EH,UL} + \left\|\widehat{w}_{prev}^T \hat{h}_{k,prev}\right\| \lambda_{prev} \tau_{DL,prev}\right)}{\Gamma\sigma^2 \tau_{UL,k}}\right), k = 1 \dots K, \tag{4.4}$$

where $\tau_{EH,UL}$ is the portion of time allocated to the sensor nodes to harvest energy for the uplink data transmission phase, $\hat{g}_k = \left[g_{k,1} \dots g_{k,Q}\right]^T, k = 1 \dots K$, ς_k is the EH efficiency at each sensor k, $0 < \varsigma_k < 1, k = 1 \dots K$, and η_k is the portion of harvested energy used for data transmission or decoding by each sensor k. $\widehat{w}_{prev}^T, \hat{h}_{k,prev}, \lambda_{prev}$, and $\tau_{DL,prev}$ are the transpose of the weight vector, channel power fading gain vector, power splitting ratio, and duration of downlink data

decoding phase in the previous time block, respectively. The chapter assumes $\varsigma_1 = \cdots = \varsigma_K = \varsigma$ and $\eta_1 = \cdots = \eta_k = \eta$ for simplicity. The $1 - \eta$ portion is used for powering the sensor circuitry.

Notice (4.4) does not include the rate achieved by sensor k when operating in backscatter mode. The uplink data rate in bps/Hz of sensor k operating in backscatter mode is calculated as follows:

$$R_{UL,B,k}\left(\tau_{UL,B}, r_{d,k}\right) = \tau_{UL,B} \log_2 \left(1 + \frac{\|\widehat{w}^T \hat{g}_k\| P_{R,k} s^2 \left(\frac{\mathrm{r}_{d,k}}{2}\right)^2 \left(\frac{4}{\pi}\right)^2}{\Gamma \sigma^2} \right), \tag{4.5}$$

where $\tau_{UL,B} = \tau_{EH}/k_B$, k_B is the number of sensors currently operating in backscatter mode determined by Algorithm 4.1, s is a scaling term related to the sensor scattering efficiency, and $\mathrm{r}_{d,k}$ is the difference between antenna reflection coefficients r_0 and r_1 calculated via antenna load impedance switching according to the data bit '0' and '1', respectively at sensor $k, k = 1 \ldots K$. Mathematically, $\mathrm{r}_{d,k} = |r_0 - r_1|$.

To maximize the sum-throughput of the combination protocol, the following optimization problem is proposed and needs to be solved:

$$(P4.1): \qquad \max_{\tau, \widehat{w}, \lambda} R_{sum}(\tau, \widehat{w}, \lambda), \tag{4.6a}$$

$$s.t. \qquad \tau_{EH,DL} + \tau_{EH,UL} + \tau_{DL} + \tau_{UL} \leq 1, \tag{4.6b}$$

$$\tau_{EH,DL}, \tau_{EH,UL}, \tau_{DL,k}, \tau_{UL,k} \geq 0, k = 1 \ldots K, \tag{4.6c}$$

$$R_{UL,k}\left(v, \widehat{w}, r_{d,k}\right) \geq 2R_{DL,k}(u, \widehat{w}, \lambda), k = 1 \ldots K, \tag{4.6d}$$

$$\|\widehat{w}\|^2 = Q, \tag{4.6e}$$

$$0 < \lambda < 1, \tag{4.6f}$$

where $\tau = \left[\tau_{EH,DL}\ \tau_{EH,UL}\ \tau_{DL,1} \cdots \tau_{DL,K}\ \tau_{UL,1} \cdots \tau_{UL,K}\right]$, $\tau_{DL} = \sum_{k=1}^{K} \tau_{DL,k}$, $\tau_{UL} = \sum_{k=1}^{K} \tau_{UL,k}$, $R_{sum}(\tau, \widehat{w}, \lambda) = R_{DL,sum}(u, \widehat{w}, \lambda) + R_{UL,sum}(v, \widehat{w}, r_{d,k})$, $u = \left[\tau_{EH,DL}\ \tau_{DL,1} \cdots \tau_{DL,K}\right]$, $v = \left[\tau_{EH,UL}\ \tau_{UL,1} \cdots \tau_{UL,K}\right]$, $R_{DL,sum}(u, \widehat{w}, \lambda) = \sum_{k=1}^{K} R_{DL,k}(u, \widehat{w}, \lambda)$, and $R_{UL,sum}(v, \widehat{w}, r_{d,k}) = \sum_{k=1}^{K} R_{UL,k}(v, \widehat{w}, r_{d,k})$. Eqn. (4.6a) is the objective function, (4.6b) is the time scheduling constraint, (4.6c) is the non-negativity constraint for the decision variables, (4.6d) is the bandwidth allocation constraint where the uplink sum-throughput is assumed to be at least twice as fast as the downlink data rate [63], (4.6e) is the weight vector constraint, (4.6f) is the power splitting ratio constraint. Eqn. (4.6d) can be modified if there are different uplink/downlink bandwidth requirements. For (*P*4.1), the objective function specified by (4.6a) is concave and its corresponding constraints are affine. Hence, (*P*4.1) is convex.

It is nearly impossible to solve problem (*P*4.1) directly due to the given number of objectives and constraints. However, it can be simplified by breaking it down into two separate sub-problems without resulting in a suboptimal solution. This is because there is a direct proportionality between the sum-throughput of the uplink or downlink data decoding phase and optimum timings, and a constant optimal ratio of harvested energy to uplink or downlink data sum-throughput exists as previously discussed in Chapter 3. Therefore, it can be solved individually in (*P*4.2) and (*P*4.3):

$$(P4.2): \qquad \max_{u,\widehat{w},\lambda} R_{DL,sum}(u, \widehat{w}, \lambda), \tag{4.7a}$$

$$s.t. \qquad \tau_{EH,DL} + \tau_{DL} \leq 1, \tag{4.7b}$$

$$\tau_{DL,k} \geq 0, k = 1, \dots K, \tag{4.7c}$$

$$\tau_{EH,DL} + \tau_{EH,UL} \geq 0, \tag{4.7d}$$

$$\|\widehat{w}\|^2 = Q, \tag{4.7e}$$

$$0 < \lambda < 1, \tag{4.7f}$$

$$(P4.3): \quad \max_{v,\hat{w},r_{d,k}} R_{UL,sum}\left(v,\hat{w},r_{d,k}\right), \tag{4.8a}$$

$$s.t. \quad \tau_{EH,UL} + \tau_{UL} \leq 1, \tag{4.8b}$$

$$\tau_{EH,UL}, \tau_{UL,k} \geq 0, k = 1 \dots K, \tag{4.8c}$$

$$\tau_{UL,B} \geq 0, k = 1 \dots K, \tag{4.8d}$$

$$0 < r_{d,k} < 1. \tag{4.8e}$$

For both (*P*4.2) and (*P*4.3), the objective function specified by (4.7a) and (4.8a) is each concave and their corresponding constraints are affine. Hence, both (*P*4.2) and (*P*4.3) are convex and can be solved using standard convex optimization techniques. Due to the constraints in (4.7b) and (4.8b) for (*P*4.2) and (*P*4.3), respectively, both will provide a solution in normalized time (i.e., $T = 1$). Note that this is an intermediate solution because adding the solutions of (*P*4.2) and (*P*4.3) together will result in a solution double the normalized time (i.e., $T = 2$), which does not satisfy the requirements for the constraint in (4.6b) in problem (*P*4.1). However, the optimal τ^* values to satisfy problem (*P*4.1) using the values obtained from sub-problems (*P*4.2) and (*P*4.3) can be calculated using the following equations from Chapter 3:

$$\tau^*_{EH,DL} = \tau_{EH,DL} BR_{DL} \mathrm{Z}, \tag{4.9}$$

$$\tau^*_{EH,UL} = \tau_{EH,UL} BR_{UL} \mathrm{Z}, \tag{4.10}$$

$$\tau^*_{DL,k} = \tau_{DL,k} BR_{DL} \mathrm{Z}, k = 1 \dots K, \tag{4.11}$$

$$\tau^*_{UL,k} = \tau_{UL,k} BR_{UL} \mathrm{Z}, k = 1 \dots K, \tag{4.12}$$

where:

$$BR_{DL} = BB_{DL} \frac{R_{DL,sum} + R_{UL,sum}}{2R_{DL,sum}}, \tag{4.13}$$

$$BR_{UL} = BB_{UL}\frac{R_{DL,sum} + R_{UL,sum}}{2R_{UL,sum}}, \tag{4.14}$$

$$\mathrm{Z} = \frac{T}{BR_{DL}\left(\tau_{EH,DL} + \tau_{DL}\right) + BR_{UL}\left(\tau_{EH,UL} + \tau_{UL}\right)}. \tag{4.15}$$

BB_{DL}, BB_{UL} are the downlink and uplink bandwidth bias, respectively, and Z is the time ratio to satisfy the constraint in (4.6b). Bandwidth bias is a parameter used to control the downlink and uplink bandwidth. As (4.6d) specified the uplink data rate to be at least twice as fast as the downlink data rate [63], setting $BB_{DL} = 2$ and $BB_{UL} = 1$ will suffice.

The optimal τ^* values to satisfy problem (P4.1) based on the solutions to sub-problems (P4.2) and (P4.3) can be calculated via (4.9) to (4.12). However, a solution to determine the optimal MS-BABF weight vector $\widehat{w}^*$ and the number of sensors to run in backscatter mode, k_B, such that the sum-throughput of the system is maximized remains to be determined. Analytical determination of both $\widehat{w}^*$ and k_B is non-trivial, hence we resort to a heuristic described in Algorithm 4.1, outlined as follows:

Algorithm 4.1 Joint MS-BABF with Combination Protocol

1. **Input:** $K, Q, P_A, BB_{DL}, BB_{UL}, p_f, I, \epsilon$
2. **Output:** $\tau^*, \widehat{w}^*, \lambda^*, R_{sum}(\tau^*, \widehat{w}^*, \lambda^*)$
3. Initialize iteration counter $\Delta = 1$ and weight vector $\widehat{w}_{best}^{[\Delta-1]}$ of size Q to any non-zero value.
4. Generate I zero mean, variance one complex normally distributed perturbation vectors $\hat{p}_i$ of dimension Q.
5. Calculate weight vectors $\widehat{w}_i^{[\Delta]}, i = 1 \ldots I$ using (4.2).

6. Select first weight vector $\widehat{w}_i^{[\Delta]}, i = 1$.

7. Solve problem (P4.2) to get the optimal $\tau_{DL,k}$ and λ values in normalized time for each sensor $k, k = 1 \dots K$.

8. Calculate $R_{DL,k}\left(\tau_{EH,DL}, \tau_{DL,k}, \widehat{w}_i, \lambda\right)$ in normalized time for all sensors, $k = 1 \dots K$ using (4.3).

9. Calculate the optimum $\tau_{EH,DL}$ in normalized time by $\tau_{EH,DL} = \left(\frac{\tau_{DL,k}\,(1-\lambda)}{\varsigma_k}\right)\left(\frac{\eta_k}{1-\eta_k}\right) - \lambda\tau_{DL}, k = 1 \dots K$.

10. Solve problem (P4.3) to get the optimal $\tau_{UL,k}$ and $r_{d,k}$ values in normalized time for each sensor $k, k = 1 \dots K$ currently not operating in backscatter mode. (No sensors are currently operating in backscatter mode on first run.)

11. Calculate $R_{UL,k}\left(\tau_{EH,UL}, \tau_{UL,k}, \widehat{w}\right)$ in normalized time for all sensors k currently not selected to be operating in backscatter mode with (4.4).

12. Calculate the bandwidth ratios BR_{DL}, BR_{UL} using (4.13) and (4.14), respectively.

13. Calculate the time ratio Z using (4.15).

14. Calculate all τ^* values using (4.9) to (4.12) to obtain $R_{sum}(\tau^*, \widehat{w}_i^{[\Delta]}, \lambda^*)$.

15. If $I \geq 2$:

Repeat Steps 7 to 14 for all remaining $\widehat{w}_i^{[\Delta]}, i = 2 \dots I$.

Endif

16. Assign the weight vector $\widehat{w}_i^{[\Delta]}$ that produces the highest $R_{sum}(\tau^*, \widehat{w}_i^{[\Delta]}, \lambda^*)$ as $\widehat{w}_{best}^{[\Delta-1]}$.

17. Check if the difference between the current $R_{sum}(\tau^*, \widehat{w}_i^{[\Delta]}, \lambda^*)$ and the previous $R_{sum}(\tau^*, \widehat{w}_{best}^{[\Delta-1]}, \lambda^*)$ exceeds ϵ.

If the difference exceeds ϵ:

Increase Δ by 1 and **repeat** Steps 4 to 16.

Else If the difference does NOT exceed ϵ:

Assign $\widehat{w}_{best}^{[\Delta-1]}$ to $\widehat{w}^*$ and continue to Line 18.

Endif

18. If there are two or more sensors remaining not currently selected for operating in backscatter mode:

Select the sensor with the lowest SNR to operate in backscatter mode.

Else

Go to Line 22.

Endif

19. Repeat Steps 10 to 14 with the backscatter sensor(s) removed from the uplink data transmission phase.

20. Calculate the rate $R_{UL,B,k}(\tau_{UL,B}^*, r_{d,k}^*)$ for the kth sensor(s) operating in backscatter mode using (4.5).

21. Check if the difference between the current $R_{sum}(\tau^*, \widehat{w}^*, \lambda^*)$ and the previous $R_{sum}(\tau^*, \widehat{w}^*, \lambda^*)$ exceeds ϵ.

If the difference does NOT exceed ϵ:

Change the last sensor that entered backscatter mode back to non-backscatter mode and go to Line 22. The τ^* values are the τ^* values before the last sensor entered backscatter mode.

Else If the difference exceeds ϵ:

Add the next lowest SNR sensor into backscatter mode and go to Line 18.

Endif

22. End

Algorithm 4.1 starts off by generating I weight vectors in Lines 3 to 5. The WPCN sum-throughput timings τ are optimized according to each weight vector $\widehat{w}_i$ and is repeated until the optimal weight vector $\widehat{w}^*$ is found in Lines 6 to 17. Lines 18 to 21 consider the sensors one at a time, starting from the one with the lowest SNR, to operate in backscatter mode until the sum-throughput cannot be further increased. Algorithm 1 provides the joint optimization solution to problem (P4.1).

The H-AP runs Algorithm 1 in the beginning of each time block of length T. The complexity of the algorithm is $O(\Delta)$ if $\Delta > K$ and $O(K)$ if $K \geq \Delta$. Implementing Algorithm 4.1 using MATLAB and running it on a 4.2 gigahertz Intel Core i7 processor [71] has a typical convergence time of 50 milliseconds when $Q = 4, K = 3$. The convergence time will reduce significantly if Algorithm 4.1 was run using optimized code on an application-specific integrated circuit chip. The figures of merit are measured by the sum-throughput and dropout percentage of the WPCN. A sensor will be temporarily disconnected during time block T if the sensor rate drops below the sensor dropout rate threshold. The sensor dropout rate is calculated by the number of disconnections divided by the total number of attempted connections. The MS-BABF/combo

protocol will be measured against the MS-BABF with time-switching (MS-BABF/TS) protocol in Chapter 3; shown in the simulation results in Section 4.5.

4.4. Sum-Throughput and Fairness Analysis and Optimization

The MS-BABF with hybrid protocol jointly optimizes the beamforming weight vector $\widehat{w}$ and system timings τ to maximize the sum-throughput and fairness of a multiple sensor WPCN for an H-AP with $Q \geq 2$ antennas. The algorithm, referred to as the sum-throughput and fairness optimization algorithm, is found in this section.

The sum-throughput and fairness optimization algorithm generates weight vector $\widehat{w}$ of size M in each time length T. $\widehat{w}$ is heuristically determined and is selected from an iteratively calculated set of weight vectors $\widehat{w}_i, i = 1 \dots I$, where I dis the perturbation vector quantity, by Algorithm 4.2.

This chapter adopts the BABF algorithm [52] with the hybrid protocol in a multiple sensor environment.

The uplink data rate in bits/second/Hz (bps/Hz) of sensor k is expressed as:

$$R_{UL,k}\left(\tau_{EH,UL}, \tau_{UL,k}, \widehat{w}\right) = \frac{\tau_{UL,k}\log_2\left(1 + \varsigma_k \eta_k P_A \|\widehat{w}^T \hat{g}_k\| \|\widehat{w}^T \hat{h}_k\| \tau_{EH,UL}\right)}{\Gamma \sigma^2 \tau_{UL,k}}, k = 1 \dots K, \quad (4.16)$$

To quantify the throughput fairness between sensors, Jain's fairness index, denoted by J, is adopted, given by [39]:

$$J = \frac{\left(\sum_{k=1}^{K}(R_{DL,k}(\tau, \widehat{w}, \lambda) + R_{UL,k}(\tau))\right)^2}{K \sum_{k=1}^{K}(R_{DL,k}(\tau, \widehat{w}, \lambda) + R_{UL,k}(\tau))^2}, \quad (4.17)$$

To maximize the sum-throughput and fairness of the hybrid protocol using MS-BABF, the following multi-objective joint optimization problem is proposed and needs to be solved:

$$(P4.2): \qquad \max_{\tau, \widehat{w}, \lambda} \{R_{sum}(\tau, \widehat{w}, \lambda), J\}, \quad (4.18a)$$

$$s.t. \qquad \tau_{EH,DL} + \tau_{EH,UL} + \tau_{DL} + \tau_{UL} \leq 1, \quad (4.18b)$$

$$\tau_{EH,DL}, \tau_{EH,UL}, \tau_{DL,k}, \tau_{UL,k} \geq 0, k = 1 \dots K, \quad (4.18c)$$

$$R_{UL,k}(\tau) \geq 2R_{DL,k}(\tau, \widehat{w}, \lambda), k = 1 \dots K, \quad (4.18d)$$

$$\|\widehat{w}\|^2 = Q, \quad (4.18e)$$

$$\frac{1}{K} \leq J \leq 1, \quad (4.18f)$$

$$0 < \lambda < 1, \quad (4.18g)$$

where (4.18a) is the objective function, (4.18b) is the time scheduling constraint, (4.18c) is the non-negativity constraint for the decision variables, (4.18d) is the bandwidth allocation constraint where the uplink sum-throughput is assumed to be at least twice as fast as the downlink data rate [63], (4.18e) is the weight vector constraint, (4.18f) is Jain's fairness index constraint, where $1/K$ is the worst case (minimum rate fairness) and 1 is the best case (maximum rate fairness), and (4.18g) is the power splitting ratio constraint. Eqn. (4.18d) can be modified if there are different uplink/downlink bandwidth requirements.

Problem (P4.2) is nearly impossible to solve directly because it is a multi-objective optimization (MOO) problem. One way to solve the problem is to decompose it to three single-objective optimization (SOO) sub-problems. The first sub-problem is given by problem (P4.3) as follows:

$$(P4.3): \quad \max_{\tau, \widehat{w}, \lambda} J, \quad (4.19a)$$

$$\frac{1}{K} \leq J \leq 1. \quad (4.19b)$$

It can be seen that J in problem (P4.3) requires the solution to $R_{DL,sum}(u, \widehat{w}, \lambda)$ and $R_{UL,sum}(v)$ from (4.16). As J, $R_{DL,sum}(u, \widehat{w}, \lambda)$, and $R_{UL,sum}(v)$ are all interdependent with each

other, problem (P4.3) needs to be solved concurrently with second sub-problem (P4.4) and third sub-problem (P4.5) defined below:

$$(P4.4): \quad \max_{u,\widehat{w},\lambda} R_{DL,sum}(u,\widehat{w},\lambda), \tag{4.20a}$$

$$s.t. \quad \tau_{EH,DL} + \tau_{DL} \leq 1, \tag{4.20b}$$

$$\tau_{DL,k} \geq 0, k = 1, \dots K, \tag{4.20c}$$

$$\tau_{EH,DL} + \tau_{EH,UL} \geq 0, \tag{4.20d}$$

$$\|\widehat{w}\|^2 = Q, \tag{4.20e}$$

$$0 < \lambda < 1. \tag{4.20f}$$

$$(P4.5): \quad \max_{v} R_{UL,sum}(v), \tag{4.21a}$$

$$s.t. \quad \tau_{EH,UL} + \tau_{UL} \leq 1, \tag{4.21b}$$

$$\tau_{EH,UL}, \tau_{UL,k} \geq 0, k = 1 \dots K. \tag{4.21c}$$

For both (P4.4) and (P4.5), the objective function specified by (4.20a) and (4.21a) is each concave and their corresponding constraints are affine. Hence, both (P4.4) and (P4.5) are convex and can be solved using standard convex optimization techniques.

Note the three sub-problems are interdependent. This decomposition is valid because there is a direct proportionality between the sum-throughput of the uplink or downlink data decoding phase and optimum timings, as well as because of a constant optimal ratio of harvested energy to uplink or downlink data sum-throughput exists discussed in Chapter 3. Due to the constraints in (4.20b) and (4.21b) for (P4.4) and (P4.5), respectively, both will provide an intermediate solution in normalized time (i.e., $T = 1$). Adding the intermediate solutions of (P4.4) and (P4.5) together will result in a solution double the normalized time (i.e., $T = 2$), which does not satisfy the constraint given by (4.18b) in problem (P4.2). However, the optimal τ^* values to satisfy problem

(*P*4.2) using the values obtained from solving the concurrent problems (*P*4.3), (*P*4.4), and (*P*4.5) can be calculated using (4.9) to (4.12).

A solution for the optimal MS-BABF weight vector $\widehat{w}^*$ such that J is maximized to achieve the optimal sum-throughput and fairness of the system remains to be determined. Solving problems (*P*4.3), (*P*4.4), and (*P*4.5) and analytical determination of $\widehat{w}^*$ that maximizes R_{sum} and J for problem (*P*4.2) is non-trivial, and may result in a sub-optimal solution because of the decomposition of an MOO to three SOO sub-problems. Hence, we propose Algorithm 4.2 to solve sub-problems (*P*4.3) to (*P*4.5) concurrently to obtain an optimal solution. The steps in Algorithm 4.2 are outlined as follows:

Algorithm 4.2 Sum-Throughput and Fairness Optimization Algorithm

1. **Input:** $K, Q, P_A, BB_{DL}, BB_{UL}, p_f, I, \epsilon$
2. **Output:** $\tau^*, \widehat{w}^*, \lambda^*, R_{sum}(\tau^*, \widehat{w}^*\lambda^*), J$
3. Initialize iteration counter $\Delta = 1$ and weight vector $\widehat{w}_{best}^{[\Delta-1]}$ of size Q to any non-zero value.
4. Generate I zero mean, variance one complex normally distributed perturbation vectors $\hat{p}_i$ of dimension Q.
5. Calculate weight vectors $\widehat{w}_i^{[\Delta]}, i = 1 \ldots I$ using (4.2).
6. Select first weight vector $\widehat{w}_i^{[\Delta]}, i = 1$.
7. Solve problem (*P*4.3) to get the optimal $\tau_{DL,k}$ and λ values in normalized time for each sensor $k, k = 1 \ldots K$.

8. Calculate $R_{DL,k}\left(\tau_{EH,DL}, \tau_{DL,k}, \widehat{w}_i, \lambda\right)$ in normalized time for all sensors, $k = 1 \ldots K$ using (4.3).

9. Calculate the optimum $\tau_{EH,DL}$ in normalized time by $\tau_{EH,DL} = \left(\frac{\tau_{DL,k}\,(1-\lambda)}{\varsigma_k}\right)\left(\frac{\eta_k}{1-\eta_k}\right) - \lambda\tau_{DL}, k = 1 \ldots K$ to solve problem (P4.4).

10. Solve problem (P4.5) to get the optimal $\tau_{UL,k}$ values in normalized time for each sensor $k, k = 1 \ldots K$.

11. Calculate $R_{UL,k}\left(\tau_{EH,UL}, \tau_{UL,k}\right)$ in normalized time for all sensors k with (4.16).

12. Calculate the bandwidth ratios BR_{DL}, BR_{UL} using (4.13) and (4.14), respectively.

13. Calculate the time ratio Z using (4.15).

14. Calculate all τ^* values using (4.9) to (4.12) to obtain $R_{sum}(\tau^*, \widehat{w}_i^{[\Delta]}, \lambda^*)$.

15. If $I \geq 2$:

Repeat Steps 7 to 14 for all remaining $\widehat{w}_i^{[\Delta]}, i = 2 \ldots I$.

Endif

16. Assign the weight vector $\widehat{w}_i^{[\Delta]}$ that produces the highest J as $\widehat{w}_{best}^{[\Delta-1]}$.

17. Check if the difference between the current J and the previous J exceeds ϵ for problem (P4.3).

If the difference exceeds ϵ:

Increase Δ by 1 and **repeat** Steps 4 to 16.

Else If the difference does NOT exceed ϵ:

Assign $\widehat{w}_{best}^{[\Delta-1]}$ to $\widehat{w}^*$ and continue to Line 18.

Endif

18. End

Algorithm 4.2 starts off by generating I weight vectors in Lines 3 to 5. The WPCN sum-throughput and fairness timings τ and power splitting ratio λ are optimized according to each weight vector $\widehat{w}_i$ and is repeated until the optimal weight vector $\widehat{w}^*$ for the maximum WPCN sum-throughput and fairness is found in Lines 6 to 17. In essence, Algorithm 4.2 provides the solution to MOO problem (*P*4.2).

The hybrid access point runs Algorithm 4.2 in the beginning of each time block of length T. The complexity of the algorithm $O(\Delta)$ if $\Delta > K$ and $O(K)$ if $K \geq \Delta$, with a typical convergence time of 80 milliseconds in a $Q = 4, K = 3$ configuration using MATLAB on a 4.2 gigahertz Intel Core i7 processor [71]. The convergence time will reduce if Algorithm 4.2 was run using optimized code on an application-specific integrated circuit chip. Algorithm 4.2's figures of merit are measured by the sum-throughput, Jain's fairness index, and dropout percentage of the WPCN. A sensor will be temporarily disconnected if the sensor rate drops below the sensor dropout rate threshold during time block T. The sensor dropout rate is calculated by the number of disconnections divided by the total number of attempted connections. The MS-BABF with hybrid protocol maximizing the sum-throughput and fairness (MS-BABF/hybrid-STF) will be measured against the MS-BABF with hybrid protocol maximizing the sum-throughput (MS-BABF/hybrid-ST); shown in the simulation results in Section 4.5.

4.5. Simulation Results and Discussion

4.5.1. System Configuration

A user is assumed to be equipped with $K = 3$ sensors located at $d_1 = d_2 = d_3 = 2$ meters away from the H-AP unless stated otherwise. The channel power gain values for sensor k, $\hat{h}_k$, are

generated using (4.1) with Gamma parameters $a = 1.192, b = 1.349$ [72] to reflect factors such as movement of other objects/people around the user of interest in a multiple input, single output (MISO) WPCN described in Section 4.2.1. The channel bandwidth is assumed to be 1MHz [66] to calculate the achievable data rate, where the sensor dropout threshold is 164kbps [68]. 164kbps is more than sufficient for most on-body applications, because a high resolution 12-bit, fast polling 10Hz 9-axis accelerometer sensor generates data at only approximately 1kbps (12 bits * 10/second * 9 axis = 1080bps). The rest of the assumed system parameter values are summarized in Table 4.1.

Table 4.1. Assumed System Parameter Values

Parameter	Definition	Value
PL_{ref}	Path loss at reference distance of 1m and transmitter frequency of 900MHz	30dB
ψ	Body shadowing loss margin	15dB [64]
φ	Path loss exponent	3.8 [65]
ς	EH efficiency at each sensor	0.5 [54]
η	Portion of harvested energy used for information transmission by each sensor	0.5 [60]
P_A	Hybrid access point transmission power	4000mW [56], [57]
Γ	SNR gap	1.5dB [67]
σ^2	Background noise power in 1MHz channels	-114dBm [66]
s	Tag scattering efficiency scaling	-1.1dB [20]
BB_{DL}	Downlink bandwidth bias	2 [63]

BB_{UL}	Uplink bandwidth bias	1 [63]
p_f	Perturbation factor	0.02 [52]
I	Perturbation vector quantity	10 [52]
ϵ	Difference checking precision	10^-4

New $\hat{h}_k$ values are generated at the beginning of each time block T of 1 second, each represented by one simulation run to simulate ongoing changes in channel quality in a dynamic environment. The length of a simulation is set to 1000 seconds per specific combination of test parameters to assure the system is operating under steady-state condition that can be completed within a reasonable amount of time.

4.5.2. Results and Discussion – MS-BABF/combo

The MS-BABF/combo protocol is investigated with regards to the scaling of the number of antennas from 2 to 8 against the MS-BABF/TS protocol. With 1 antenna, the WPCN functions as a single input, single output (SISO) configuration. Each data point in Fig. 4.1 represents the average of 1000 runs in the simulator. It is observed from Fig. 4.1 that, as the number of antennas increase, the average sum-throughput for both protocols consistently increased. However, the MS-BABF/combo always outperformed MS-BABF/TS protocol by an average of 25.1% with a maximum of 26.2%. This is because sensors can harvest more energy and utilize backscatter communication with the MS-BABF/combo protocol compared to the MS-BABF/TS protocol. The H-AP with 8 antennas running the MS-BABF/combo protocol (i.e., MISO MS-BABF/combo) also increased the sum-throughput by 48.8% compared to a SISO MS-BABF/combo protocol. The recorded dropout rate is zero for all protocols with a channel width of 1MHz. The dropout rate

may increase if the channel width is decreased because there will be a decrease in sensor rate in bits per second.

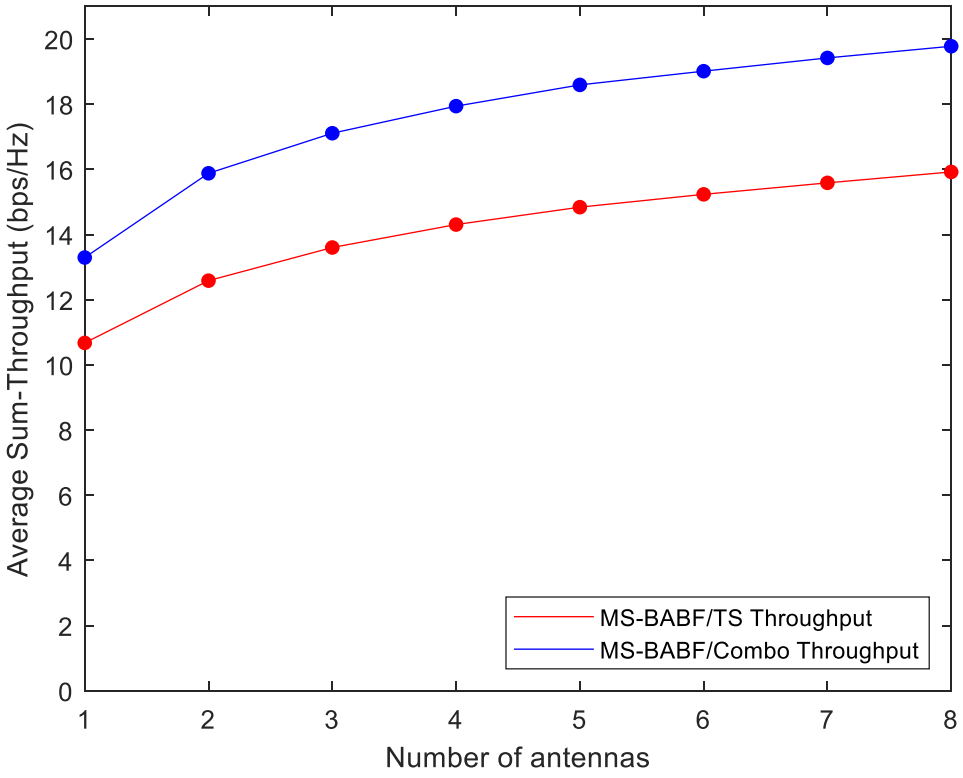

Fig. 4.1. System sum-throughout versus number of antennas.

The sensitivity of the average sum-throughput and dropout rate to the distance between an H-AP with $Q = 4$ antennas and its sensors is presented in Fig. 4.2, where the distance is varied from 1.5m to 7.5m. The average sum-throughput decreases as the separation distance increases due to a decrease in average received power. The MS-BABF/combo protocol always outperformed the MS-BABF/TS protocol by an average of 23.0% with a maximum 26.4%. However, the dropout rate for the MS-BABF/combo protocol is only 0.43% at 7.5m compared to 1.0% for the MS-BABF/TS protocol. Once again, the MS-BABF/combo protocol outperformed MS-BABF/TS because its sensors can harvest more energy and utilize time more efficiently in the same time

block. These results are significant because it shows the MS-BABF/combo protocol can meet higher sum-throughput and dropout rate requirements compared to MS-BABF/TS without increasing the H-AP transmission power, which is limited by government regulations [56], [57].

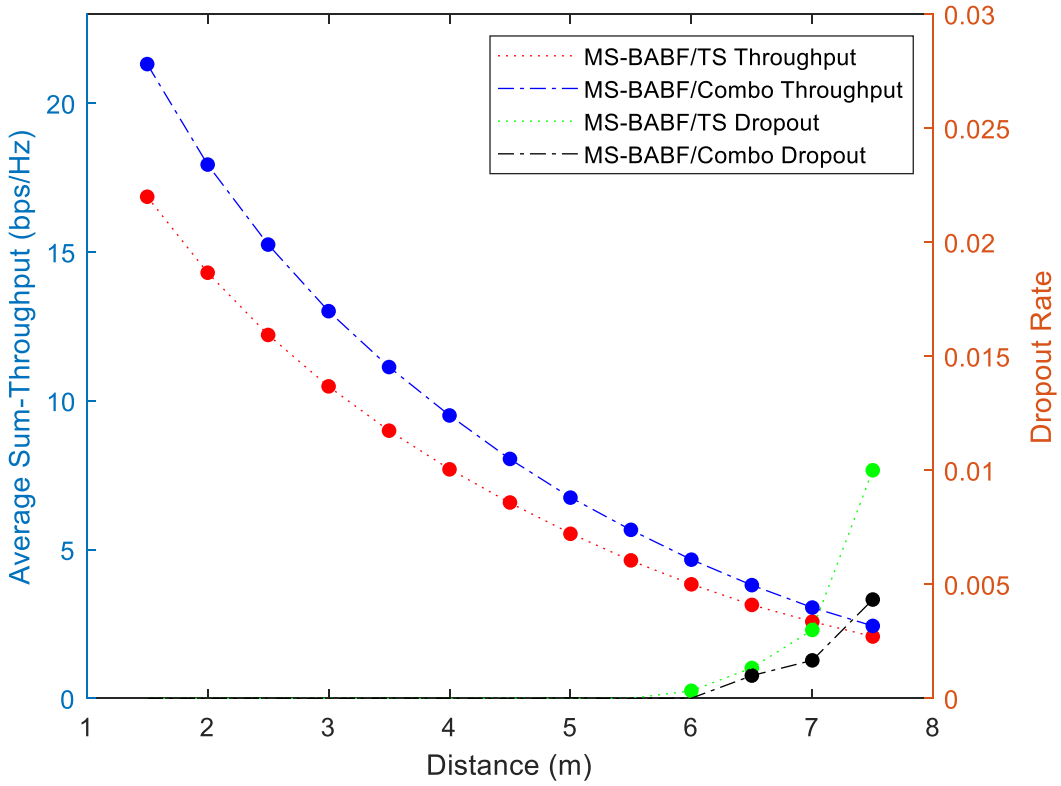

Fig. 4.2. System sum-throughout and dropout rate versus radial distance between the H-AP and sensors.

4.5.3. Results and Discussion – MS-BABF/hybrid-STF

The MS-BABF/hybrid-STF protocol is investigated by varying the number of antennas of the H-AP from 2 to 8 with $K = 3$ sensors against the MS-BABF/hybrid-ST protocol. With 1 antenna, the WPCN functions as a SISO configuration. Each data point in Fig. 4.3 represents the average of 1000 seconds in the simulator. It is observed from Fig. 4.3 that, as the number of antennas increases, both the average WPCN throughput and fairness between sensors consistently increased

for both MS-BABF/hybrid-STF and MS-BABF/hybrid-ST. The only exception is MS-BABF/hybrid-STF when going from 1 to 2 antennas, where a slight decrease in WPCN throughput was noticed. This is because more H-AP antennas mean more transmitted energy from the H-AP, which increases the harvested energy at the sensors. However, when going from 1 to 2 antennas, some throughput was sacrificed to increase fairness. The fairness between sensors in the WPCN is, on average, 20.5% higher when the sum-throughput and fairness is maximized compared to when the sum-throughput is maximized for $1 \leq Q \leq 3$. The increase in fairness comes at the expense of WPCN throughput, where optimizing the sum-throughput and fairness decreased the WPCN throughput by an average of 19.3% for $1 \leq Q \leq 3$. Little fairness gain can be realized for $Q > 3$ antennas when $K = 3$ sensors considering $J = 0.97$ when $Q = 3$. Increasing the number of antennas from 1 to 2 also increased the sum-throughput and fairness by 36.7% using MS-BABF/hybrid-STF. The recorded dropout rate is zero for all protocols with a channel width of 1MHz, but the dropout rate may increase if the channel width is decreased due to a reduction of sensor rate in bits per second.

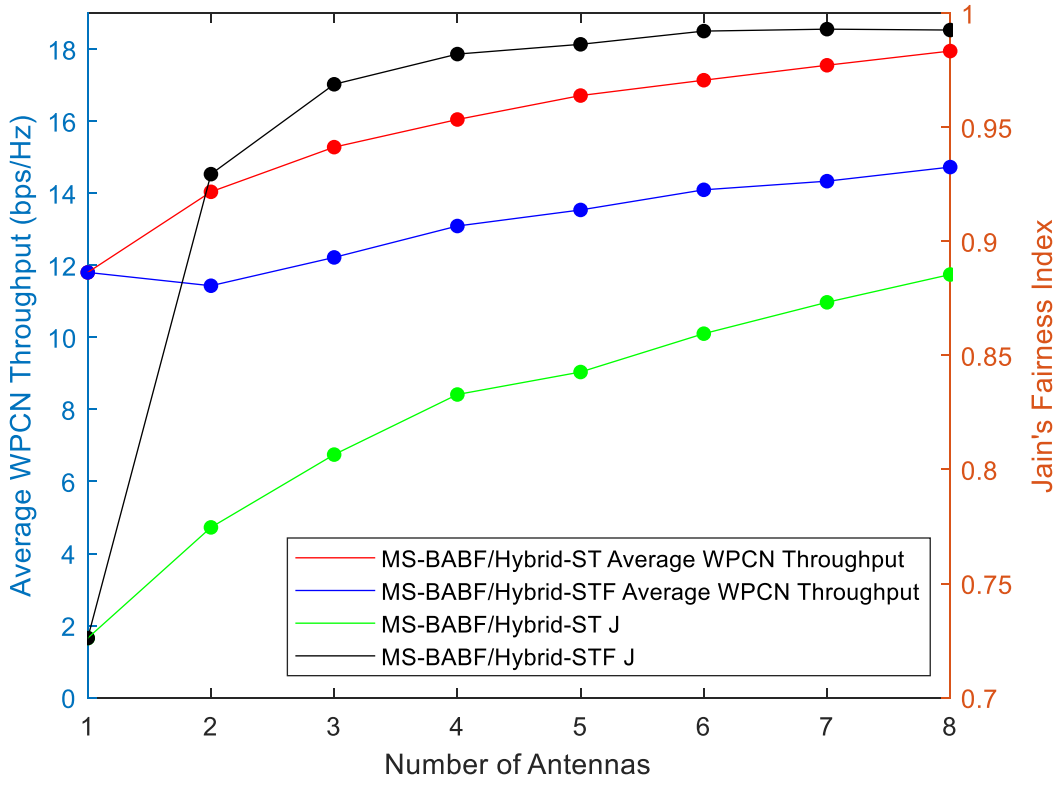

Fig. 4.3. WPCN sum-throughout and *J* versus number of antennas. MS-BABF/hybrid-ST Average WPCN Throughput and MS-BABF/hybrid-STF Average WPCN Throughput is the average sum-throughput of the WPCN of their respective protocols with the units on the left axis. MS-BABF/hybrid-ST J and MS-BABF/hybrid-STF J is Jain's fairness index of their respective protocols with the units on the right axis.

Next, the WPCN throughput and fairness between sensors was investigated by varying the number of sensors from 2 to 8 in the network. The results for a WPCN with a $Q = 4$ antennas H-AP is presented in Fig. 4.4. Increasing the number of sensors increases the throughput of the WPCN because increasing the number of sensors also increases the average amount of harvested energy in the WPCN. MS-BABF/hybrid-STF has an average fairness gain of 19.1% over MS-BABF/hybrid-ST, maintaining $J = 0.96$ when $K = 4$ sensors at the expense of 15.9% average decrease in WPCN throughput when $2 \leq K \leq 8$. The recorded dropout rate is zero for all protocols with a channel width of 1MHz.

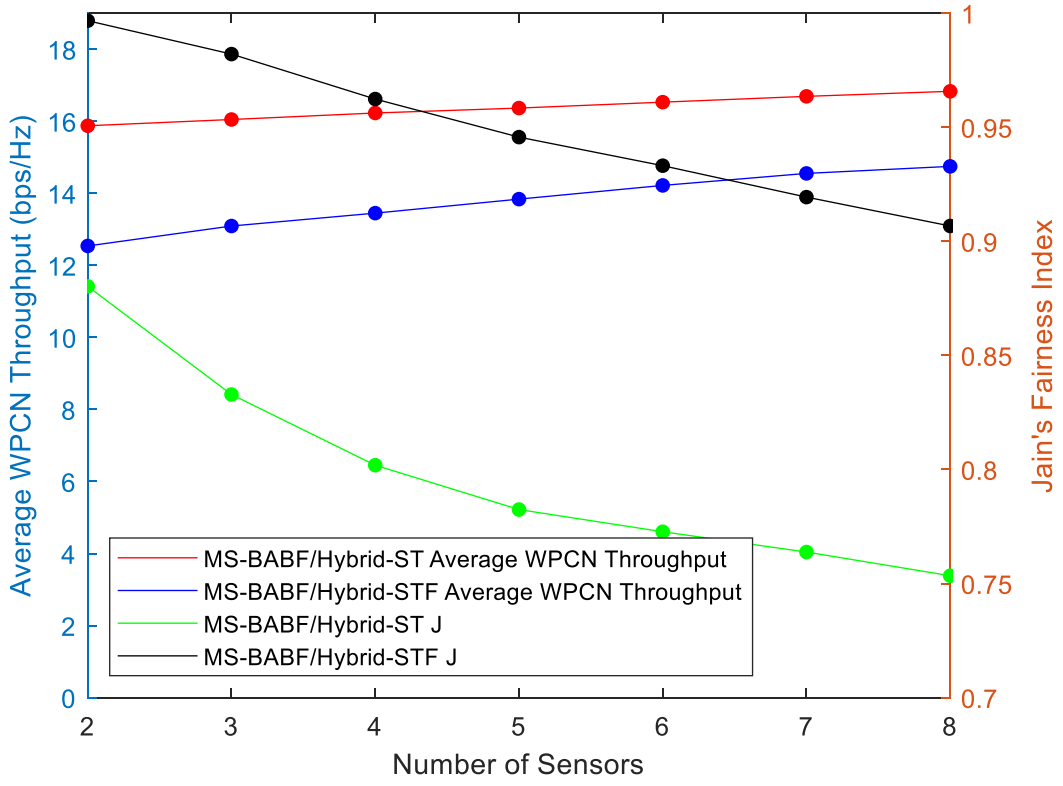

Fig. 4.4. WPCN sum-throughout and *J* versus number of sensors.

These results are significant because the multi-objective WPCN throughput and fairness problem can be solved by a beamforming H-AP using the MS-BABF/hybrid-STF algorithm. This can be used to ensure sensors will harvest sufficient energy to support the transmission of its sensed data with the required quality by alleviating the doubly near far problem. Furthermore, the tradeoff of optimizing the WPCN sum-throughput and fairness using MS-BABF/hybrid-STF versus the sum-throughput is justified given the percentage increase in fairness exceeds the percentage decrease of throughput. Lastly, different performance requirements, such as the WPCN throughput or fairness between sensors, for different scenarios can be achieved by increasing or decreasing the number of H-AP antennas.

4.6. Summary

A solution for maximizing the sum-throughput of a two-way communication WPCN by jointly optimizing the system timings and a beamforming weight vector using a multi-sensor blind adaptive beamforming with combination protocol was presented in this chapter. It was found that the MISO MS-BABF/combo protocol significantly increased the sum-throughput of a WPCN compared to a SISO configuration by 48.8% and the MS-BABF/TS by up to 26.4%. The MS-BABF/combo protocol also decreased the dropout rate to 0.43% at 7.5m from 1.0% achieved with MS-BABF/TS at the same distance.

A solution for maximizing the sum-throughput and fairness of a two-way communication WPCN by jointly optimizing the system timings and a beamforming weight vector using a multi-sensor blind adaptive beamforming with hybrid protocol was also presented in this chapter. It was found that the MS-BABF/hybrid-STF protocol significantly increased the fairness between sensors of a WPCN compared to a SISO configuration by 36.7% and MS-BABF/hybrid-ST by an average of 20.1% at the expense of 19.3% decrease in WPCN throughput. When varying the number of sensors from 2 to 8, it was found that MS-BABF/hybrid-STF has an average fairness gain of 19.1% over MS-BABF/hybrid-ST at the expense of 15.9% average decrease in WPCN throughput.

CHAPTER 5: PERFORMANCE OPTIMIZATION OF A MULTI-SOURCE, MULTI-SENSOR BEAMFORMING WIRELESS POWERED COMMUNICATION NETWORK WITH BACKSCATTER COMMUNICATION[3]

5.1. Introduction

This chapter formulates and solves a multi-objective joint optimization problem where both the sum-throughput and fairness of a radio frequency (RF) energy harvesting (EH) wireless powered communication network (WPCN) are maximized using multiple beamforming hybrid access points (H-APs) and backscatter communication-enabled combination sensors. The chapter proposes the multi-source, multi-sensor blind adaptive beamforming (BABF) with combination sensors (MS2-BABF/combo) protocol. The protocol is analyzed to determine its performance with metrics including WPCN sum-throughput, fairness in the achievable rates by sensors, sum-throughput and fairness tradeoff, and sensor dropout rate.

5.2. System Model

5.2.1. System Architecture

A body area WPCN is considered. The system architecture comprises N H-APs each with Q antennas. A user with K on-/in-body sensors, where sensor $k, k = 1 \dots K$ is located at a certain radial distance $d_{n,k}$ away from H-AP $n, n = 1 \dots N$, shown in Fig. 5.1. In the considered system, all H-APs are connected to the global controller. The N H-APs and the global controller are powered by the same mains supply whereas the K sensors are battery-less and harvest energy wirelessly from the N H-APs for their operation. The harvested energy by each sensor is

[3] The content of this chapter has generated one journal paper [34]: J. C. Kwan and A. O. Fapojuwo, "Performance Optimization of a Multi-Source, Multi-Sensor Beamforming Wireless Powered Communication Network With Backscatter," in *IEEE Sensors Journal*, vol. 19, no. 22, pp. 10898-10909, Nov. 15, 2019.

temporarily stored in a capacitor, which will be fully discharged in the subsequent downlink or uplink data transmission phases to maximize the WPCN throughput.

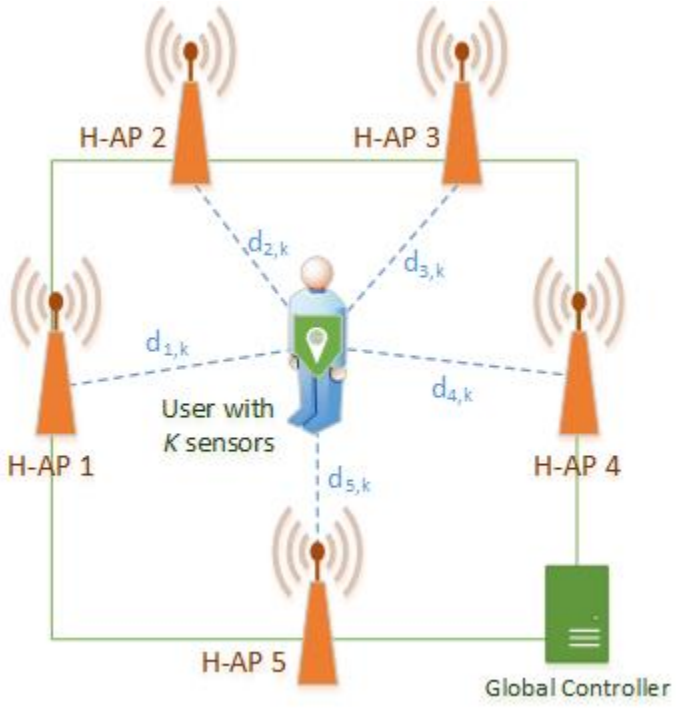

Fig. 5.1. A WPCN with K sensors on/in a human body located at radial distance $d_{n,k}, n = 1 \dots N, k = 1 \dots K$ from $N = 5$ hybrid access points for illustration.

To prevent destructive wireless interference, all H-APs and sensors in the WPCN can transmit only during their allocated time slot enabled by the global network controller (Fig. 5.1), which has knowledge of all the H-APs and sensors in the WPCN within its coverage area [14]. The sensed data is then transmitted to the H-AP with the uplink highest channel gain, which subsequently uploads the sensed data to places like a health care service provider's database via the Internet. All H-APs can also transmit data such as device configuration changes or health alerts/data query requests from the health care service provider to the sensors.

The sensors can make themselves known to the global network controller via a registration message piggy-backed on the first data packet transmission as in Chapter 3. Therefore, it is

reasonable to assume the global network controller has knowledge of all sensors in the WPCN. The received power at each sensor from each H-AP can be piggy-backed on each uplink data packet transmission to keep the information up to date without incurring additional signaling overhead. Each node in the network only receives or transmits during its allocated time slot.

The combination protocol combines the time-switching and power splitting receiver structure with backscatter communication and requires an algorithm that runs in the global network controller to determine which and how many sensors to operate in backscatter mode described in Chapter 3.

5.2.2. Channel Propagation Model

The WPCN operates in a dynamic environment whose propagation channel is modeled by path loss, shadowing, and small-sale fading. The log-distance path loss model is assumed with path loss exponent φ and small-scale fading modeled by Nakagami-*m* fading with fading depth parameter m and average power parameter Ω, as in Chapter 4. Randomness of shadow fading is not considered for analytic simplicity. Instead, shadow fading is modeled by a fixed body shadowing loss margin. The channel power gain between sensor k and H-AP n's antenna q, $h_{n,k,q}$, is calculated using the following formula [59]:

$$h_{n,k,q} = 10^{-\frac{(PL_{ref}+\psi_{n,k,q})}{10}} \left(\frac{d_{n,k}}{d_{ref}}\right)^{-\varphi} \beta_{n,k,q},$$
$$n = 1 \dots N, k = 1 \dots K, q = 1 \dots Q, d_{n,k} > d_{ref}, \quad (5.1)$$

where PL_{ref} is the path loss in dB at the reference distance d_{ref}, $\psi_{n,k,q}$ is the body shadowing loss margin in dB between antenna q on the H-AP and sensor k, $d_{n,k}$ is the distance between H-AP n and sensor k, and $\beta_{n,k.q}$ is the small-scale fading channel power gain between the sensor k and H-AP n's antenna q. Based on the assumed Nakagami-*m* small-scale fading, $\beta_{n,k,q}$ is Gamma

distributed with the shape parameter $a = m$ and the scale parameter $b = \Omega/m$ [59]. For simplicity, the chapter assumes $\psi_{1.1,1} = \cdots = \psi_{N,K.Q} = \psi$ and channel reciprocity holds, so that the uplink channel power gain between sensor k and H-AP n's antenna q, $g_{n,k,q}$, is equal to $h_{n,k,q}$, i.e. $g_{n,k,q} = h_{n,k,q}, n = 1 \dots N, k = 1 \dots K, q = 1 \dots Q$. The fading channel power gain is assumed to remain constant for an entire time block T for transmission and energy harvesting, but varies from block to block.

5.3. Multi-Source, Multi-Sensor Blind Adaptive Beamforming

For WPCNs with $N \geq 2$ H-APs each with $Q \geq 2$ antennas, the MS2-BABF/combo protocol is proposed to increase the received power at the sensors. Each H-AP transmits to all sensors in its allocated time slot. The MS2-BABF/combo protocol jointly optimizes:

1) The beamforming weight vector at each H-AP n, $\widehat{w}_n, n = 1 \dots N$.

2) The proportion of time RF source n spends in transmitting energy, $\alpha_n, n = 1 \dots N$.

3) System timings τ to maximize the sum-throughput of a multiple sensor WPCN at each H-AP.

The step-by-step procedure for the MS2-BABF/combo protocol algorithm is presented as Algorithm 5.1 in Section 5.4.

The MS2-BABF/combo algorithm generates weight vector $\widehat{w}_n$ of dimension Q for each H-AP in each time block T. $\widehat{w}_n$ is heuristically determined and is selected from an iteratively calculated set of weight vectors $\widehat{w}_{n,i}, n = 1 \dots N, i = 1 \dots I$, where I is the perturbation vector quantity, calculated as follows [52]:

$$\widehat{w}_{n,i}^{[\Delta]} = \sqrt{Q} \frac{\widehat{w}_{n,best}^{[\Delta-1]} + p_f \hat{p}_{w,n,i}}{\left\| \widehat{w}_{n,best}^{[\Delta-1]} + p_f \hat{p}_{w,n,i} \right\|}, \tag{5.2}$$

where Δ is the current iteration index, $\hat{w}_{n,best}^{[\Delta-1]}$ is the best weight vector for H-AP n from the previous iteration, p_f is the perturbation factor, $\hat{p}_{w,n,i}$ is the ith randomly generated perturbation vector of dimension Q for H-AP n, $n = 1 \ldots N, i = 1 \ldots I$, and $||x||$ is the Euclidean norm of vector x. When $\Delta = 1$, $\hat{w}_{n,best}^{[0]}$ is randomly selected.

Similarly, the MS2-BABF/combo algorithm generates optimal values of α_n, the proportion of time RF source n spends in transmitting energy during τ_{EH}, shown in Fig. 5.2. Clearly, the α_n values are constantly changing because of the dynamic environment. It is of critical importance to be able to increase the harvested energy fairness between sensors to alleviate the doubly near far problem. However, it is also of critical importance to allocate energy transmission time to the most favorable RF sources in the sense of high channel power gain and allocate little or no transmission time to the least favorable sources at each point in time as well. This will directly affect the optimal values of α, where $\alpha = [\alpha_1 \ldots \alpha_N]$ and $\sum_{n=1}^{N} \alpha_n = 1$.

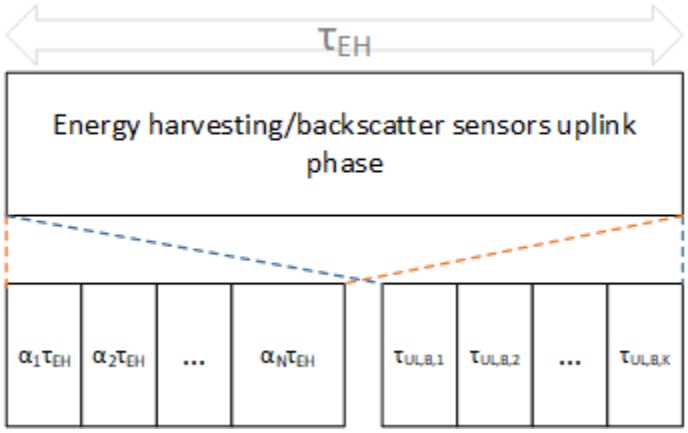

Fig. 5.2. Timing diagram for the energy harvesting/backscatter sensors uplink phase.

Although α can be solved by brute force as done in a previously published work by this author [14], the corresponding algorithm is exponentially complex and thus inefficient. Therefore,

in this chapter, α is heuristically determined and is selected from an iteratively obtained set of timing vectors $\hat{\alpha}_i, i = 1 \dots I$, calculated as follows:

$$\hat{\alpha}_i^{[\Delta]} = \frac{\left|\hat{\alpha}_{best}^{[\Delta-1]} + p_f \hat{p}_{\alpha,i}\right|}{\left\|\hat{\alpha}_{best}^{[\Delta-1]} + p_f \hat{p}_{\alpha,i}\right\|}, \tag{5.3}$$

where $\hat{\alpha}_{best}^{[\Delta-1]}$ is the best timing vector from the previous iteration, $\hat{p}_{\alpha,i}$ is the ith perturbation vector of dimension N, and $|y|$ is the absolute value of y. When $\Delta = 1$, $\hat{\alpha}_{best}^{[0]}$ is randomly selected.

It is important to point out that the sum of $\hat{\alpha}_{best}^{[\Delta]}$, the best timing vector from the current iteration, generated from (5.3) is not equal to 1 because it is unnormalized. The normalized values of α_n that sum to unity are calculated as follows:

$$\alpha_n = \frac{\alpha_{n,best}^{[\Delta]}}{\sum \alpha_{n,best}^{[\Delta]}}, n = 1 \dots N, \tag{5.4}$$

where $\alpha_{n,best}^{[\Delta]}$ is the nth element of $\hat{\alpha}_{best}^{[\Delta]}$.

Algorithm 5.1 provides a heuristic determination of α that can reliably deliver identical results as the brute force method, but with a linear rather than exponentially complexity and thus significantly reduces convergence time and computational resources.

5.4. WPCN Throughput/Fairness Analysis and Optimization

The focus of this section is on sum-throughput/fairness analysis and optimization, where the latter is achieved through determining the optimal timing values for each H-AP and each combination sensor. Based on the assumed system model, the timing optimization problem in an EH system is formulated and solved both mathematically and algorithmically.

It is important to note that sum-throughput/fairness optimization is not equivalent to common throughput optimization. Common throughput optimization guarantees the Jain's fairness index *J*

[39] equals to unity, but at the expense of high computational complexity. Sum-throughput/fairness optimization presented in this section is not strictly focused on guaranteeing $J = 1$. Instead, the goal is maintaining high sum-throughput and equalizing the harvested energy at each sensor by controlling the timings of the H-APs to achieve high J with reduced computational complexity compared to that of common throughput optimization. To quantify the tradeoff between sum-throughput and fairness, a unified metric called the sum-throughput and fairness index product ($STFIP$) is proposed. The definition and implications of $STFIP$ are introduced later in this section.

Firstly, the length of energy harvesting/backscatter uplink phase τ_{EH}, length of downlink data decoding phase τ_{DL}, and uplink data transmission phase τ_{UL} must satisfy the constraint given by:

$$\sum_{n=1}^{N} \alpha_n \tau_{EH} + \sum_{k=1}^{K} \tau_{DL,k} + \sum_{k=1}^{K} \tau_{UL,k} \leq 1, \tag{5.5}$$

which follows from Fig. 5.2.

Assuming $P_{A,n}$, the transmission power of H-AP n is sufficiently large to negate receiver noise, the amount of energy harvested at each sensor k from each H-AP n is $E_{n,k} = \left\|\widehat{w}_n^T \hat{h}_{n,k}\right\| P_{A,n} \varsigma_k \alpha_n \tau_{EH}, n = 1 \dots N$ and the total energy harvested by sensor k from all the N H-APs, $E_k = \sum_{n=1}^{N} E_{n,k}$, is expressed as:

$$E_k = \varsigma_k \sum_{n=1}^{N} \alpha_n \left\|\widehat{w}_n^T \hat{h}_{n,k}\right\| P_{A,n} \tau_{EH}, k = 1 \dots K, \tag{5.6}$$

where $\widehat{w}_n^T$ is the transpose of the MS2-BABF complex weight vector for H-AP n, $\hat{h}_{n,k} = \left[h_{n,k,1} \dots h_{n,k,Q}\right]^T, n = 1 \dots N, k = 1 \dots K$, and ς_k is the EH efficiency at each sensor k, $0 < \varsigma_k < 1, k = 1 \dots K$. For simplicity, the chapter assumes $\varsigma_1 = \cdots = \varsigma_K = \varsigma$.

Following that, the received power $P_{R,k}$ at sensor $k, k = 1 \dots K$ is given by:

$$P_{R,k}(\alpha, \widehat{w}) = \sum_{n=1}^{N} \alpha_n \left\| \widehat{w}_n^T \hat{h}_{n,k} \right\| P_{A,n}, k = 1 \dots K, \tag{5.7}$$

where $\widehat{w} = [\widehat{w}_1 \dots \widehat{w}_N]$. Recall that $\widehat{w}_n$ is the beamforming weight vector of dimension Q at H-AP $n, n = 1 \dots N$.

Thus, the downlink data rate in bps/Hz of sensor k is expressed as:

$$R_{DL,k}(\tau_{EH,DL}, \tau_{DL,k}, \alpha, \widehat{w}, \lambda) = \tau_{DL,k} \log_2 \left(1 + \frac{P_{R,k}(1-\lambda)}{\Gamma \sigma^2}\right), \tag{5.8}$$

where $\tau_{EH,DL}$ is the portion of time allocated to the sensor nodes to harvest energy for the downlink data decoding phase, $R_{DL,k}(\tau_{EH,DL}, \tau_{DL,k}, \alpha, \widehat{w}, \lambda)$ is the rate of the sensor k calculated using the Shannon-Hartley theorem [61], Γ is the signal to noise ratio (SNR) gap from Shannon channel capacity due to use of a practical modulation and coding scheme, and σ^2 is the thermal noise power.

The uplink data rate in bits/second/Hz (bps/Hz) of sensor k operating in non-backscatter mode is expressed as:

$$R_{UL,k}(\tau_{EH,UL}, \tau_{UL,k}, \alpha, \widehat{w}) = \tau_{UL,k} \log_2 (1 + \varsigma_k \eta_k g_k \left(\frac{\sum_{n=1}^{N} \alpha_n P_{A,n} \left\| \widehat{w}_n^T \hat{h}_{n,k} \right\| \tau_{EH,UL}}{\Gamma \sigma^2 \tau_{UL,k}} + \frac{\sum_{n=1}^{N} \alpha_{n,prev} P_{A,n} \left\| \widehat{w}_{n,prev}^T \hat{h}_{n,k,prev} \right\| \lambda_{prev} \tau_{DL,prev}}{\Gamma \sigma^2 \tau_{UL,k}}\right)), k = 1 \dots K, \tag{5.9}$$

where $\tau_{EH,UL}$ is the portion of time allocated to the sensor nodes to harvest energy for the uplink data transmission phase, g_k is highest beamformed channel gain from sensor k, expressed as $g_k = \max\left(\left\| \widehat{w}_n^T \left[g_{n,k,1} \dots g_{n,k,Q} \right]^T \right\|\right), n = 1 \dots N$. ς_k is the EH efficiency at each sensor k, $0 < \varsigma_k < 1, k = 1 \dots K$, and η_k is the portion of harvested energy used for data transmission or decoding by each sensor k. The chapter assumes $\eta_1 = \cdots = \eta_K = \eta$ for simplicity.

Harvested energy from the previous time block needs to be considered because if sensor k operated in backscatter mode in the previous time block, there will be unused harvested energy remaining in the sensor k's capacitor previously discussed in Chapter 3. Therefore, $\alpha_{n,prev}, \widehat{w}_{n,prev}^{T}, \hat{h}_{n,k,prev}$, λ_{prev}, and $\tau_{DL,prev}$ are the proportion of time RF source n spends in transmitting energy, transpose of the weight vector, channel power fading gain vector, power splitting ratio, and duration of downlink data decoding phase in the previous time block, respectively. Note that $\alpha_{n,prev}, \widehat{w}_{n,prev}^{T}, \hat{h}_{n,k,prev}$, λ_{prev}, and $\tau_{DL,prev}$ are all zero if sensor k did not operate in backscatter mode in the previous time block.

Notice (5.9) does not include the rate achieved by sensor k when operating in backscatter mode. Let $R_{UL,B,k_B}(.,.)$ denote the uplink data rate in bits/second/Hz (bps/Hz) of sensor k_B (where the subscript B indicates sensor k is operating in backscatter mode). $R_{UL,B,k_B}(.,.)$ is calculated as follows [20]:

$$R_{UL,B,k_B}(\tau_{UL,B,k}, r_{d,k}) = \tau_{UL,B,k_B} \log_2\left(1 + \frac{g_k P_{R,k} s^2 \left(\frac{\mathrm{r}_{d,k}}{2}\right)^2 \left(\frac{4}{\pi}\right)^2}{\Gamma\sigma^2}\right), \tag{5.10}$$

where τ_{UL,B,k_B} is the amount of time k_B is operating in backscatter mode, s is a scaling term related to the sensor scattering efficiency, and $\mathrm{r}_{d,k}$ is the difference between antenna reflection coefficients r_0 and r_1 calculated via antenna load impedance switching according to the data bit '0' and '1', respectively at sensor $k, k = 1 \ldots K$. Mathematically, $\mathrm{r}_{d,k} = |r_0 - r_1|$.

To quantify the throughput rate fairness between sensors, Jain's fairness index, denoted by J, is adopted, given by [39]:

$$J = \frac{\left(\sum_{k=1}^{K}(R_{DL,k} + R_{UL,k})\right)^2}{K\sum_{k=1}^{K}(R_{DL,k} + R_{UL,k})^2}, \tag{5.11}$$

where $1/K \leq J \leq 1$, $1/K$ being the worst case (minimum rate fairness) and 1 is the best case (maximum rate fairness).

To maximize jointly the sum-throughput and fairness of the MS2-BABF/combo protocol, the following multi-objective joint optimization problem is formulated:

$$(P5.1): \quad \max_{\tau,\alpha,\widehat{w},\lambda}\{R_{sum}(\tau,\alpha,\widehat{w},\lambda), J\}, \tag{5.12a}$$

$$s.t. \left(\sum_{n=1}^{N} \alpha_n\left(\tau_{EH,DL} + \tau_{EH,UL} + \tau_{DL}\right)\right) + \tau_{UL} \leq 1, \tag{5.12b}$$

$$\tau_{EH,DL}, \tau_{EH,UL}, \tau_{DL,k}, \tau_{UL,k} \geq 0, k = 1 \dots K, \tag{5.12c}$$

$$R_{UL,k}\left(v,\alpha,\widehat{w},r_{d,k}\right) \geq 2R_{DL,k}(u,\alpha,\widehat{w},\lambda), k = 1 \dots K, \tag{5.12d}$$

$$\|\widehat{w}_n\|^2 = Q, n = 1 \dots N, \tag{5.12e}$$

$$0 < \lambda < 1, \tag{5.12f}$$

where $\tau = \left[\tau_{EH,DL}\ \tau_{EH,UL}\ \tau_{DL,1} \cdots \tau_{DL,K}\ \tau_{UL,1} \cdots \tau_{UL,K}\right]$, $\tau_{DL} = \sum_{k=1}^{K} \tau_{DL,k}$, $\tau_{UL} = \sum_{k=1}^{K} \tau_{UL,k}$, and $R_{sum}(\tau,\alpha,\widehat{w},\lambda) = R_{DL,sum}(u,\alpha,\widehat{w},\lambda) + R_{UL,sum}(v,\alpha,\widehat{w},r_{d,k})$. Furthermore, $u = \left[\tau_{EH,DL}\ \tau_{DL,1} \cdots \tau_{DL,K}\right]$, $v = \left[\tau_{EH,UL}\ \tau_{UL,1} \cdots \tau_{UL,K}\right]$, $R_{DL,sum}(u,\alpha,\widehat{w},\lambda) = \sum_{k=1}^{K} R_{DL,k}(u,\alpha,\widehat{w},\lambda)$, and $R_{UL,sum}\left(v,\alpha,\widehat{w},r_{d,k}\right) = \sum_{k=1}^{K} R_{UL,k}\left(v,\alpha,\widehat{w},r_{d,k}\right)$. Eqn. (5.12a) is the objective function whose decision variables are $\tau, \alpha, \widehat{w}$, and λ, (5.12b) is the time scheduling constraint from (5.5), (5.12c) is the non-negativity constraint for the decision variables, (5.12d) is the bandwidth allocation constraint where the uplink sum-throughput is assumed to be at least twice as fast as the downlink data rate [63], (5.12e) is the weight vector constraint, and (5.12f) is the power splitting ratio constraint. Eqn. (5.12d) can be modified if there are different uplink/downlink bandwidth requirements.

It is nearly impossible to solve problem (P5.1) directly because it is a multi-objective optimization (MOO) problem. One way to solve problem (P5.1) is to decompose it to three single-objective optimization (SOO) sub-problems. Given α_n is a proportion of τ_{EH} for the H-AP n, it follows that $\sum_{n=1}^{N} \alpha_n = 1$. To maintain high sum-throughput while equalizing the received power at each sensor, controlling the timings of the H-APs to maximize J can be done by finding the optimal α_n values denoted as α_n^*. These values can be obtained by solving the first sub-problem (P5.2):

$$(P5.2): \quad \max_{\alpha} J, \tag{5.13a}$$

$$s.t. \quad \sum_{n=1}^{N} \alpha_n = 1, \tag{5.13b}$$

$$\alpha_n \geq 0, n = 1 \dots N, \tag{5.13c}$$

$$\frac{1}{K} \leq J \leq 1. \tag{5.13d}$$

Like (P5.1), (P5.2) has a dependency on $\tau, \alpha, \widehat{w}$, and λ, which are all unknown at this point. However, if the optimal weight vectors $\widehat{w}^*$ for all the H-APs are known, an arbitrary non-zero value can be assumed for τ_{EH} to solve for a set of intermediate $E_k, k = 1 \dots K$ values to calculate α^* [14]. This means that the calculated α^* in (P5.2) will not result in a suboptimal solution for (P5.1). The calculated α^* can then be used to solve the two remaining sub-problems given by (P5.3) and (P5.4):

$$(P5.3): \quad \max_{u,\alpha,\widehat{w},\lambda} R_{DL,sum}(u, \alpha, \widehat{w}, \lambda), \tag{5.14a}$$

$$s.t. \quad \left(\sum_{n=1}^{N} \alpha_n (\tau_{EH,DL} + \tau_{DL}) \right) \leq 1, \tag{5.14b}$$

$$\tau_{DL,k} \geq 0, k = 1 \dots K, \tag{5.14c}$$

$$\tau_{EH,DL} + \tau_{EH,UL} \geq 0, \tag{5.14d}$$

$$\|\widehat{w}_n\|^2 = Q, n = 1 \dots N \tag{5.14e}$$

$$0 < \lambda < 1. \tag{5.14f}$$

$$(P5.4): \quad \max_{v,\alpha,\widehat{w},r_{d,k}} R_{UL,sum} \left(v, \alpha, \widehat{w}, r_{d,k}\right), \tag{5.15a}$$

$$s.t. \quad \left(\sum_{n=1}^{N} \alpha_n \tau_{EH,UL}\right) + \tau_{UL} \leq 1, \tag{5.15b}$$

$$\tau_{EH,UL}, \tau_{UL,k} \geq 0, k = 1 \dots K, \tag{5.15c}$$

$$\tau_{UL,B} \geq 0, k = 1 \dots K, \tag{5.15d}$$

$$0 < r_{d,k} < 1. \tag{5.15e}$$

The solutions to sub-problems (*P*5.3) and (*P*5.4) contribute to the solution of (*P*5.1) without resulting in a suboptimal solution because there is a direct proportionality between the sum-throughput of the uplink or downlink data decoding phase and optimum timings, and a constant optimal ratio of harvested energy to uplink or downlink data sum-throughput exists discussed in Chapter 3.

For both (*P*5.3) and (*P*5.4), the objective function specified by (5.14a) and (5.15a) is each concave and their corresponding constraint is affine. Hence, both (*P*5.3) and (*P*5.4) are each convex and can be solved using standard convex optimization techniques. Due to the constraints in (5.14b) and (5.15b) for (*P*5.3) and (*P*5.4), respectively, both will provide a solution in normalized time (i.e., $T = 1$). Note that this is an intermediate solution because adding the solutions of (*P*5.3) and (*P*5.4) together will result in a solution double the normalized time (i.e., $T = 2$), which does not satisfy the requirements for the constraint in (5.12b) in problem (*P*5.1).

However, the optimal τ^* values to satisfy problem (P5.1) using the values obtained from sub-problems (P5.3) and (P5.4) can be calculated using the following equations from Chapter 3:

$$\tau^*_{EH,DL} = \tau_{EH,DL} BR_{DL} \mathrm{Z}, \tag{5.16}$$

$$\tau^*_{EH,UL} = \tau_{EH,UL} BR_{UL} \mathrm{Z}, \tag{5.17}$$

$$\tau^*_{DL,k} = \tau_{DL,k} BR_{DL} \mathrm{Z}, k = 1 \dots K, \tag{5.18}$$

$$\tau^*_{UL,k} = \tau_{UL,k} BR_{UL} \mathrm{Z}, k = 1 \dots K, \tag{5.19}$$

where:

$$BR_{DL} = BB_{DL} \frac{R_{DL,sum} + R_{UL,sum}}{2R_{DL,sum}}, \tag{5.20}$$

$$BR_{UL} = BB_{UL} \frac{R_{DL,sum} + R_{UL,sum}}{2R_{UL,sum}}, \tag{5.21}$$

$$\mathrm{Z} = \frac{T}{BR_{DL}(\tau_{EH,DL} + \tau_{DL}) + BR_{UL}(\tau_{EH,UL} + \tau_{UL})}. \tag{5.22}$$

BB_{DL} and BB_{UL} are the downlink and uplink bandwidth bias, respectively, and Z is the time ratio to satisfy the constraint in (5.12b). Bandwidth bias is a parameter used to control the downlink and uplink bandwidth. As (5.12d) specifies the uplink data rate to be at least twice as fast as the downlink data rate [63], setting $BB_{DL} = 2$ and $BB_{UL} = 1$ will suffice.

Earlier in this section, $STFIP$ is introduced to quantify the tradeoff between sum-throughput and fairness, now defined mathematically as:

$$STFIP = R_{sum} \times J. \tag{5.23}$$

Clearly, to maintain the $STFIP$ at a given value, an increase in sum-throughput R_{sum} must be counter-balanced by a decrease in fairness index J. Now, if two protocols A and B achieves $STFIP_A$ and $STFIP_B$, respectively such that $STFIP_A > STFIP_B$, then protocol A exhibits a better tradeoff than protocol B. This follows from (5.23) where $STFIP$ increases with both R_{sum} and J,

so that the higher the $STFIP$, the better the balance in the tradeoff between the sum-throughput and fairness. $STFIP$ has the units of bps/Hz because J is dimensionless.

Analytical determination of $\alpha^*, \widehat{w}^*$, and k_B is non-trivial, hence we resort to a hybrid deterministic and heuristic method described in Algorithm 5.1 that jointly solves the three SOO sub-problems (*P*5.2), (*P*5.3), and (*P*5.4), which, in essence, provides a solution to the MOO problem (P5.1) as follows:

Algorithm 5.1 MS2-BABF/Combo Algorithm

1. **Input:** $N, K, Q, P_A, BB_{DL}, BB_{UL}, p_f, I, \epsilon$
2. **Output:** $\tau^*, \alpha^*, \widehat{w}^*, \lambda^*, R_{sum}(\tau^*, \alpha^*, \widehat{w}^*, \lambda^*), J$
3. Initialize H-AP time proportion value $\alpha_n = 1$, counter $\Delta = 1$, and weight vector $\widehat{w}_{n,best}^{[\Delta-1]}$ of size Q to any non-zero value for H-AP $n = 1$.
4. Generate I zero mean, variance one complex normally distributed perturbation vectors for H-AP $n = 1$, $\hat{p}_{w,1,i}$, of dimension Q.
5. Calculate weight vectors for the H-AP $n = 1$, $\widehat{w}_{1,i}^{[\Delta]}, i = 1 \dots I$ using (5.2).
6. Calculate the total received power $P_{sum,n}(\alpha_n, \widehat{w}_{n,i}^{[\Delta]}), n = 1 \dots N$ for all sensors from H-AP $n = 1$, $P_{sum,1} = \sum_{k=1}^{K} P_{R,k}(\alpha, \widehat{w}_{1,i}^{[\Delta]})$, assuming $\alpha_1 = 1$, using (5.7).
7. **If** $I \geq 2$:

   Repeat Step 6 for all remaining $\widehat{w}_{1,i}^{[\Delta]}, i = 2 \dots I$.

   Endif
8. Select $\widehat{w}_{1,i}^{[\Delta]}$ that produces the highest total received power $P_{sum,1}(\alpha_1, \widehat{w}_{1,i}^{[\Delta]})$ and assign it to $\widehat{w}_{1,best}^{[\Delta]}$.

9. **If** $\left|P_{sum,1}\left(\alpha_1, \widehat{w}_{1,best}^{[\Delta]}\right) - P_{sum,1}\left(\alpha_1, \widehat{w}_{1,best}^{[\Delta-1]}\right)\right| > \epsilon$:

Increase Δ by 1 and **repeat** Steps 4 to 8.

Else If $\left|P_{sum,1}\left(\alpha_1, \widehat{w}_{1,best}^{[\Delta]}\right) - P_{sum,1}\left(\alpha_1, \widehat{w}_{1,best}^{[\Delta-1]}\right)\right| \leq \epsilon$:

Assign $\widehat{w}_{1,best}^{[\Delta-1]}$ to $\widehat{w}_1^*$ and continue to Line 10.

Endif

10. **If** $N \geq 2$:

Repeat Steps 3 to 9 for all remaining H-APs $n, n = 2 \ldots N$ to find all remaining $\widehat{w}^*$ values.

Endif

11. **If** $N > K$:

Find $N - K$ H-AP(s) with the lowest $P_{sum,n}(\alpha_n, \widehat{w}_n^*)$ and set their corresponding $\alpha_n^* = 0$.

Endif

12. Reset iteration counter to $\Delta = 1$ and $\hat{\alpha}_{best}^{[\Delta-1]}$ of size N to any non-zero value.

13. Generate I zero mean, variance one normally distributed perturbation vectors $\hat{p}_{\alpha,i}$, of dimension N.

14. Calculate α vectors $\hat{\alpha}_i^{[\Delta]}, i = 1 \ldots I$ using (5.3).

15. Calculate the received power for each sensor k, $P_{R,k}\left(\hat{\alpha}_1^{[\Delta]}, \widehat{w}^*\right), k = 1 \ldots K$ using (5.7).

16. **If** $I \geq 2$:

Repeat Step 14 for all remaining $\hat{\alpha}_i^{[\Delta]}, i = 2 \ldots I$.

Endif

17. Select $\hat{\alpha}_i^{[\Delta]}$ that produces the lowest received power variance between sensors and assign it to $\hat{\alpha}_{best}^{[\Delta]}$. Received power variance between sensors is expressed as $var\left(P_{R,k}, k = 1 \dots K\right)$.

18. If $\left|var\left(P_{R,k}\left(\hat{\alpha}_{best}^{[\Delta]}, \hat{w}^*\right), k = 1 \dots K\right) - var\left(P_{R,k}\left(\hat{\alpha}_{best}^{[\Delta-1]}, \hat{w}^*\right), k = 1 \dots K\right)\right| > \epsilon$:

Increase Δ by 1 and **repeat** Steps 13 to 17.

Else If $\left|var\left(P_{R,k}\left(\hat{\alpha}_{best}^{[\Delta]}, \hat{w}^*\right), k = 1 \dots K\right) - var\left(P_{R,k}\left(\hat{\alpha}_{best}^{[\Delta-1]}, \hat{w}^*\right), k = 1 \dots K\right)\right| \leq \epsilon$:

Assign $\hat{\alpha}_{best}^{[\Delta-1]}$ as $\hat{\alpha}_{best}^{[\Delta]}$ and continue to Line 19.

Endif

19. Calculate $\alpha_n^*, n = 1 \dots N$ using (5.4).

20. Solve problem (P5.3) to get the optimal $\tau_{DL,k}$ and λ values in normalized time for each sensor $k, k = 1 \dots K$.

21. Calculate $R_{DL,k}(u, \alpha, \hat{w}, \lambda)$ in normalized time for all sensors, $k = 1 \dots K$ using (5.8).

22. Calculate the optimum $\tau_{EH,DL}$ in normalized time by $\tau_{EH,DL} = \left(\frac{\tau_{DL,k}\,(1-\lambda)}{\varsigma_k}\right)\left(\frac{\eta_k}{1-\eta_k}\right) - \lambda\tau_{DL}, k = 1 \dots K$.

23. Solve problem (P5.4) to get the optimal $\tau_{UL,k}$ and $r_{d,k}$ values in normalized time for each sensor $k, k = 1 \dots K$ currently not operating in backscatter mode. (If this is the first run, no sensors are currently operating in backscatter mode.)

24. Calculate $R_{UL,k}(v)$ in normalized time for all sensors k currently not selected to be operating in backscatter mode with (5.9). (If this is the first run, no sensors are currently operating in backscatter mode.)

25. Calculate the bandwidth ratios BR_{DL} and BR_{UL} using (5.20) and (5.21), respectively.

26. Calculate the time ratio Z using (5.22).

27. Calculate all τ^* values using (5.16) to (5.19) to obtain $R_{sum}(\tau, \alpha, \widehat{w}, \lambda)$.

28. If there are two or more sensors remaining not currently selected for operating in backscatter mode:

Select the sensor with the lowest SNR to operate in backscatter mode.

Else

Go to Line 32.

Endif

29. Repeat Steps 20 to 27 with the backscatter sensor(s) removed from the uplink data transmission phase.

30. Calculate the rate $R_{UL,B,k}(\tau^*_{UL,B,k}, r^*_{d,k})$ for the kth sensor(s) operating in backscatter mode using (5.10). τ^*_{UL,B,k_B} is determined such that all R_{UL,B,k_B} are equal.

31. Check if the difference between the current $R_{sum}(\tau^*, \alpha^*, \widehat{w}^*, \lambda^*)$ and the previous $R_{sum}(\tau^*, \alpha^*, \widehat{w}^*, \lambda^*)$ exceeds ϵ.

If the difference does not exceed ϵ:

Change the last sensor that entered backscatter mode back to non-backscatter mode and go to Line 32. The τ^* values are the τ^* values before the last sensor entered backscatter mode.

Else If the difference exceeds ϵ:

Add the next lowest SNR sensor into backscatter mode and go to Line 28.

Endif

32. End

The global controller in Fig. 5.1 runs Algorithm 5.1 at the beginning of each iteration of length T. For convenience, we assume $T = 1$ second.

Algorithm 5.1 starts off by selecting the input parameters of number of sensors in the system K, number of antennas per H-AP Q, transmit power of the H-AP P_A, downlink and uplink bandwidth bias BB_{DL} and BB_{UL}, respectively, MS2-BABF perturbation factor p_f, number of MS2-BABF perturbation vectors I, and convergence tolerance ϵ. Lines 3 to 11 find the optimal weight vectors $\widehat{w}^*$ for each H-AP. Lines 12 to 19 find the optimal α values α^* for each H-AP in concert with $\widehat{w}^*$. Lines 20 to 27 attempt to maximize the WPCN throughput with the current $\widehat{w}^*$ and α^* with no sensors in backscatter mode. Lines 28 to 32 consider the sensors one at a time, starting from the one with the lowest SNR, to operate in backscatter mode. The algorithm will keep at least one sensor in non-backscatter mode to ensure the τ_{EH} phase will not reduce to zero. Line 31 checks if there is any improvement in the WPCN throughput compared to the previous sensors' operation mode configuration. If not, it means adding more sensors to backscatter mode will not further increase the WPCN throughput and the global optimum solution has already been found. The algorithm will stop checking and revert to the previously calculated τ^* values for the global optimum solution.

The complexity of Algorithm 5.1 is $O(\Delta)$ if $\Delta \geq K$ and $O(K)$ if $\Delta < K$ because its complexity increases linearly with the number of iterations in lines 7, 10, 16, and 28. The length of vector I is typically set at 10 [52] because $\widehat{w}^*$ and α^* are found by a descent method that gets closer to the optimal solution after each perturbation. If I is too small, the algorithm will keep advancing the descent rather than conducting good descent steps, wasting processor resources and increasing the convergence time. However, if I is too large, more time will be spent finding the next descent step rather than advancing the descent, thus also increasing the convergence time. Algorithm 5.1 is a computationally light, linear complexity algorithm. The typical convergence time when $N = 5,\ Q = 4,\ K = 3$ is 110 milliseconds when Algorithm 5.1 is implemented using MATLAB and executed on a 4.2 gigahertz Intel Core i7 processor [71].

Algorithm 5.1 jointly optimizes τ, α, and $\widehat{w}$. This is different from the algorithm presented in Chapter 3, which only concerns τ and the algorithms in Chapter 4, which do not consider α.

5.5. Numerical Results and Discussion

5.5.1. System Configuration

Unless otherwise stated, a user is assumed to be equipped with $K = 3$ sensors. The network consists of $N = 5$ hybrid access points each with $Q = 4$ antennas spread out in a 10m^2 room with a 3m ceiling height. The H-APs are located 2m above the sensors that are mounted on-body 1m above ground. The user's location inside the room is random but uniformly distributed. The channel power gain values between antenna sensor k and H-AP n's antenna q, $h_{n,k,q}$, are calculated using (5.1), where, for the factor $\beta_{n,k,q}$, the Gamma parameters are $a = 1.192, b = 1.349$ [72] to reflect factors such as movement of the user of interest in a multiple input, single output (MISO) WPCN.

The sensor dropout threshold is the minimum throughput rate required by the sensor application. The channel bandwidth is assumed to be 1MHz like Bluetooth [66] to calculate the achievable data rate, where the sensor dropout threshold is 164kbps [68]. 164kbps is more than sufficient for most on-body applications, because a high resolution 12-bit, fast polling 10Hz 9-axis accelerometer sensor generates data at only approximately 1kbps (12 bits * 10/second * 9 axis = 1080bps). If a sensor's achievable data rate is below this threshold, the sensor will disconnect or drop out and come back online in the subsequent time block. The rest of the assumed system parameter values are listed in Table 5.1.

Table 5.1. Assumed System Parameter Values

Parameter	Definition	Value
PL_{ref}	Path loss at reference distance of 1m and transmitter frequency of 900MHz	30dB
ψ	Body shadowing loss margin	15dB [64]
φ	Path loss exponent	3.8 [65]
ς	EH efficiency at each sensor	0.5 [54]
η	Portion of harvested energy used for information transmission by each sensor	0.5 [60]
P_A	Hybrid access point transmission power	4000mW [56], [57]
Γ	SNR gap	1.5dB [67]
σ^2	Background noise power in 1MHz channels	-114dBm [66]
s	Tag scattering efficiency scaling	-1.1dB [20]
BB_{DL}	Downlink bandwidth bias	2 [63]

BB_{UL}	Uplink bandwidth bias	1 [63]
p_f	Perturbation factor	0.02 [52]
I	Perturbation vector quantity	10 [52]
ϵ	Difference checking precision	10^-4

The MS2-BABF/combo algorithm (Algorithm 5.1) was implemented and tested in a WPCN simulator using MATLAB with the assumed system parameter values listed in Table 5.1, unless otherwise stated. New $\hat{h}_{n,k,q}$ values and updated user location coordinates are generated at the beginning of each iteration of length $T = 1$ second to simulate ongoing changes in channel quality in a dynamic environment. The length of a simulation run is set to 1000 seconds (i.e., 1000 iterations) per specific combination of test parameters to assure the system is operating under steady-state condition that can be completed within a reasonable amount of time. Each data point in Figs. 5.3 to 5.11 represents the average of 1000 simulation runs.

The performance of the proposed MS2-BABF/combo protocol is compared against the MS2-BABF/hybrid protocol and the time-switching (TS) protocol. The MS2-BABF/hybrid protocol is a special case of the MS2-BABF/combo protocol. MS2-BABF/combo becomes MS2-BABF/hybrid when no sensors are operating in backscatter mode, which is skipping lines 28 to 31 in Algorithm 5.1. The TS protocol is a standard energy harvesting protocol in literature [13].

5.5.2. Results and Discussion

First, the MS2-BABF/combo protocol performance was investigated with regards to scaling the H-AP transmission power from 10mW (typical for a low power transmitter like Bluetooth [66]) to 4000mW (maximum allowed under Canadian and United States government

regulations [56], [57]) and compared against the performance of the MS2-BABF/hybrid and standard TS protocols. From Fig. 5.3 presenting the sum-throughput performance, the sum-throughput of all three protocols increase with the H-AP transmission power because a sensor's throughput is proportional to the harvested energy. MS2-BABF/combo consistently outperformed MS2-BABF/hybrid by an average of 17.8% with the highest percentage gain of 20.2% at 10mW. This is due to MS2-BABF/combo's increase in energy harvested with relation to available time for MS2-BABF/hybrid; made possible by utilizing a previously unused uplink data transmission phase. The WPCN sum-throughput of MS2-BABF/combo is always higher than MS2-BABF/hybrid for the range of the transmission power considered, because Algorithm 1 will default to MS2-BABF/hybrid if utilizing sensors in backscatter mode does not increase the WPCN throughput. Similarly, MS2-BABF/combo consistently outperformed TS by an average of 146.1% with highest gain of 295.5% at 10mW. Compared to TS, MS2-BABF/combo increases the harvested energy at the sensors via its multi-sensor optimized beamforming and multi-source selection and timing control.

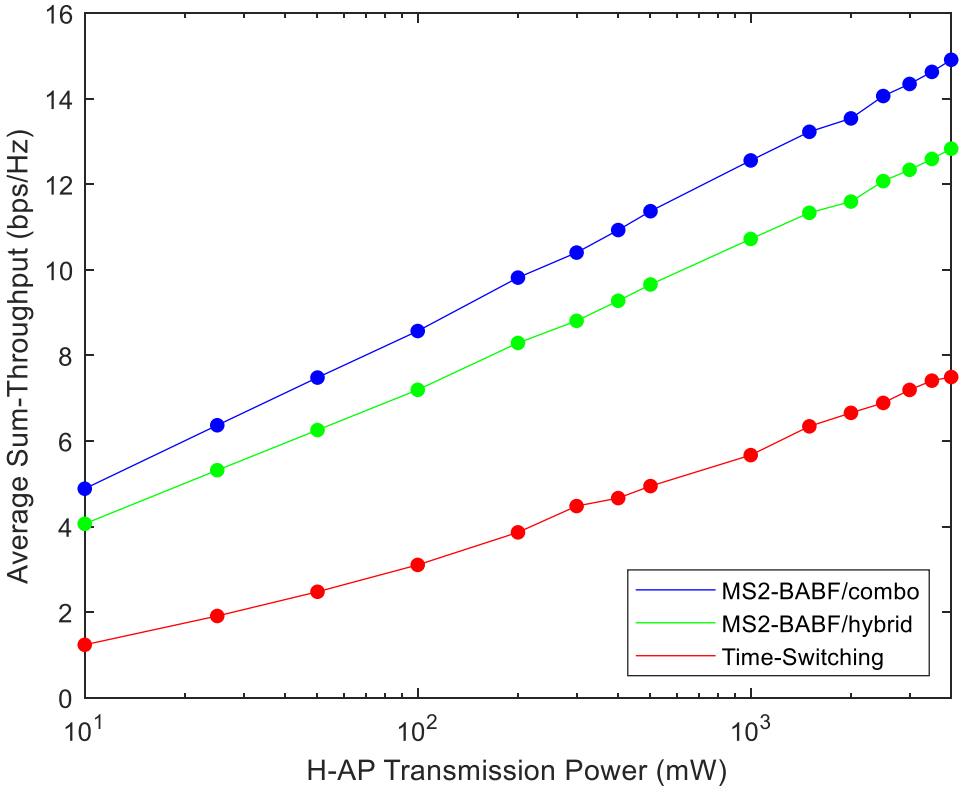

Fig. 5.3. Average sum-throughput versus H-AP transmission power.

From Fig. 5.4, MS2-BABF/hybrid and TS maintained $J \cong 0.85$ and $J \cong 0.77$, respectively, regardless of transmission power, whereas for the MS2-BABF/combo J slowly but steadily decreased from $J = 0.88$ to 0.80 as the transmission power increased from 10mW to 4000mW. The J for MS2-BABF/hybrid and TS does not increase with transmitted power because increasing the H-AP transmit power generally means proportionately increased received power at the sensors, so only the sum-throughput is increased. However, while all sensors benefit from an increase in harvested energy, MS2-BABF/combo's ability to operate some sensors in backscatter mode also mean some sensors gain more in individual throughput than others, resulting in reduced J.

Dropout rate for both the MS2-BABF/combo and MS2-BABF/hybrid was approximately zero at all transmission power settings because all sensors can harvest sufficient energy to maintain the minimum required throughput rate. On the other hand, TS has a dropout rate of 28.5% at 10mW because the sensors were unable to harvest sufficient energy to achieve the minimum required throughput rate. As the transmission power is increased, the TS dropout rate decreases monotonically to 1.6% at 100mW; a consequence of increased throughput rate at high transmission power thus increasing the likelihood of exceeding the minimum required throughput rate. The lower dropout rate for the MS2-BABF/combo and MS2-BABF/hybrid is a result of better time utilization and increased harvested energy compared to TS as described earlier.

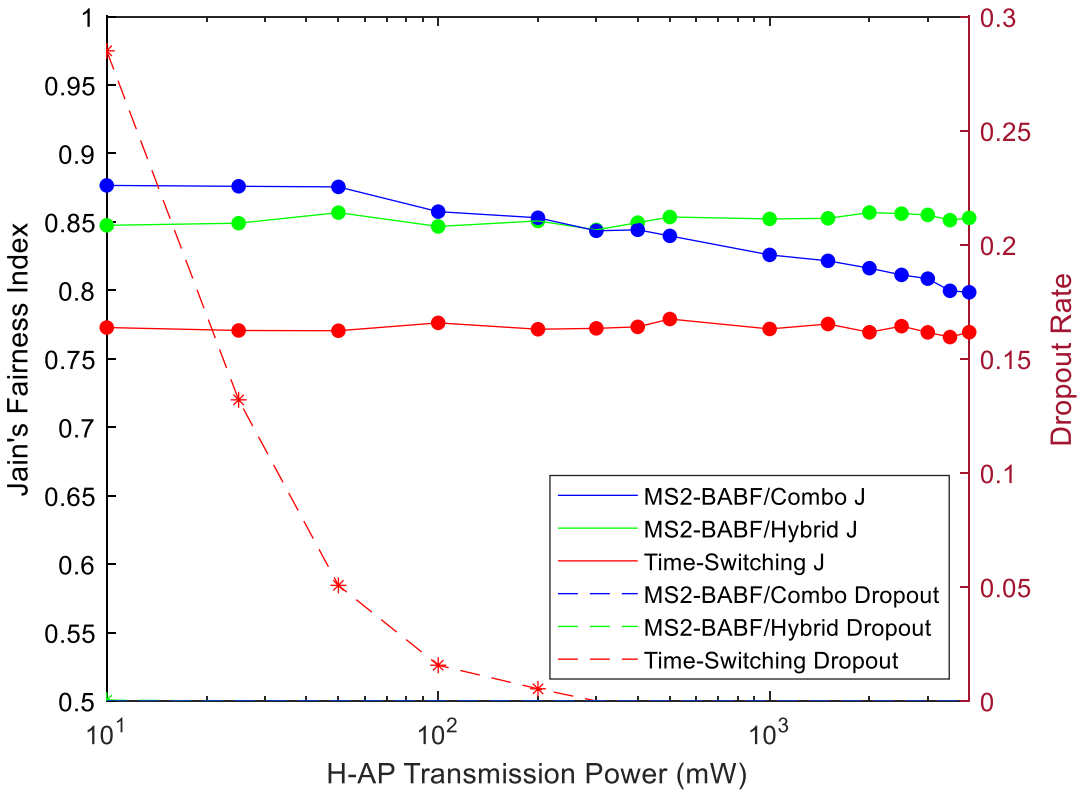

Fig. 5.4. Jain's fairness index and dropout rate versus H-AP transmission power.

Fig. 5.5 presents the tradeoff between sum-throughput and fairness, where the MS2-BABF/combo's $STFIP$ exceeds those of MS2-BABF/hybrid and TS over the range of transmission power considered. This is because the MS2-BABF/combo's sum-throughput increases faster than its decrease in J. From Fig. 5.5, increasing the transmission power of the H-AP achieves a better balance in the tradeoff between sum-throughput and fairness for MS2-BABF/hybrid and TS as well. This is because increasing the transmission power for MS2-BABF/hybrid and TS increases the sum-throughput without decreasing fairness as either protocol does not have a backscatter communication phase.

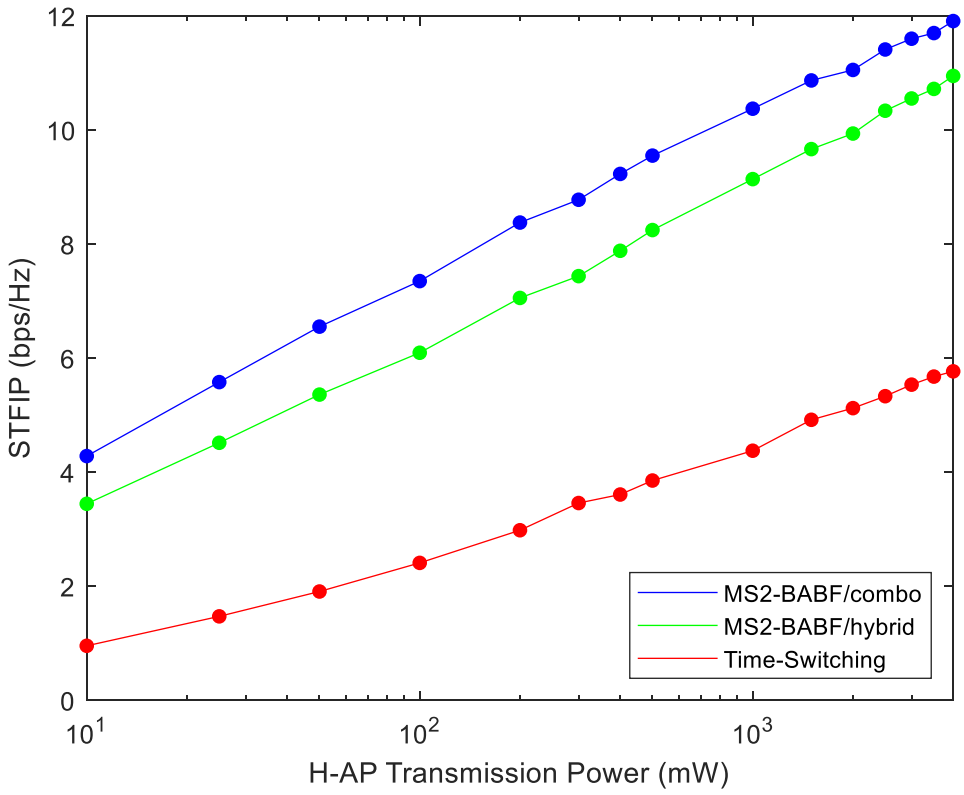

Fig. 5.5. STFIP versus H-AP transmission power.

Next, the impact of Q, the number of antennas per H-AP on the protocol performance was studied by varying Q from 1 to 8 considering the form factor of an H-AP. Clearly, $Q = 1$ and $Q >$

1 correspond to the single input, single output (SISO) and MISO configuration, respectively. It is observed from Fig. 5.6 that, as the number of antennas increases, the average sum-throughput for all three protocols consistently increases. This is because more antennas mean improved beamforming, hence higher received power at the sensors. However, MS2-BABF/combo consistently outperformed MS2-BABF/hybrid by an average of 16.1% due to its ability to utilize the backscatter communication phase. MS2-BABF/combo also consistently outperformed TS by an average of 93.3% because of increased harvested energy with its multi-sensor optimized beamforming and multi-source selection and timing control provided by Algorithm 5.1.

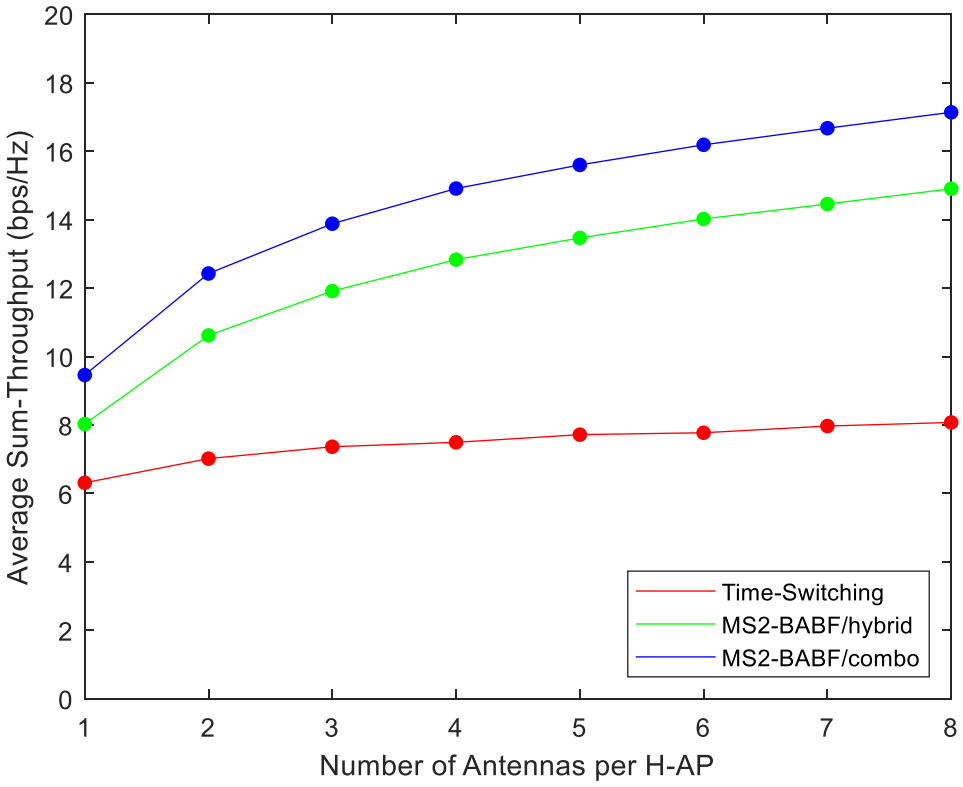

Fig. 5.6. Sum throughput versus number of antennas per H-AP.

From Fig. 5.7 showing fairness performance with respect to Q, it is observed that the WPCN fairness increased with Q in MS2-BABF/hybrid. This is because more antennas allow more

effective beamforming, thus better control for harvested energy at each sensor, resulting in increased fairness in the WPCN. On the other hand, the MS2-BABF/combo and TS's fairness remained at $J \cong 0.80$ and $J \cong 0.76$, respectively, regardless of Q. Although MS2-BABF/combo is based off MS2-BABF/hybrid and should exhibit an increase in J with Q, the MS2-BABF/combo's backscatter communication phase causes J to decrease as harvested energy increases as seen previously in Fig. 5.5. This means the increase in fairness due to more effective beamforming cancels out the decrease in fairness from the backscatter communication phase, keeping the MS2-BABF/combo's J approximately flat with Q. In Fig. 5.8, the MS2-BABF/combo's $STFIP$ exceeds that of the MS2-BABF/hybrid and TS for all Q; the best tradeoff between sum-throughput and fairness among its comparatives.

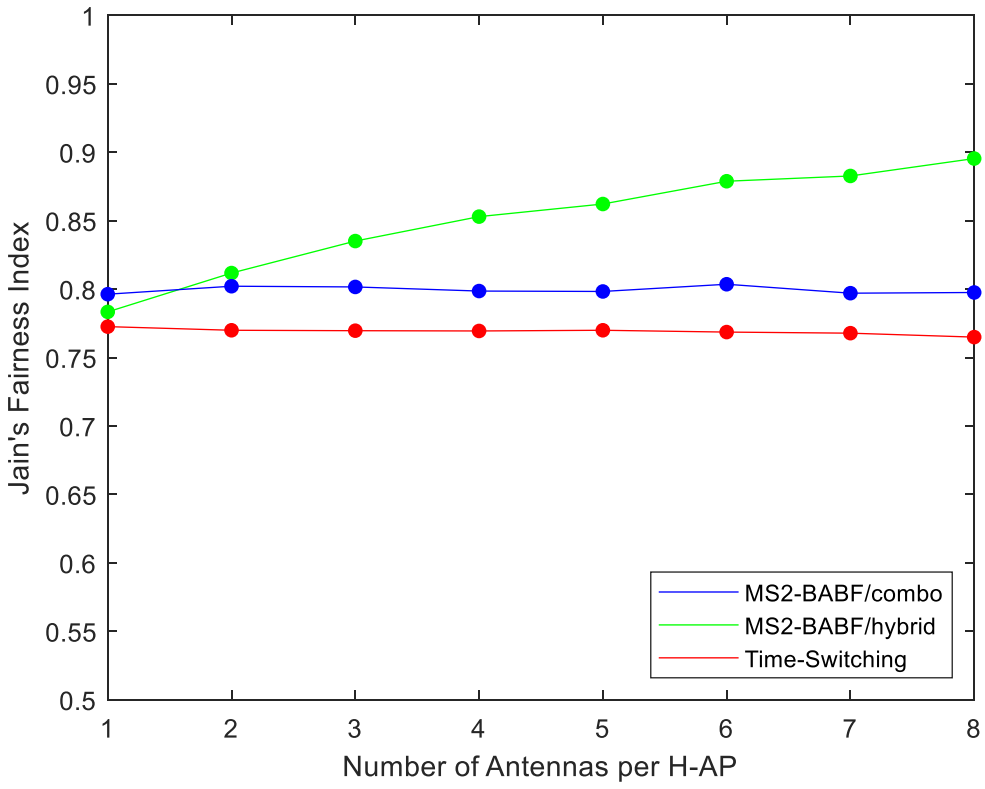

Fig. 5.7. Jain's fairness index versus number of antennas per H-AP (Dropout rate is zero in all cases).

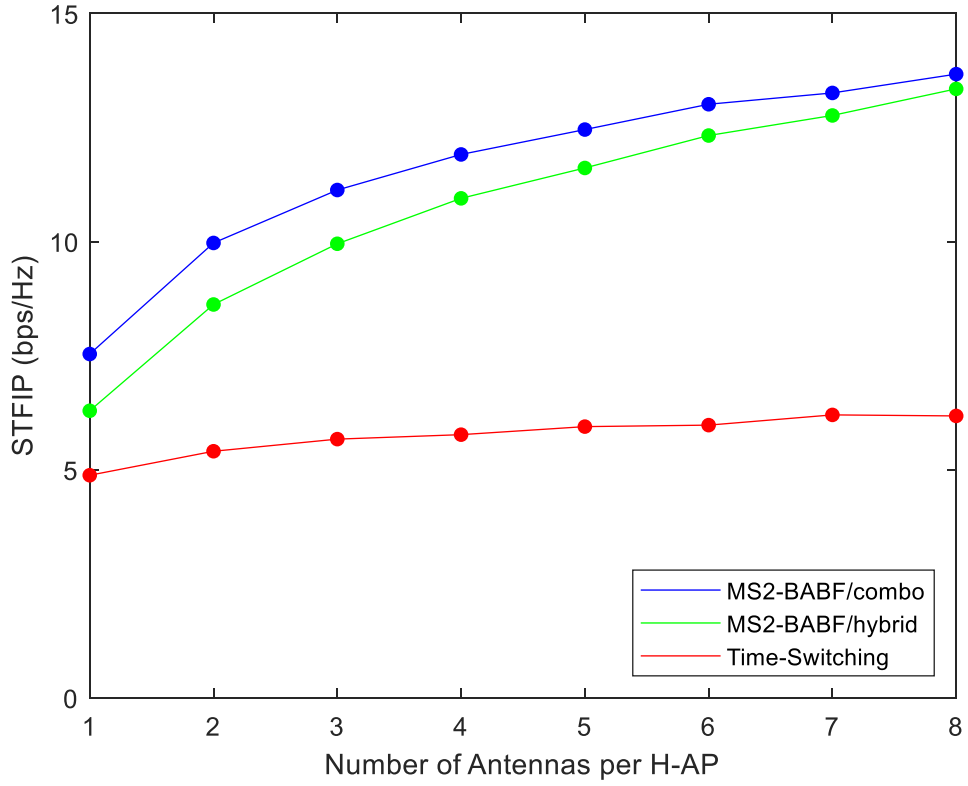

Fig. 5.8. STFIP versus number of antennas per H-AP.

Lastly, Figs. 5.9 to 5.11 present the effect of the number of transmitting H-APs on the protocol performance. The number of H-APs was varied from 1 to 5 considering a reasonable number of H-APs that can be placed inside a 10m^2 room.

In Fig. 5.9, the sum-throughput increases as the number of H-APs increase. This is not surprising considering more H-APs inside a room provide better coverage, which in turn increases the harvested energy. The proportion of time each H-AP spends in transmitting energy, α, is optimized to equalize the harvested energy between sensors, which increases fairness as well. This can be seen in Fig. 5.10, where J increased from 0.83 and 0.86 for MS2-BABF/hybrid when N

increases from 1 to 5. There is no significant increase in J when $N \geq 2$ because of the superior source scenario [14]. The superior source scenario suggests the H-AP from which the lowest energy is harvested by all sensors should be allocated no time in the time block T. The standard TS protocol's J ranged from only 0.73 to 0.77 with no source selection algorithm. Meanwhile, MS2-BABF/combo's J decreased slightly from 0.83 to 0.80 because the harvested energy equalization provided by Algorithm 1 does not affect the fairness of the WPCN when sensors communicate using backscatter mode. Both MS2-BABF/hybrid and MS2-BABF/combo have higher J compared to TS even at $N = 1$ is due to the multi-sensor optimized blind adaptive beamforming.

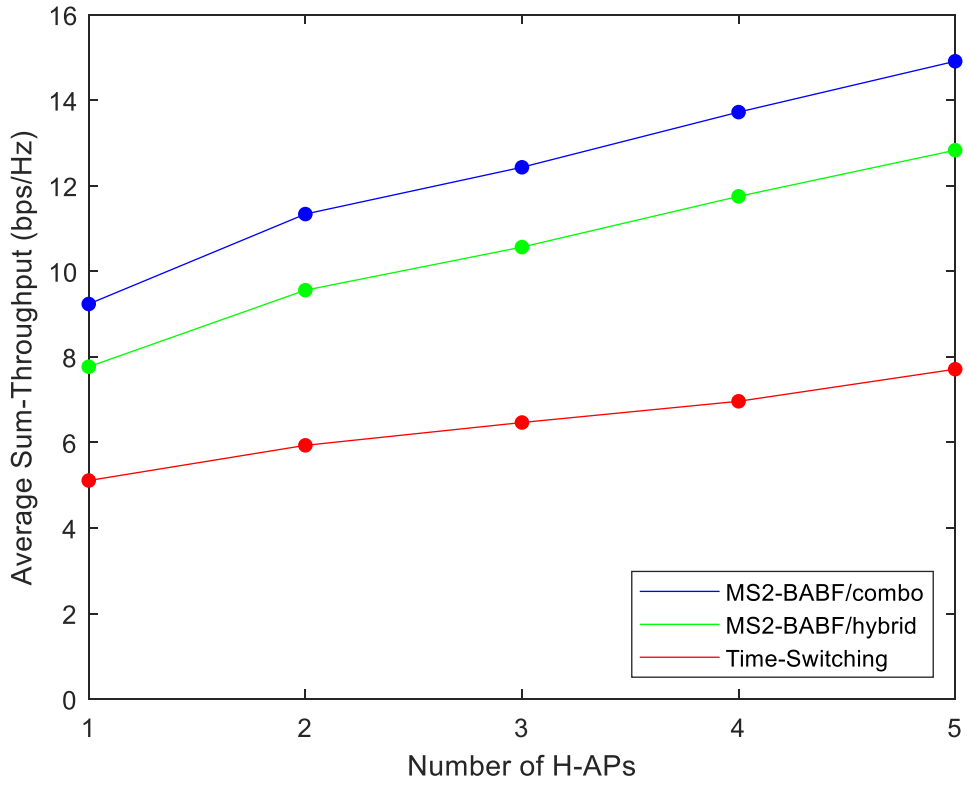

Fig. 5.9. Sum throughput versus number of H-APs.

Fig. 5.10. Jain's fairness index versus number of H-APs (Dropout rate is zero in all cases).

In Fig. 5.11, $STFIP$ performance for MS2-BABF/combo is better than MS2-BABF/hybrid and TS, meaning that the MS2-BABF/combo exhibits the best tradeoff between sum-throughput and fairness. Fig. 5.11 shows that increasing the number of H-APs has a positive impact on achieving a good balance in the tradeoff between sum-throughput and fairness.

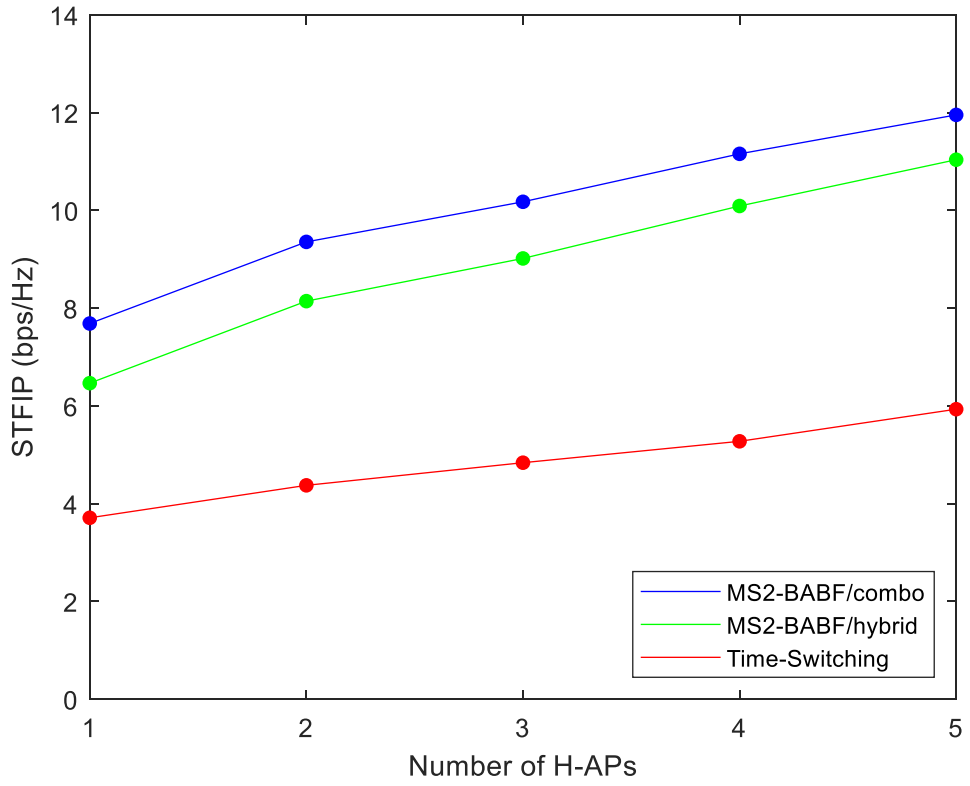

Fig. 5.11. STFIP versus number of H-APs.

From the results shown in Figs. 5.3 to 5.11, the MS2-BABF/combo and MS2-BABF/hybrid protocols always delivered higher performance than the reference TS protocol. Achieving the highest $STFIP$, the MS2-BABF/combo protocol positively trades fairness for higher sum-throughput compared to the MS2-BABF/hybrid protocol in all cases. However, if maximum J is

desired, MS2-BABF/combo can easily switch to MS2-BABF/hybrid when needed by not moving sensors into backscatter mode.

5.6. Summary

A multi-objective joint optimization problem where both the sum-throughput and fairness of an RF energy harvesting WPCN are maximized using multiple beamforming H-APs and backscatter communication-enabled combination sensors was formulated and solved in this chapter. Numerical results show that the MS2-BABF/combo protocol delivered the highest sum-throughput – up to approximately 296% increase compared to the reference standard time-switching energy harvesting protocol – with high fairness index J. The increase in J depends on the H-AP transmission power or number of H-APs. The MS2-BABF/combo protocol also resulted in a lower sensor dropout rate at low H-AP transmission power than that of the standard TS protocol.

CHAPTER 6: A COORDINATED AMBIENT/DEDICATED RADIO FREQUENCY ENERGY HARVESTING SCHEME USING MACHINE LEARNING[4]

6.1. Introduction

This chapter proposes a coordinated ambient/dedicated (CA/D) protocol where backscatter-enabled combination sensors are optimized to harvest energy from intended radio frequency (RF) sources when available and fall back to harvesting energy from unintended sources when only unintended sources are available. The CA/D protocol can use either of the two new machine learning techniques proposed, the linear forecaster with near-time linear regression-based enhancer (LFNTLRE) algorithm and an artificial neural network with environment detection (ANN-ED) algorithm, to determine the optimum energy harvesting (EH) schedule. These machine learning algorithms can reliably operate in environments where there is unpredictable availability of unintended sources and ongoing changes in channel conditions between the sensors and the unintended sources.

6.2. System Model

6.2.1. System Architecture

A user with K on-body sensors is considered. All sensors are equipped with a capacitor to temporarily store the harvested energy for operation. Each sensor using the CA/D RF EH protocol operates in dedicated mode when at least one hybrid access point (H-AP) running the multi-source, multi-sensor blind adaptive beamforming with combination sensors (MS2-BABF/combo protocol)

---

[4] The content of this chapter has generated one journal paper [35]: J. C. Kwan, J. M. Chaulk and A. O. Fapojuwo, "A Coordinated Ambient/Dedicated Radio Frequency Energy Harvesting Scheme using Machine Learning," in *IEEE Sensors Journal*, vol. PP, pp. 1-16, Jun. 2020.
The content of this chapter has generated one conference paper [36]: J. C. Kwan, J. M. Chaulk and A. O. Fapojuwo, "Artificial Neural Networks-based Ambient Radio Frequency Energy Harvesting with Environment Detection," to be submitted.

introduced in Chapter 5 is within the sensor range. Each sensor is considered connected to a wireless powered communication network (WPCN) when operating in dedicated mode. The CA/D RF EH protocol operating in dedicated mode encapsulates the backscatter-enabled MS2-BABF/combo protocol, which supports both downlink and uplink data communication between sensors and H-APs. An MS2-BABF/combo protocol-enabled WPCN comprises N H-APs each with Q antennas, which wirelessly communicates with the K on-body battery-less sensors. Each sensor $k, k = 1 \dots K$ is located at a certain radial distance $d_{1,1} = d_{1,2} = \cdots = d_{n,k}, n = 1 \dots N, k = 1 \dots K$ away, previously shown in Fig. 5.1. All H-APs are connected to the mains supply for power and are controlled by a global controller.

To prevent destructive wireless interference, all H-APs and sensors in the WPCN can transmit only during their allocated time slot. As such, all H-APs are connected to an Internet-enabled global controller, which has knowledge of all the H-APs and sensors in the WPCN within the global controller's coverage area; consistent with previous chapters. The sensors can make themselves known to the global controller via a registration message piggy-backed on the first data packet transmission to incur minimal signalling overhead. Sensed data is transmitted from the sensors to the H-APs in the WPCN, which subsequently can be uploaded to the Internet. The H-APs in the WPCN can also transmit data such as location coordinates and artificial neural network data from the cloud via the H-APs to the sensors.

Each sensor using the CA/D RF EH protocol operates in ambient mode when all H-APs using the MS2-BABF/combo protocol are out of sensor range. In this case, the sensor is not connected to the WPCN. The sensors will harvest energy from unintended RF energy sources such as the nearby cell phone towers. Due to the unpredictable nature and low amount of energy that can be harvested from unintended RF energy sources [18], [30], all wireless data communication

functions on the sensors will be disabled when operating in ambient mode. Instead, the sensors will sleep when harvesting energy and wake up periodically, whose wake-up frequency depends on how much energy can be harvested to sense data such as heart rate or body temperature. The sensed data will be temporarily stored on the sensors' internal memory until at least one H-AP using the MS2-BABF/combo protocol is within range. Once an H-AP is within sensor range, the sensors will operate in dedicated mode again with its wireless data communication functions enabled to upload the temporarily stored data to the Internet.

6.2.2. Spatial Configuration of Ambient Sources

For simplicity, only cell phone towers are considered as ambient RF EH sources for on-body sensors due to their ubiquity, range of operating frequencies, and continuous signal nature [18]. Wi-Fi access points are not considered because of their non-continuous signal nature, low transmission power, and generally indoor-only availability [18]. Other potential ambient RF EH sources such as radio stations are not considered because their low operating frequency requires large antennas, which cannot be used with on-body sensors. The Ginibre point process is used to represent the spatial configuration of these cell phone towers [30] due to its suitability for networks with repulsion, and the process can be efficiently simulated using a method described in [73].

Consistent with the literature [30], this chapter considers two operating scenarios of interest: (1) the urban environment, and (2) the rural environment. In the urban environment, 142 cell phone towers are distributed over a 2.5 km by 1.8 km region with the probability factor 0.86, shown in Fig. 6.1 [30]. In the rural environment, 149 cell phone towers are distributed over a 75 km by 65 km region with the probability factor 0.02, shown in Fig. 6.2 [30].

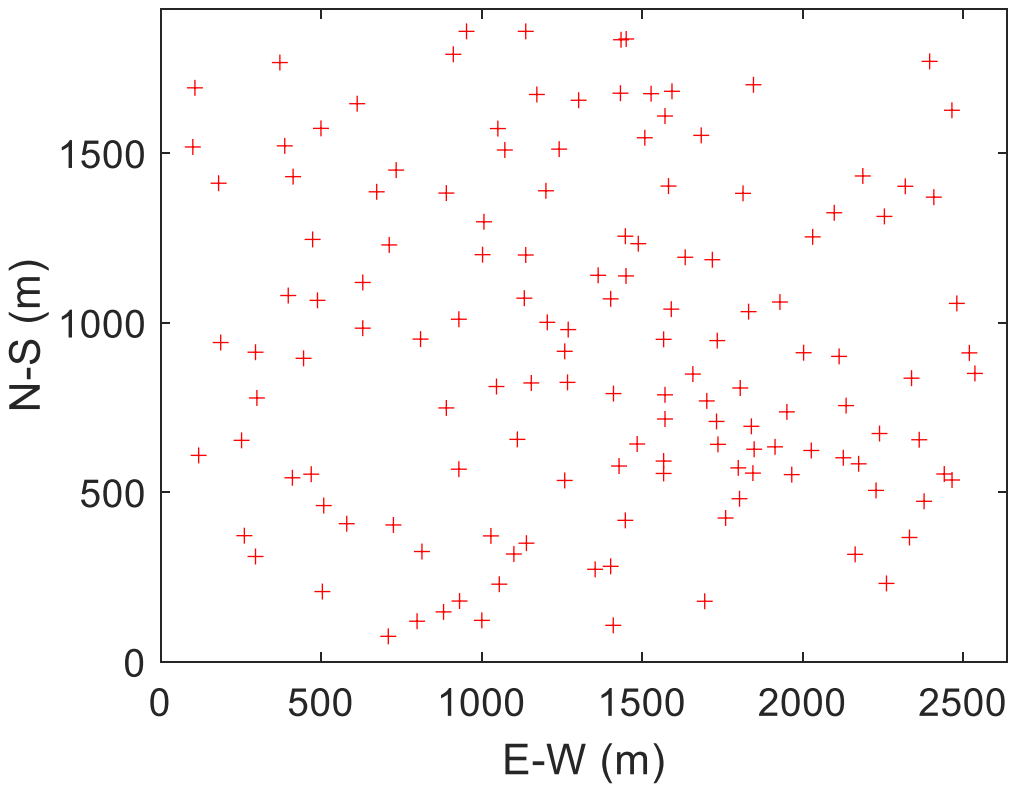

Fig. 6.1. Cell phone tower locations in the urban environment.

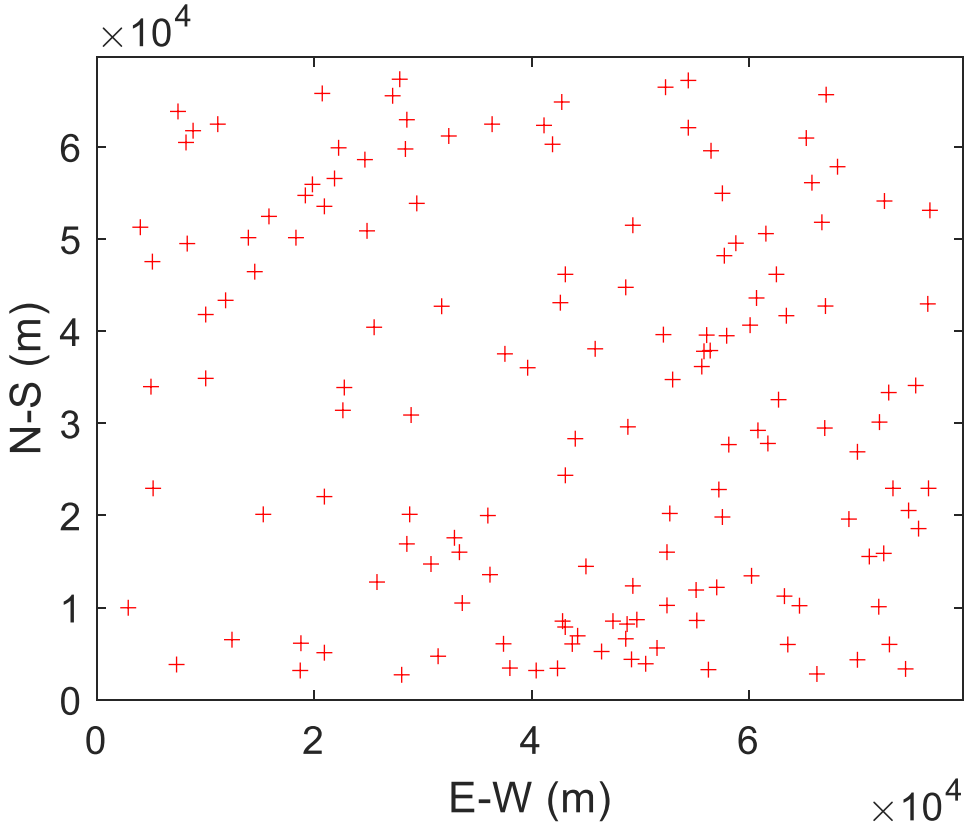

Fig. 6.2. Cell phone tower locations in the rural environment.

6.2.3. Channel Propagation Model

The propagation channel is modeled by path loss, shadowing, and small-scale fading. The log-distance path loss model is assumed with path loss exponent φ and small-scale fading is modeled by Nakagami-*m* fading with fading depth parameter m and average power parameter Ω. Shadow fading is modeled by a fixed body shadowing loss margin ψ for analytic simplicity.

The channel power gain between sensor k and source n's antenna q, $h_{n,k,q}$, is calculated using [59]:

$$h_{n,k,q} = 10^{-\frac{(PL_{ref}+\psi_{n,k,q})}{10}} \left(\frac{d_{n,k}}{d_{ref}}\right)^{-\varphi} \beta_{n,k,q}, n = 1 \dots N, k = 1 \dots K, q = 1 \dots Q, d_{n,k} > d_{ref}, \quad (6.1)$$

where PL_{ref} is the path loss in dB at the reference distance d_{ref}, $\psi_{n,k,q}$ is the body shadowing loss margin in dB between antenna q at the source n and sensor k, $d_{n,k}$ is the distance between source n and sensor k, and $\beta_{n,k.q}$ is the small-scale fading channel power gain between the sensor k and H-AP n's antenna q. Recall that in dedicated mode the source is an H-AP in a WPCN and in ambient mode the source is a cell phone tower.

Based on the assumed Nakagami-*m* small-scale fading, $\beta_{n,k,q}$ is Gamma distributed with the shape parameter $A = m$ and the scale parameter $B = \Omega/m$ [59]. For simplicity, the chapter assumes $\psi_{1.1,1} = \cdots = \psi_{n,k.q} = \psi, n = 1 \dots N, k = 1 \dots K, q = 1 \dots Q$. In dedicated mode, the channel reciprocity holds; where the uplink channel power gain between sensor k and H-AP n's antenna q, $g_{n,k,q}$, is equal to $h_{n,k,q}$, i.e. $g_{n,k,q} = h_{n,k,q}, n = 1 \dots N, k = 1 \dots K, q = 1 \dots Q$. In ambient mode, the cell phone towers are assumed to radiate power evenly and constantly in all directions. As such, Q is set to 1 in this chapter for simplicity because the maximum output power is limited by government regulations.

The fading channel power gain is assumed to remain constant for an entire time block $T = 1$ second, but varies from block to block. A time block is a logical base unit of time to represent real time in simulation. $T = 1$ second is chosen because it is easy to work with and short enough to ensure the assumption of constant fading channel power gain during that time period is reasonable.

6.3. Proposed Coordinated Ambient/Dedicated Radio Frequency Energy Harvesting Protocol

The coordinated ambient/dedicated radio frequency energy harvesting (CA/D RF EH) protocol proposed in this chapter enables sensors to operate in two modes: ambient and dedicated.

In the ambient mode, the harvested energy at each sensor $k, k = 1 \ldots K$ during time block $T = 1$ second from the N cell phone towers within range of the K sensors can be calculated as follows:

$$E_{H,k} = \varsigma_k P_C \sum_{n=1}^{N} h_{n,k}\,, \tag{6.2}$$

where ς_k is the EH efficiency at each sensor k, $0 < \varsigma_k < 1$, and P_C is the transmission power of each cell phone tower. For simplicity, the chapter assumes $\varsigma_1 = \cdots = \varsigma_K = \varsigma$. $E_k^{[\Delta_B]}$, the capacitor energy level of sensor k at the beginning of a session, is related to the harvested energy $E_{H,k}$, as the capacitor energy level increases due to $E_{H,k}$, where Δ_B is the beginning of the corresponding session. Hence, $E_k^{[\Delta]}$, the current capacitor energy level of sensor k at the end of the ambient session counter Δ, decreases due to operations like data sensing.

The CA/D RF EH protocol is presented in Algorithm 6.1. The input variable $E_{C,k}$ is the energy required for sensor k to wake up and check the capacitor energy level.

Algorithm 6.1 Coordinated Ambient/Dedicated Algorithm

1. **Input:** $E_{C,k}$, `WPCN_signal_strength, signal_strength_threshold, default_next_wake_up_time`.
2. **Output:** $E_k^{[\Delta_B]}$, `operating_mode` (ambient or dedicated).
3. Check $E_k^{[\Delta_B]}$. This hardware parameter can be simulated by $E_k^{[\Delta_B]}$ = last known capacitor energy level + any capacitor energy level changes since the sensor last woke up.
4. **If** $E_k^{[\Delta_B]} \geq E_{C,k}$

   Go to Step 5.

Else

A sensor outage has occurred. Sleep and wait for `default_next_wake_up_time` to wake up, then go back to Step 3.

Endif

5. **If** the `WPCN_signal_strength >= signal_strength_threshold`

   Reset the ambient session counter Δ to 0 and set `operating_mode = dedicated`.

   Else

   Set the ambient session counter Δ to 0 if uninitialized and set `operating_mode = ambient`. Invoke Algorithm 6.2 if it is an LFNTLRE sensor or Algorithm 6.4 if it is an ANN sensor.

   Endif

Line 1 lists the input parameters required by Algorithm 6.1, comprising $E_{C,k}$, `WPCN_signal_strength` (the received signal strength at each sensor from the H-APs in the WPCN), `signal_strength_threshold` (the minimum received signal strength at each sensor from the H-APs in the WPCN to operate in dedicated mode), and `default_next_wake_up_time`. Line 2 lists the output parameters: $E_k^{[\Delta_B]}$ and the operating mode the algorithm will operate in. Lines 3 and 4 check if the sensor has sufficient harvested energy stored in the capacitor to operate its onboard electronics and sense data. Line 5 checks the signal strength and decides whether to operate the sensor in ambient or dedicated mode. When `operating_mode = dedicated`, the sensor will run the backscatter-enabled MS2-

BABF/combo protocol [34]. When `operating_mode = ambient`, the sensor will continue with either Algorithm 6.2 if it is an LFNTLRE sensor or 6.4 if it is an artificial neural network (ANN) sensor, described in the next section. Algorithm 6.1 runs on every sensor. Algorithm 6.1 has complexity $O(1)$ because it runs in constant time.

6.4. Machine Learning Algorithms for Determining Optimum Sensor Data Collection Schedule

The problem of operating the sensors in dedicated mode was solved in Chapter 5 with the MS2-BABF/combo protocol. However, operating sensors in the CA/D RF EH protocol's ambient mode has not yet been solved, which forms a contribution of this chapter.

Due to the unpredictable availability and often slow energy harvesting rate from ambient sources compared to those of dedicated sources, sensors operating in ambient mode should be in sleep mode by default and only wake up when there is sufficient energy to sense data. However, a sensor will not know the currently stored energy level until it wakes up and checks the internal capacitor charge status. But energy is expended at each wake up, so if there is insufficient energy to operate the electronic circuits for sensing data, the energy used to wake the sensor will be wasted or may even cause a sensor power outage. Ideally, sensors should only wake up when there is sufficient energy to sense data, but practically proves to be a challenging problem when the energy arrival rate and capacitor charge status are not known a-priori.

To address this challenge, this chapter proposes two separate machine learning algorithms to determine the optimum sensor data sensing schedule (i.e., the optimum time for the sensor to wake up and sense data). The first is the linear forecaster with near-time linear regression-based enhancer (LFNTLRE), while the second is based on an artificial neural network (ANN).

6.4.1. Linear Forecaster with Near-Time Linear Regression-Based Enhancer (LFNTLRE)

The proposed LFNTLRE (Algorithm 6.2) has the ability to adapt to the environment it operates in on-the-fly. However, it requires a limited history of live data for it to work well and hence requires more sensor memory than ANN.

For a simple linear forecaster, the relationship between the predicted capacitor energy level at the beginning of the next session, $E_k^{[\Delta_B+1]}$, and the next wake up time for sensor k, $T_{w,k}^{[\Delta]}$, can be expressed as:

$$E_k^{[\Delta_B+1]} = \overline{E_{HR,k}^{[\Delta]}} T_{w,k}^{[\Delta]} + E_k^{[\Delta]}, k = 1 \dots K, \tag{6.3}$$

where $\overline{E_{HR,k}^{[\Delta]}}$ is the most recent known average energy harvesting rate. $\overline{E_{HR,k}^{[\Delta]}}$ can be obtained by comparing $E_k^{[\Delta-1]}$ in relation to $E_k^{[\Delta_B]}$, compensating for the energy used for sensor k to wake up and check the capacitor energy level:

$$\overline{E_{HR,k}^{[\Delta]}} = \frac{E_k^{[\Delta_B]} - E_k^{[\Delta-1]} + E_{C,k}}{T_{w,k}^{[\Delta-1]}}. \tag{6.4}$$

where $E_k^{[\Delta-1]} = 0$ if $E_k^{[\Delta-1]}$ is undefined, $T_{w,k}^{[\Delta-1]}$ is the time since sensor k last woke up, and $E_k^{[\Delta-1]}$ is the capacitor energy level at the end of the previous session.

Since $E_k^{[\Delta_B+1]} \geq E_{C,k} + E_{S,k}$ for the sensor k to sense data at least once, where $E_{S,k}$ is the energy required for sensor k to sense data once, we write:

$$E_{C,k} + E_{S,k} \leq \overline{E_{HR,k}^{[\Delta]}} T_{w,k}^{[\Delta]} + E_k^{[\Delta]}. \tag{6.5}$$

Rearranging (6.5) to calculate the minimum required $T_{w,k}^{[\Delta]}$ using the most recent known average energy harvesting rate:

$$T_{w,k}^{[\Delta]} = \frac{E_{C,k} + E_{S,k} - E_k^{[\Delta]}}{\overline{E_{HR,k}^{[\Delta]}}}. \tag{6.6}$$

Note that the linear forecaster only considers the most recent known average energy harvesting rate to predict the next wake up time based on the sensor energy consumption. This technique, while simple, is inadequate in an ambient RF EH environment where the user can walk closer or further away from a cell phone tower, which will quickly cause considerable increases or decreases in the energy harvesting rate. The dynamic ambient RF EH environment's channel conditions are also affected by factors such as fast fading, which will cause the energy harvesting rate to fluctuate. This may result in an overly conservative next wake up time prediction (i.e., wake up time is excessively long) when the user is walking towards a cell phone tower, resulting in the capacitor to charge to its maximum capacity and the sensor not sensing as much data as it could. It may also result in an overly aggressive next wake up time prediction (i.e., very short wake up time) when the user is walking away from a cell phone tower, resulting in sensor outages.

Adding a near-time linear regression-based enhancer rectifies this problem by considering the current capacitor charge level in conjunction with the average energy harvesting rate trend via a capacitor energy depletion ratio, $S_{R,k}, k = 1 \ldots K, 0 \leq S_{R,k} \leq 1$. Physically, $S_{R,k}$ is the maximum fraction of the remaining energy stored in sensor k's capacitor that can be used to predict its next wake up time. From an algorithm perspective, $S_{R,k}$ fine tunes how aggressive or conservative $T_{w,k}^{[\Delta]}$ is. A value closer to 1 increases the aggression for a faster wake up time. Conversely, a value closer to 0 is more conservative, where the sensor should wait longer to harvest energy based on information from the linear forecaster.

The LFNTLRE algorithm considers four near-time trends of various depths, where the trends are learned using the least squares method in linear regression [74]. The depth of the near-time trends is expressed as D, where $D = 2, 3, 5,$ or 10 for the trends of the current plus 1, 2, 4, or 9 previous session's average energy harvesting rates, respectively. Four near-time trends of various depths with a maximum trend depth of 10 is selected so the LFNTLRE algorithm has enough information to establish reasonable confidence in near-time for determining $S_{R,k}$. However, it will also prevent the algorithm from taking too long to determine $S_{R,k}$ such that it becomes ineffective in adapting to the environment. When there is insufficient information to determine $S_{R,k}$, it is initialized to zero.

Using the linear regression least squares method, consider time on the X axis and average energy harvesting rate on the Y axis at each time point. Let $T_{t,k}$ denote the total elapsed time since a reference start time of zero when the value on the Y axis is $\overline{E_{HR,k}^{[\Delta-(\mathrm{D}-1)]}}$ to the time when the value on the Y axis is $\overline{E_{HR,k}^{[\Delta]}}$. The total elapsed time over D depths since the reference start time, $T_{t,k}$, is calculated by:

$$T_{t,k} = \sum_{d=1}^{D-1} T_{w,k}^{[\Delta-\mathrm{d}]}. \tag{6.7}$$

The average $\bar{T}_{t,k}, k = 1 \ldots K$, can be obtained as follows:

$$\bar{T}_{t,k} = \frac{\sum_{d=0}^{D-1}\left(T_{t,k} - \sum_{i=1}^{d} T_{w,k}^{[\Delta-i]}\right)}{D}. \tag{6.8}$$

The current (i.e., most recent) average energy harvesting rate $\overline{E_{HR,k}^{[\Delta]}}$ is at time $T_{t,k}$, meaning we are calculating the total average elapsed time over D depths since the reference start time in Fig. 6.3.

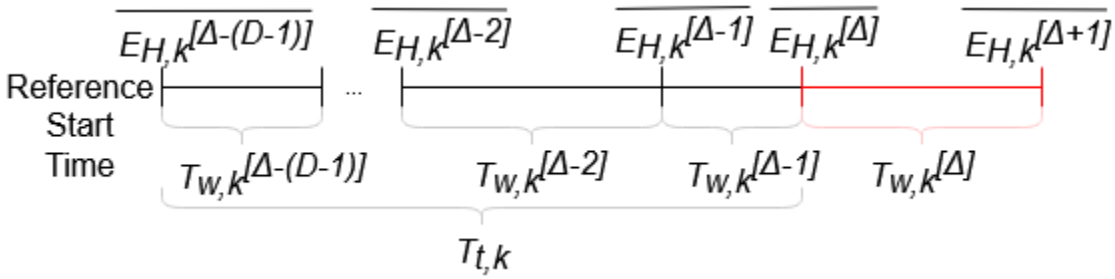

Fig. 6.3. Timing diagram illustrating the relationship between time and energy.

Next, the average energy harvesting rate in the considered D for sensor k, $\bar{E}_{D,k},, k = 1 \dots K$ can be calculated:

$$\bar{E}_{D,k} = \frac{\sum_{d=0}^{D-1} \overline{E_{HR,k}^{[\Delta-\mathrm{d}]}}}{D}. \tag{6.9}$$

Therefore, average energy harvesting acceleration (if positive) or deceleration (if negative) for sensor k at depth D, $\bar{E}_{T,D,k}, k = 1 \dots K$, can be learned:

$$\bar{E}_{T,D,k} = \frac{\sum_{d=0}^{D-1} \left(\left(\left(T_{t,k} - \sum_{i=1}^{d} T_{w,k}^{[\Delta-i]} \right) - \bar{T}_{t,k} \right) \left(\overline{E_{HR,k}^{[\Delta-\mathrm{d}]}} - \bar{E}_{D,k} \right) \right)}{\sum_{d=0}^{D-1} \left(\left(T_{t,k} - \sum_{i=1}^{d} T_{w,k}^{[\Delta-i]} \right) - \bar{T}_{t,k} \right)^2}. \tag{6.10}$$

The normalized average energy harvesting acceleration, denoted by $\bar{E}_{T,D,k}$, $x_{E_{T,D,k}}, D = 2, 3, 5, 10$, for each k where $k = 1 \dots K$ is calculated by:

$$x_{\bar{E}_{T,D,k}} = \frac{\bar{E}_{T,D,k} - \min\left(\bar{E}_{T,D,k}, D = 2,3,5,10\right)}{\max\left(\bar{E}_{T,D,k}, D = 2,3,5,10\right) - \min\left(\bar{E}_{T,D,k}, D = 2,3,5,10\right)}, \tag{6.11}$$

where $\max(.)$ and $\min(.)$ are functions returning the largest and smallest of their arguments, respectively.

Consider the case when sensor k still has sufficient energy at the end of the session to wake up again and sense data at least once. In this case, there is no risk of a sensor miss in the next session. Therefore, $S_{R,k}$ can be more aggressive (i.e., closer to 1). $S_{R,k}, k = 1 \dots K$ is calculated as

a weighted sum of the four normalized average energy harvesting acceleration $x_{\bar{E}_{T,D,k}}, D = 2,3,5,10, k = 1 \dots K$:

$$S_{R,k} = 0.4x_{\bar{E}_{T,2,k}} + 0.3x_{\bar{E}_{T,3,k}} + 0.2x_{\bar{E}_{T,5,k}} + 0.1x_{\bar{E}_{T,10,k}}, \tag{6.12}$$

where the weights in (6.12) are heavier for more recent trends to ensure a quick response to changes in the environment. Note that the weights in (6.12) must sum to unity.

Next, consider the other case when the sensor k does not have sufficient energy at the end of the session to wake up again and sense data at least once. For this scenario, there is some risk of a sensor miss occurring in the next session if the sensor does not harvest enough energy. Therefore, $S_{R,k}$ needs to be more conservative (i.e., closer to 0).

First, sort the values of $x_{\bar{E}_{T,D,k}}, D = 2,3,5,10$, for each k where $k = 1 \dots K$ in ascending order into the array $\hat{x}_{\bar{E}_{T,k}}$:

$$\hat{x}_{\bar{E}_{T,k}} = \begin{bmatrix} \min\left(x_{\bar{E}_{T,D,k}}, D = 2,3,5,10\right) \\ \vdots \\ \max\left(x_{\bar{E}_{T,D,k}}, D = 2,3,5,10\right) \end{bmatrix} = \begin{bmatrix} x_{\bar{E}_{T,k}}^{[1]} \\ x_{\bar{E}_{T,k}}^{[2]} \\ x_{\bar{E}_{T,k}}^{[3]} \\ x_{\bar{E}_{T,k}}^{[4]} \end{bmatrix}, \tag{6.13}$$

where the superscript j in $x_{\bar{E}_{T,k}}^{[j]}, j = 1, 2, 3, 4$ denotes the value of $x_{\bar{E}_{T,k}}$ in the jth position of the sorted set.

Next, use $\hat{x}_{\bar{E}_{T,k}}$ to determine $S_{R,k}, k = 1 \dots K$:

$$S_{R,k} = 0.7x_{\bar{E}_{T,k}}^{[1]} + 0.15x_{\bar{E}_{T,k}}^{[2]} + 0.1x_{\bar{E}_{T,k}}^{[3]} + 0.05x_{\bar{E}_{T,k}}^{[4]}, \tag{6.14}$$

where the weights in (6.14) are heavier for slower trends, resulting in a more conservative $S_{R,k}$.

Modifying the linear forecaster in (6.6) by adding the near-time linear regression-based enhancer parameter $S_{R,k}$, the next wake up time for sensor $k, k = 1 \dots K$ can be predicted:

$$T_{w,k}^{[\Delta]} = \left\lceil \frac{E_{C,k} + E_{S,k} - E_k^{[\Delta]} S_{R,k}}{\overline{E_{HR,k}^{[\Delta]}}} \right\rceil, \tag{6.15}$$

The ceiling function is used in (6.15) to prevent lower than expected harvested energy due to a down-rounded predicted next wake up time. Using only positive integer values for $T_{w,k}^{[\Delta]}$ makes better use of limited computational resources on a sensor due to reduced memory usage and to also allow compatibility with low-precision clocks.

The LFNTLRE algorithm is presented in Algorithm 6.2. The input variable S_{max} is the maximum number of times a sensor can sense data in one session regardless of the capacitor energy level. S_{max} is arbitrarily set by the user depending on user preference. The input variables E_k and $T_{w,k}$ respectively store the values of energy level and wake up time for all the previous sessions. Sensor reserve energy is necessary to prevent the sensor from using all of its harvested energy to sense data thus completely running out of energy. A good value of E_{res} is $E_{C,k}$ to ensure the sensor will have sufficient energy to wake up and complete Algorithm 6.2 in the next session.

Algorithm 6.2 Linear Forecaster with Near-Time Linear Regression-Based Enhancer Algorithm

1. **Input:** $E_k^{[\Delta_B]}, E_{C,k}, E_{S,k}, E_k, T_{w,k}, S_{max}, E_{res}$, `operating_mode = ambient`.
2. **Output:** $T_{w,k}^{[\Delta]}$.
3. **If** the ambient session counter, Δ, is not defined:

   Initialize $\Delta = 0$.

   Endif
4. **If** the sensor miss counter, `sensor_miss_count`, is not defined:

Initialize `sensor_miss_count` = 0.

Endif

5. If $E_k^{[\Delta_B]} \geq E_{C,k} + E_{S,k} + E_{res}$

If $E_k^{[\Delta_B]} \geq E_{C,k} + S_{max}E_{S,k} + E_{res}$

- Sense data S_{max} times.

- Update $E_k^{[\Delta]} = E_k^{[\Delta_B]} - (E_{C,k} + S_{max}E_{S,k})$.

Else

- Sense data $\left\lfloor \frac{E_k^{[\Delta_B]} - E_{C,k} - E_{res}}{E_{S,k}} \right\rfloor$ times.

- Update $E_k^{[\Delta]} = E_k^{[\Delta_B]} - (E_{C,k} + \left\lfloor \frac{E_k^{[\Delta_B]} - E_{C,k} - E_{res}}{E_{S,k}} \right\rfloor E_{S,k})$.

Endif

Else

A sensor miss has occurred because $E_{C,k} \leq E_k^{[\Delta_B]} < E_{C,k} + E_{S,k} + E_{res}$.

Increase `sensor_miss_count` by 1.

Endif

6. Calculate $\overline{E_{HR,k}^{[\Delta]}}$ using (6.4).

7. If $\Delta \geq 10$

- Calculate $E_{T,D,k}$ for $D = 2,3,5$, and 10 using (6.10).

- Calculate $x_{\bar{E}_{T,D,k}}, D = 2,3,5,10$ using (6.11).

If $E_k^{[\Delta]} \geq E_{C,k} + E_{S,k} + E_{res}$

Calculate $S_{R,k}$ using (6.12).

Else

Determine $\hat{x}_{\bar{E}_{T,k}}$ and $S_{R,k}$ using (6.13) and (6.14), respectively.

Endif

Else

Set $S_{R,k} = 0$.

Endif

8. Determine $T_{w,k}^{[\Delta]}$ using (6.15) with $\overline{E_{HR,k}^{[\Delta]}}$ calculated in Step 6.

9. Increment Δ by 1.

10. Wait $T_{w,k}^{[\Delta]}$ seconds and start from the beginning of Algorithm 6.1.

Each LFNTLRE sensor runs Algorithm 6.2 when set to operate in the ambient mode from Algorithm 6.1. Line 1 lists the input parameters required by Algorithm 2. Line 2 lists the output parameter, which is $T_{w,k}^{[\Delta]}$. Uninitialized variables are initialized in lines 3 and 4. Line 5 determines how much data to sense in the current session and senses the data. Line 7 finds the $S_{R,k}$ value. The condition $\Delta \geq 10$ is set in line 7 because of the maximum depth $D = 10$. $T_{w,k}^{[\Delta]}$ is determined by executing line 8. Algorithm 6.2 has complexity $O(1)$ because it runs in constant time. Its low complexity allows it to run on sensors with limited resources.

6.4.2. Artificial Neural Network

The second machine learning algorithm (Algorithms 6.3 and 6.4) proposed for the CA/D RF EH protocol's ambient mode uses an artificial neural network (ANN) [75]. The ANN takes the

last successful wake up time $T_{w,k}^{[\Delta-1]}$ and current energy level at the beginning of a session $E_k^{[\Delta_B]}$ to predict the next wake up time. A successful wake up time is defined as the $T_{w,k}^{[\Delta-1]}$ that immediately precedes a session where the sensor wakes up and successfully senses data at least once.

The training of the ANN starts off with data being processed in the cloud. When a sensor is connected to the WPCN, the sensor will upload to the cloud the training data set comprising information collected when it was operating in ambient mode. This information includes its full history of times since the sensor last successfully woke up, its corresponding history of capacitor energy level at the beginning of the sessions, and its corresponding record of all accurately predicted wake up times. Energy consumption for sensor-to-cloud communication and vice-versa do not need to be considered here. This is because the sensor-to-cloud communication and vice-versa only occur when a sensor is connected to the WPCN. When connected to the WPCN, sensors have a relatively reliable and consistent RF EH source.

The full history of all successful last wake up times for all sensors will be stored in the array $\hat{T}_w$ in the cloud. The entire corresponding history of capacitor energy levels at the beginning of the sessions will be stored in the array $\hat{E}$ in the cloud. The entire corresponding history of all accurately predicted wake up times will be stored in the array $\hat{T}_p$ in the cloud. The cloud will process the data to train a neural network to predict the next wake up time, which will be periodically sent to the sensors as updates when connected to the WPCN. As more sensors collect and upload data to the cloud, the more accurate the model will become.

The advantage of ANN is that the sensor algorithm is extremely simple and requires minimal sensor memory for storing a history of live data, because all the training was previously done in the cloud. Furthermore, it requires only the immediate live data to accurately function.

However, it is not adaptive to the environment it operates in and instead depends on a trained artificial neural network, which is technically offline to the environment and can be inaccurate if insufficiently trained.

The inputs, otherwise known as features, need to be normalized for the ANN to ensure the features have the same scale. The average of all known successful wake up times for all sensors, $\bar{T}_w$, is calculated as follows:

$$\bar{T}_w = \frac{1}{Z}\sum_{z=1}^{Z} \hat{T}_w^{[z]}, \tag{6.16}$$

where z is the array indexing element and Z is the size of the training data set. The size of all three arrays are the same.

The standard deviation for all known successful wake up times for all sensors, $\sigma_{\hat{T}_w}$, is obtained by:

$$\sigma_{\hat{T}_w} = \sqrt{\frac{\sum_{z=1}^{Z}\left(\hat{T}_w^{[z]} - \bar{T}_w\right)^2}{Z}}. \tag{6.17}$$

Next, the average of all known capacitor energy levels for all sensors at the beginning of the sessions, $\bar{E}$, is calculated by:

$$\bar{E} = \frac{1}{Z}\sum_{z=1}^{Z} \hat{E}^{[z]}. \tag{6.18}$$

The standard deviation for $\hat{E}$, $\sigma_{\hat{E}}$, can be obtained from the following equation:

$$\sigma_{\hat{E}} = \sqrt{\frac{\sum_{z=1}^{Z}\left(\hat{E}^{[z]} - \bar{E}\right)^2}{Z}}. \tag{6.19}$$

The maximum value in the array $\hat{T}_p$, denoted as $T_{p,max}$, is expressed as:

$$T_{p,max} = \max\left(\hat{T}_p\right). \tag{6.20}$$

Physically, $T_{p,max}$ is the longest accurately predicted wake up time for all sensors.

The normalized last successful wake up times, $\hat{x}_T$, and normalized corresponding capacitor energy levels, $\hat{x}_E$, used for training is calculated as follows:

$$\hat{x}_T = \begin{bmatrix} x_T^{[1]} \\ x_T^{[2]} \\ \vdots \\ x_T^{[Z]} \end{bmatrix} = \frac{1}{\sigma_{\hat{T}_w}} \begin{bmatrix} \hat{T}_w^{[Z]} - \bar{T}_w \\ \hat{T}_w^{[Z-1]} - \bar{T}_w \\ \vdots \\ \hat{T}_w^{[1]} - \bar{T}_w \end{bmatrix}, \tag{6.21}$$

$$\hat{x}_E = \begin{bmatrix} x_E^{[1]} \\ x_E^{[2]} \\ \vdots \\ x_E^{[Z]} \end{bmatrix} = \frac{1}{\sigma_{\hat{E}}} \begin{bmatrix} \hat{E}^{[Z]} - \bar{E} \\ \hat{E}^{[Z-1]} - \bar{E} \\ \vdots \\ \hat{E}^{[1]} - \bar{E} \end{bmatrix}. \tag{6.22}$$

The corresponding normalized known accurately predicted wake up times, $\hat{y}_T$, used for training is calculated using:

$$\hat{y}_T = \begin{bmatrix} y_T^{[1]} \\ y_T^{[2]} \\ \vdots \\ y_T^{[Z]} \end{bmatrix} = \frac{1}{T_{p,max}} \begin{bmatrix} \hat{T}_p^{[Z]} \\ \hat{T}_p^{[Z-1]} \\ \vdots \\ \hat{T}_p^{[1]} \end{bmatrix}. \tag{6.23}$$

The normalized training data needs to be fed forward into the ANN. Two different activation functions $f_A(x)$, rectified linear unit (ReLU) and logistic, and their corresponding derivatives, $f_A{}'(x)$, are used for the urban and rural environments, respectively. ReLU works better for urban environments and logistic works better for rural environments from our experimentation. x is any numerical input value operated on element-wise.

The ReLU activation function and its derivative are defined as follows [76]:

$$ReLU(x) = \max(0, x), \tag{6.24}$$

$$ReLU'(x) = \begin{cases} 1, & \text{if x} > 0 \\ 0, & \text{otherwise.} \end{cases} \tag{6.25}$$

The logistic activation function and its derivative are [77]:

$$\sigma(x) = \frac{1}{1 + e^{-x}}, \tag{6.26}$$

$$\sigma'(x) = \sigma(x)\big(1 - \sigma(x)\big). \tag{6.27}$$

The ANN used for the CA/D RF EH protocol's ambient mode has 1 input layer, 2 hidden layers with 64 neurons per layer, and 1 output layer as shown in Fig. 6.4. This ANN topology was chosen to achieve the best balance in the tradeoff between the complexity of the ANN and its prediction accuracy. The feed forward equation for the first 64-neuron hidden layer, $\hat{z}_1$, as a function of x_T and x_E is:

$$\hat{z}_1 = \begin{bmatrix} z_1^{[1]} \\ z_1^{[2]} \\ \vdots \\ z_1^{[64]} \end{bmatrix} = \widehat{w}_1 \begin{bmatrix} x_T \\ x_E \end{bmatrix} + \hat{b}_1, \tag{6.28}$$

where $\widehat{w}_1 \in \mathbb{R}^{64\times 2}$ and $\hat{b}_1 \in \mathbb{R}^{64\times 1}$ are matrix of the weights and vector of the biases of the first layer, respectively.

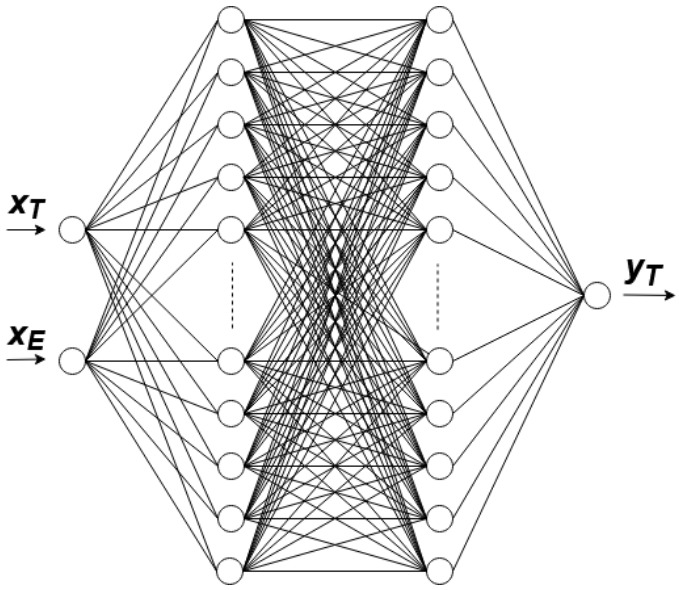

Fig. 6.4. Artificial neural network architecture that has 2 hidden layers with 64 neurons each.

The values to be fed into the second 64-neuron hidden layer, $\hat{a}_1$, can be obtained by:

$$\hat{a}_1 = \begin{bmatrix} a_1^{[1]} \\ a_1^{[2]} \\ \vdots \\ a_1^{[64]} \end{bmatrix} = f_A(\hat{z}_1). \tag{6.29}$$

The feed forward equation for the second 64-neuron hidden layer, $\hat{z}_2$, is:

$$\hat{z}_2 = \begin{bmatrix} z_2^{[1]} \\ z_2^{[2]} \\ \vdots \\ z_2^{[64]} \end{bmatrix} = \hat{w}_2 \hat{a}_1 + \hat{b}_2, \tag{6.30}$$

where $\hat{w}_2 \in \mathbb{R}^{64\times64}$ and $\hat{b}_2 \in \mathbb{R}^{64\times1}$ are matrix of the weights and vector of the biases of the second layer, respectively.

Consequently, the values to be fed into the output layer, $\hat{a}_2$, are:

$$\hat{a}_2 = \begin{bmatrix} a_2^{[1]} \\ a_2^{[2]} \\ \vdots \\ a_2^{[64]} \end{bmatrix} = f_A(\hat{z}_2). \tag{6.31}$$

The feed forward equation for the output layer, $\hat{z}_3$, is:

$$\hat{z}_3 = \left[z_3^{[1]}\right] = \hat{w}_3 \hat{a}_2 + \hat{b}_3, \tag{6.32}$$

where $\hat{w}_3 \in \mathbb{R}^{1\times 64}$ and $\hat{b}_3 \in \mathbb{R}^{1\times 1}$ are matrices of the weights and biases of the output layer, respectively.

The values to be fed into the output error calculation, $\hat{a}_3$, are:

$$\hat{a}_3 = \left[a_3^{[1]}\right] = \left[z_3^{[1]}\right]. \tag{6.33}$$

The output error, $\hat{\delta}_3$, as a function of y_T, is given by:

$$\hat{\delta}_3 = \left[\delta_3^{[1]}\right] = \left(\left[a_3^{[1]}\right] - [y_T]\right). \tag{6.34}$$

The output error needs to be back propagated. From $\hat{\delta}_3$, the output error for the second layer, $\hat{\delta}_2$, can be calculated:

$$\hat{\delta}_2 = \begin{bmatrix} \delta_2^{[1]} \\ \delta_2^{[2]} \\ \vdots \\ \delta_2^{[64]} \end{bmatrix} = \left(\hat{w}_3{}^T \hat{\delta}_3\right) \odot f_A{}'^{(\hat{z}_2)}, \tag{6.35}$$

where the notation $\odot$ denotes element-by-element multiplication.

Following that, the output error for the second layer is back propagated to the first layer. The output error for the first layer, $\hat{\delta}_1$, is:

$$\hat{\delta}_1 = \begin{bmatrix} \delta_1^{[1]} \\ \delta_1^{[2]} \\ \vdots \\ \delta_1^{[64]} \end{bmatrix} = \left(\hat{w}_2{}^T \hat{\delta}_2\right) \odot f_A{}'(\hat{z}_1). \tag{6.36}$$

A gradient descent optimizer known as root mean square propagation (RMSprop) [77] is used to accelerate convergence of the error between the target and predicted outputs.

The exponential weighted moving average of gradients for the first layer's weights and biases, $RMS_{w,1}$ and $RMS_{b,1}$, respectively, are:

$$\widehat{RMS}_{w,1}^{[i]} = 0.9[\widehat{RMS}_{w,1}]^{[i-1]} + 0.1\begin{bmatrix} x_T\delta_1^{[1]} & x_E\delta_1^{[1]} \\ x_T\delta_1^{[2]} & x_E\delta_1^{[2]} \\ \vdots & \vdots \\ x_T\delta_1^{[64]} & x_E\delta_1^{[64]} \end{bmatrix}^2 + \begin{bmatrix} \varepsilon & \varepsilon \\ \varepsilon & \varepsilon \\ \vdots & \vdots \\ \varepsilon & \varepsilon \end{bmatrix}, \tag{6.37}$$

$$\widehat{RMS}_{b,1}^{[i]} = 0.9[\widehat{RMS}_{b,1}]^{[i-1]} + 0.1\left[\hat{\delta}_1\right]^2 + \begin{bmatrix} \varepsilon \\ \varepsilon \\ \vdots \\ \varepsilon \end{bmatrix}, \tag{6.38}$$

where $\widehat{RMS}_{w,1} \in \mathbb{R}^{64\times 2}$ and $\widehat{RMS}_{b,1} \in \mathbb{R}^{64\times 1}$. In (37) and (38), the superscript i is the iteration indexing element and ε is a very small arbitrary number used to prevent division by zero. In this case, $\varepsilon = 10^{-20}$. If $i = 0$, all the RMS values are initialized to zero. The selected weights of 0.9 and 0.1 are standard constants for optimum performance in RMSprop [77].

Next, the exponential weighted moving average of gradients for the second layer's weights and biases, $RMS_{w,2}$ and $RMS_{b,2}$, respectively, are:

$$\widehat{RMS}_{w,2}^{[i]} = 0.9\left[\widehat{RMS}_{w,2}\right]^{[i-1]} + 0.1\begin{bmatrix} a_1^{[1]}\delta_2^{[1]} & \cdots & a_1^{[64]}\delta_2^{[1]} \\ a_1^{[1]}\delta_2^{[2]} & \cdots & a_1^{[64]}\delta_2^{[2]} \\ \vdots & \ddots & \vdots \\ a_1^{[1]}\delta_2^{[64]} & \cdots & a_1^{[64]}\delta_2^{[64]} \end{bmatrix}^2 + \begin{bmatrix} \varepsilon & \cdots & \varepsilon \\ \varepsilon & \cdots & \varepsilon \\ \vdots & \ddots & \vdots \\ \varepsilon & \cdots & \varepsilon \end{bmatrix}, \tag{6.39}$$

$$\widehat{RMS}_{b,2}^{[i]} = 0.9\begin{bmatrix} RMS_{b,2}^{[1]} \\ RMS_{b,2}^{[2]} \\ \vdots \\ RMS_{b,2}^{[64]} \end{bmatrix}^{[i-1]} + 0.1\left[\hat{\delta}_2\right]^2 + \begin{bmatrix} \varepsilon \\ \varepsilon \\ \vdots \\ \varepsilon \end{bmatrix}, \tag{6.40}$$

where $\widehat{RMS}_{w,2} \in \mathbb{R}^{64\times 64}$ and $\widehat{RMS}_{b,2} \in \mathbb{R}^{64\times 1}$.

Finally, the exponential weighted moving average of gradients for the output layer's weights and biases, $RMS_{w,3}$ and $RMS_{b,3}$, respectively, are:

$$\widehat{RMS}_{w,3}^{[i]} = 0.9\left[\widehat{RMS}_{w,3}\right]^{[i-1]} + 0.1\left[a_2^{[1]}\delta_3^{[1]} \quad \dots \quad a_2^{[64]}\delta_3^{[1]}\right]^2 + [\varepsilon \quad \cdots \quad \varepsilon], \tag{6.41}$$

$$\widehat{RMS}_{b,3}^{[i]} = 0.9\left[\widehat{RMS}_{b,3}\right]^{[i-1]} + 0.1\left[\hat{\delta}_3\right]^2 + \epsilon, \tag{6.42}$$

where $\widehat{RMS}_{w,3} \in \mathbb{R}^{1\times 64}$ and $\widehat{RMS}_{b,3} \in \mathbb{R}^{1\times 1}$.

The change in error with respect to its weights in the first, second, and output layers, respectively, is:

$$\partial_w Err_1 = \hat{\delta}_1 \begin{bmatrix} x_T \\ x_E \end{bmatrix}^T = \begin{bmatrix} x_T\delta_1^{[1]} & x_E\delta_1^{[1]} \\ x_T\delta_1^{[2]} & x_E\delta_1^{[2]} \\ \vdots & \vdots \\ x_T\delta_1^{[64]} & x_E\delta_1^{[64]} \end{bmatrix}, \tag{6.43}$$

$$\partial_w Err_2 = \hat{\delta}_2 \hat{a}_1{}^T = \begin{bmatrix} a_1^{[1]}\delta_2^{[1]} & \cdots & a_1^{[64]}\delta_2^{[1]} \\ a_1^{[1]}\delta_2^{[2]} & \cdots & a_1^{[64]}\delta_2^{[2]} \\ \vdots & \ddots & \vdots \\ a_1^{[1]}\delta_2^{[64]} & \cdots & a_1^{[64]}\delta_2^{[64]} \end{bmatrix}, \tag{6.44}$$

$$\partial_w Err_3 = \hat{\delta}_3 \hat{a}_2{}^T = \left[a_2^{[1]}\delta_3^{[1]} \quad \cdots \quad a_2^{[64]}\delta_3^{[1]}\right]. \tag{6.45}$$

The weight and bias vectors for the layer $L, L = 1,2,3$ in the current iteration i, $\widehat{w}_L^{[i]}$, are:

$$\widehat{w}_L^{[i]} = \widehat{w}_L^{[i-1]} - \mathrm{H}\frac{\partial_w Err_L}{\sqrt{\widehat{RMS}_{w,L}^{[i]}}}, \tag{6.46}$$

$$\hat{b}_L^{[i]} = \hat{b}_L^{[i-1]} - \mathrm{H}\frac{\partial_b Err_L}{\sqrt{\widehat{RMS}_{b,L}^{[i]}}}, \tag{6.47}$$

where H is the learning rate, $\partial_b Err_L = \hat{\delta}_L$. When $i = 1$, we set:

$$\widehat{w}_L^{[0]} = \begin{cases} \widehat{w}_L^{[-1]}, & L = 1, \\ \sqrt{\dfrac{1}{32}}\,\widehat{w}_L^{[-1]}, & L = 2,3, \end{cases} \tag{6.48}$$

where $\widehat{w}_L^{[-1]}$ is a Gaussian distributed function with a mean of zero and variance of one. The weight vector $\widehat{w}_L^{[-1]}$ is multiplied by a constant $\sqrt{2/64} = \sqrt{1/32}$ for layers 2 and 3 because there are 64 columns in the corresponding weight vectors in (6.30) and (6.32).

To prevent $\widehat{w}_L^{[i]}, L = 1,2,3$ in (6.46) from blowing up, it is normalized as follows:

$$\widehat{w}_L^{[i]} = \begin{cases} \widehat{w}_L^{[i]}, & \max\left(\widehat{w}_L^{[i]}\right) \leq 1, \\ \dfrac{\widehat{w}_L^{[i]}}{\max\left(\widehat{w}_L^{[i]}\right)}, & \max\left(\widehat{w}_L^{[i]}\right) > 1. \end{cases} \tag{6.49}$$

The artificial neural network algorithm for processing data in the cloud is presented in Algorithm 6.3.

Algorithm 6.3 Artificial Neural Network (Cloud) Algorithm

1. **Input:** $T_{w,k}, E_k, T_{p,k}$, H, `batch_size`, `epochs`.
2. **Output:** $\widehat{w}_1, \hat{b}_1, \widehat{w}_2, \hat{b}_2, \widehat{w}_3, \hat{b}_3, \overline{T}_w, \sigma_{\hat{T}_w}, \overline{E}, \sigma_{\hat{E}}, T_{p,max}$.
3. Servers in the cloud system receive new training data $T_{w,k}, E_k$, and $T_{p,k}$ from sensor k and appends the data to the corresponding arrays in the cloud $\hat{T}_w, \hat{E}$, and $\hat{T}_p$.
4. Calculate $\overline{T}_w, \sigma_{\hat{T}_w}, \overline{E}, \sigma_{\hat{E}}$, and $T_{p,max}$ using (6.16), (6.17), (6.18), (6.19), and (6.20), respectively.
5. Calculate $\hat{x}_T, \hat{x}_E$, and $\hat{y}_T$, using (6.21), (6.22), and (6.23), respectively.
6. Initialize iteration index $i = 1$.
7. Shuffle the arrays $\hat{x}_T, \hat{x}_E$, and $\hat{y}_T$.

8. Read a batch of unread values of $\hat{T}_w, \hat{E}$, and $\hat{T}_p$ in size of `batch_size`.

9. **If** the input data is from an urban environment:

Calculate $f_A(x)$ and $f_A{}'(x)$ using (6.24) and (6.25), respectively.

Else

Calculate $f_A(x)$ and $f_A{}'(x)$ using (6.26) and (6.27), respectively.

Endif

10. Calculate $\hat{z}_1$ and $\hat{a}_1$ using (6.28) and (6.29), respectively.

11. Calculate $\hat{z}_2$ and $\hat{a}_2$ using (6.30) and (6.31), respectively.

12. Calculate $\hat{z}_3$ and $\hat{a}_3$ using (6.32) and (6.33), respectively.

13. Calculate $\hat{\delta}_3$, $\hat{\delta}_2$, and $\hat{\delta}_1$ using (6.34), (6.35), and (6.36), respectively.

14. Calculate $\widehat{RMS}_{w,1}^{[i]}$ and $\widehat{RMS}_{b,1}^{[i]}$ using (6.37) and (6.38), respectively.

15. Calculate $\widehat{RMS}_{w,2}^{[i]}$ and $\widehat{RMS}_{b,2}^{[i]}$ using (6.39) and (6.40), respectively.

16. Calculate $\widehat{RMS}_{w,3}^{[i]}$ and $\widehat{RMS}_{b,3}^{[i]}$ using (6.41) and (6.42), respectively.

17. Calculate $\partial_w Err_1$, $\partial_w Err_2$, and $\partial_w Err_3$ using (6.43), (6.44), and (6.45), respectively.

18. Calculate $\widehat{w}_L^{[i]}$ for layers $L = 1,2,3$ using (6.46).

19. Adjust $\widehat{w}_L^{[i]}$ for all layers $L = 1,2,3$ using (6.49).

20. Calculate $\hat{b}_L^{[i]}$ for layers $L = 1,2,3$ using (6.47).

21. Repeat Steps 8 to 20 until all data in the arrays $\hat{T}_w, \hat{E}$, and $\hat{T}_p$ are read and processed.

22. Increment $i = i + 1$.

23. Repeat Steps 7 to 22 until $i =$ `epochs`.

Algorithm 6.3 runs in the cloud and is assumed to have virtually unlimited computational resources.

Line 1 lists the input parameters required by Algorithm 6.3. Line 2 lists the required output parameters: $\widehat{w}_1, \hat{b}_1, \widehat{w}_2, \hat{b}_2, \widehat{w}_3, \hat{b}_3, \bar{T}_w, \sigma_{\hat{T}_w}, \bar{E}, \sigma_{\hat{E}}$, and $T_{p,max}$. Line 3 updates the training data in the cloud. Line 4 calculates the ANN constants. Lines 5 to 8 shuffles and reads the input data in batches of size `batch_size`. Lines 9 to 12 implement the feed forward procedure. Line 13 calculates the output error. Lines 14 to 20 perform the error backpropagation using the gradient descent optimizer. Algorithm 6.3 has complexity $O(\text{epochs})$. Although it is low complexity, it will require significant processing power and system memory depending on the quantity of data the ANN needs to process.

Algorithm 6.3's output are matrices of weights and biases for a trained ANN and transmitted from the cloud via the H-APs to the sensors.

On the sensors' side, the normalized inputs $x_{T,k}$ and $x_{E,k}$ for sensor $k, k = 1 \dots K$, corresponding to $T_{w,k}^{[\Delta-1]}$ and $E_k^{[\Delta_B]}$, respectively, are:

$$x_{T,k} = \frac{T_{w,k}^{[\Delta-1]} - \bar{T}_w}{\sigma_{\hat{T}_w}}, \tag{6.50}$$

$$x_{E,k} = \frac{E_k^{[\Delta_B]} - \bar{E}}{\sigma_{\hat{E}}}. \tag{6.51}$$

The predicted next wake up time for sensor $k, k = 1 \dots K$, $T_{w,k}^{[\Delta]}$, is given by:

$$T_{w,k}^{[\Delta]} = \left\lceil T_{p,max} \cdot y_{T,k} \right\rceil, \tag{6.52}$$

where $y_{T,k}$ is the normalized predicted wake up time calculated from the trained ANN for sensor $k, k = 1 \ldots K$. Like the LFNTLRE algorithm (Algorithm 6.2), $T_{w,k}^{[\Delta]}$ is a positive integer value to reduce memory usage and also to allow compatibility with low-precision clocks.

The artificial neural network algorithm for predicting $T_{w,k}^{[\Delta]}$ in each sensor $k, k = 1 \ldots K$, is presented in Algorithm 6.4.

Algorithm 6.4 Artificial Neural Network (Sensor) Algorithm

1. **Input:** $E_k^{[\Delta_B]}, E_{C,k}, E_{S,k}, E_k, T_{w,k}, S_{max}, E_{res}$, `operating_mode = ambient`.

   $\widehat{w}_1, \widehat{b}_1, \widehat{w}_2, \widehat{b}_2, \widehat{w}_3, \widehat{b}_3, \overline{T}_w, \sigma_{\hat{T}_w}, \overline{E}, \sigma_{\hat{E}}, T_{p,max}$ *(Only updated when sensor is connected to the WPCN)*

2. **Output:** $T_{w,k}^{[\Delta]}$.

   $T_{w,k}, E_k, T_{p,k}$ *(Only uploaded when sensor is connected to the WPCN)*

3. **If** the ambient session counter, Δ, is not defined:

   Initialize $\Delta = 0$.

   Endif

4. **If** the sensor miss counter, `sensor_miss_count`, is not defined:

   Initialize `sensor_miss_count` = 0.

   Endif

5. **If** $E_k^{[\Delta_B]} \geq E_{C,k} + E_{S,k} + E_{res}$

   Save $T_{w,k}^{[\Delta-2]}, E_k^{[\Delta_B-1]}$, and $T_{w,k}^{[\Delta-1]}$ into the local arrays $\hat{T}_{w,k}, \hat{E}_k$, and $\hat{T}_{p,k}$, respectively. *(This data will be uploaded to the corresponding arrays $\hat{T}_w, \hat{E}$, and $\hat{T}_p$ in the cloud the next time the sensor is connected to the WPCN.)*

If $E_k^{[\Delta_B]} \geq E_{C,k} + S_{max}E_{S,k} + E_{res}$

Sense data S_{max} times.

Else

Sense data $\left\lfloor \frac{E_k^{[\Delta_B]} - E_{C,k} - E_{res}}{E_{S,k}} \right\rfloor$ times.

Endif

Else

- A sensor miss has occurred.

- Discard the data $T_{w,k}^{[\Delta-2]}$, $E_k^{[\Delta_B-1]}$, and $T_{w,k}^{[\Delta-1]}$.

- Increase sensor miss counter by 1.

Endif

6. Calculate $x_{T,k}$ using (6.50).

7. Calculate $x_{E,k}$ using (6.51).

8. Calculate $\hat{z}_1$ using (6.28) with $\widehat{w}_1$ and $\hat{b}_1$ downloaded from the cloud.

9. Calculate $\hat{a}_1$ using (6.29).

10. Calculate $\hat{z}_2$ using (6.30) with $\widehat{w}_2$ and $\hat{b}_3$ downloaded from the cloud.

11. Calculate $\hat{a}_2$ using (6.31).

12. Calculate $\hat{z}_3$ using (6.32) with $\widehat{w}_3$ and $\hat{b}_3$ downloaded from the cloud.

13. Calculate $\hat{a}_3$ using (6.33). The result of $\hat{a}_3$ is $y_{T,k}$.

14. Determine $T_{w,k}^{[\Delta]}$ using (6.52).

15. If $T_{w,k}^{[\Delta]} < 1$

Set $T_{w,k}^{[\Delta]} = 1$.

Endif

16. Increment Δ by 1.

17. Wait $T_{w,k}^{[\Delta]}$ seconds and start from the beginning of Algorithm 6.1.

Each ANN sensor runs Algorithm 6.4 when set to operate in the ambient mode from Algorithm 6.1.

Line 1 lists the input parameters required by Algorithm 6.4. Line 2 lists the output parameters, which are $T_{w,k}^{[\Delta]}$ when an ANN sensor is disconnected from the cloud and $T_{w,k}, E_k,$ and $T_{p,k}$ when the ANN sensor is connected to the cloud. Uninitialized variables are initialized in lines 3 and 4. Line 5 determines how much data to sense in the current session and senses the data. Lines 6 to 14 are used to predict $T_{w,k}^{[\Delta]}$. Line 15 prevents $T_{w,k}^{[\Delta]}$ from being a negative or fractional (less than unity) value. Algorithm 6.4 has complexity $O(1)$ because it runs in constant time. Its low complexity allows it to run on sensors with limited resources.

6.5. Cascading Artificial Neural Networks

Adding environment detection (ED) to the CA/D protocol's ambient mode that uses an artificial neural network is necessary because ANN sensors can then operate reliably without the need to download a different trained ANN from the cloud every time the ambient operating environment changes from urban to rural, and vice-versa. This is done by adding another ANN and performance-enhancing filters cascaded in front of the wake up time predictor ANN shown in Fig. 6.5, to be referred to as ANN-ED. The increase in complexity is negligible the algorithm is still $O(1)$. Its low complexity allows it to run on sensors with limited resources. It is not necessary

to add ED to LFNTLRE sensors because LFNTLRE sensors already have the native ability to adapt to the environment it operates in on-the-fly.

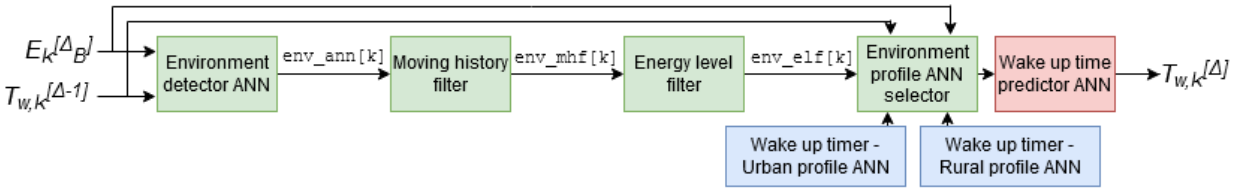

Fig. 6.5. Cascading artificial neural networks with performance-enhancing filters.

6.5.1. Environment Detector Artificial Neural Network

The training of the environment detector ANN starts off with data being processed in the cloud, similar to the wake up time predictor ANN in Section 6.4.2. When a sensor is connected to the cloud via the WPCN, the sensor will upload the training data set comprising information collected when it was operating in ambient mode. In addition to the full history of times since the sensor last successfully woke up (stored in the cloud array $\hat{T}_w$) and its corresponding history of capacitor energy level at the beginning of the sessions (stored in the cloud array $\hat{E}$) required by the wake up time predictor ANN, the corresponding record of all accurate environment detections (stored in the cloud arrays $\hat{y}_U$ and $\hat{y}_R$, where the subscripts U and R denote urban and rural environment, respectively) is also uploaded.

The ANN used for the environment detector has 1 input layer, 2 hidden layers with 64 neurons per layer, and 1 output layer. The activation function used is the logistic function. This ANN topology was chosen to best balance between the complexity of the ANN and accuracy as well as to correspond to the wake up time predictor ANN.

Since the environment detector ANN has the same topology as the wake up time predictor ANN, most equations will remain unchanged and thus will not be rewritten in this section for

brevity. Similarly, the corresponding ANN cloud and sensor algorithms are also similar, therefore only the differences will be discussed.

In the environment detector ANN, $T_{p,max}$ is not needed, because it is a classifier ANN. The wake up time predictor output, $\hat{y}_T$, is now replaced with the corresponding known accurately detected numerical values corresponding to the urban and rural environments, $\hat{y}_U$ and $\hat{y}_R$, respectively, as follows:

$$\hat{y}_U = \begin{bmatrix} y_U^{[1]} \\ y_U^{[2]} \\ \vdots \\ y_U^{[z]} \end{bmatrix}, \tag{6.53}$$

$$\hat{y}_R = \begin{bmatrix} y_R^{[1]} \\ y_R^{[2]} \\ \vdots \\ y_R^{[z]} \end{bmatrix}. \tag{6.54}$$

Correspondingly, the feed forward equation for the output layer $\hat{z}_3$, is:

$$\hat{z}_3 = \begin{bmatrix} z_3^{[1]} \\ z_3^{[2]} \end{bmatrix} = \hat{w}_3 \hat{a}_2 + \hat{b}_3. \tag{6.55}$$

The values to be fed into the output error calculation, $\hat{a}_3$, are:

$$\hat{a}_3 = \begin{bmatrix} a_3^{[1]} \\ a_3^{[2]} \end{bmatrix} = \begin{bmatrix} z_3^{[1]} \\ z_3^{[2]} \end{bmatrix}. \tag{6.56}$$

The output error, $\hat{\delta}_3$, as a function of y_T, is given by:

$$\hat{\delta}_3 = \left(\hat{a}_3 - \begin{bmatrix} y_U \\ y_R \end{bmatrix} \right), \tag{6.57}$$

where $\hat{\delta}_3 \in \mathbb{R}^{2\times 1}$.

The conversion from the environment detector ANN's numerical output to the detected environment for sensor $k, k = 1 \ldots K$, `env_ann[k]`, is given in Psuedocode 6.1. The numerical values y_U and y_R are obtained from the trained ANN's output $\hat{z}_3 = \begin{bmatrix} y_U \\ y_R \end{bmatrix}$ in (6.55).

Pseudocode 6.1 Numerical Output to Detected Environment

1. **If** $y_U > y_R$:
2. `env_ann[k] = urban`
3. **Else**
4. `env_ann[k] = rural`
5. **Endif**

6.5.2. Moving History Filter

The environment detector ANN in Section 6.5.1 is not perfectly accurate. Given it is extremely unlikely, if not physically impossible, for a person to rapidly move from one environment to the other and back, a moving history filter can be used to enhance its accuracy by filtering out random detection errors from the environment detector ANN.

A moving history filter can be implemented by taking the 5 most recent `env_ann[k]`, all stored in the array `env_ann_last5[k]`, and finding the most frequent value using the function mode in Pseudocode 6.2. A history of 5 is used as it balances between filtering out random detection errors and adaptability to environmental changes. The moving history filter can be bypassed if there is insufficient history information.

Pseudocode 6.2 Moving History of 5 Filter

1. **If** `mode(env_ann_last5[k])` == urban:

2. `env_mhf[k] = urban`
3. **Else**
4. `env_mhf[k] = rural`
5. **Endif**

6.5.3. Energy Level Filter

The data sensing schedule for the sensors can be optimized by using an energy level filter after the moving history filter. If the energy level is greater than what is required for the sensor to wake up and sense data at least once, force the urban profile. This is because if the sensor uses the urban profile, the predicted next wake up time is going to be shorter compared to the rural profile, so more data can be sensed. Even if the actual operating environment is rural, there is still no risk of outage. The energy level filter is described in Pseudocode 6.3.

Pseudocode 6.3 Energy Level Filter

1. **If** $E_k^{[\Delta_B]} \geq E_{C,k} + E_{S,k} + E_{res}$:
2. `env_elf[k] = urban`
3. **Else**
4. `env_elf[k] = env_mhf[k]`
5. **Endif**

6.5.4. Environment Profile ANN Selector, Wake Up Time Predictor ANN

The environment profile ANN selector selects either the trained urban or rural ANN already on the sensor depending on the input from the energy level filter. The wake up time predictor using the loaded urban or rural ANN takes the inputs $E_k^{[\Delta_B]}$ and $T_{w,k}^{[\Delta-1]}$ to predict $T_{w,k}^{[\Delta]}$.

6.6. Numerical Results and Discussion

The CA/D RF EH protocol uses the MS2-BABF/combo protocol in dedicated mode and its performance is well-documented in Chapter 5, hence this section will present and discuss the simulation results of the CA/D RF EH protocol operating in ambient mode only. Note that there is no possible results comparison between the ambient and dedicated modes. This is because the two operation modes are fundamentally different; ambient mode only concerns data sensing in a limited and unpredictable RF EH environment, whereas dedicated mode concerns both data sensing and wireless data communication with reliable RF EH sources.

The CA/D RF EH protocol's ambient mode performance with the two proposed machine learning algorithms, LFNTLRE (Algorithm 6.2) and ANN-ED (Algorithms 6.3 and 6.4 with Section 6.5 enhancements), will be compared against two benchmarks that use no machine learning algorithm: (1) ideal knowledge sensors, and (2) sensors with a constant polling rate.

The figures of merit used to measure the sensors' performance (i.e., performance metrics) include battery outage count, miss count, hit count, and accuracy percentage. Battery outage count is defined as the number of times a sensor was unable to complete a sensor energy level check as a result of complete energy depletion. Miss count is defined as the number of times a sensor had sufficient energy to complete a sensor energy level check, but insufficient energy to sense data. Hit count is defined as the number of times a sensor was successful in sensing data. Lastly, the accuracy percentage is defined as the ratio of the number of sessions a sensor was able to

successfully sense data at least once to the total number of data sensing attempts and then multiplied by 100.

The ideal knowledge sensor has a perfectly accurate wake up schedule with respect to its energy level. This means the ideal knowledge sensor always has no battery outage, no miss count, maximum possible hit count given the amount of harvested energy, 100% accuracy, and requires no machine learning. The sensor with a constant polling rate wakes up periodically by a constant preset $T_{w,k}$ and also does not use any machine learning algorithm.

6.6.1. System Configuration

A user with 5 on-body sensors is assumed (i.e., $K = 5$). The channel power gain values between cell phone tower n and sensor k are generated using (6.1) at the beginning of each time block of length 1 second to simulate ongoing changes in channel quality in a dynamic environment. For the factor $\beta_{n,k,q}$, the Gamma parameters are $A = 1.80, B = 0.11$ to realize Rician fading that holds true for the rural environment and are also set as $A = 1.00, B = 0.11$ to obtain Rayleigh fading for the urban environment [59]. The results are averaged over the random fading channel power gains and cell tower locations in each simulation run of length 10,000 seconds. We assume all sensors are the same for simplicity, therefore $E_{C,1} = \cdots = E_{C,K} = E_C$ and $E_{S,1} = \cdots = E_{S,K} = E_S$. The maximum number of times a sensor can sense data in one session, S_{max}, is set at 10 to ensure data will be more evenly sensed over a period of time at a reasonable poll rate.

The sensors are modeled by a design using Texas Instruments' CC1350 microcontroller unit [78] and NXP's MMA8491Q 3-axis multifunction digital accelerometer [79]. Each trial begins with the user in a random starting position in the urban environment (Fig. 6.2) or the rural environment (Fig. 6.3). The user is assumed to be either walking at a speed of 1.4m/s or biking at

4.2m/s on a random path. If a user is at a distance less than or equal to 1m from a cell phone tower, the path loss is assumed as PL_{ref} dB.

The time interval between successive wake ups of the sensors using a constant poll rate is set to $T_{w,k} = 60$ and 300 seconds when operating in the urban and rural environment, respectively. The default next wake up time for all sensors are set to 60 and 300 seconds when operating in the urban and rural environment, respectively, as well. These numbers can be configured to other desired values, but a higher number is selected for the rural environment to anticipate for reduced harvested energy. Meanwhile, the ANN-ED sensors are pre-trained with 3.2 million data points downloaded from the cloud servers when previously connected to the WPCN. In the cloud servers, 80% of the data are used for training and 20% for validation. The resulting ANN-ED configuration parameters are `epochs` = 10, `batch_size` = 3000, and H $= 10^{-5}$ in this particular case for best training accuracy and will change depending on the size of the training data set.

The rest of the assumed system parameter values are listed in Table 6.1.

Table 6.1. Assumed System Parameter Values

Parameter	Definition	Value
PL_{ref}	Path loss at reference distance of 1m and transmitter frequency of 900MHz	30dB
φ	Path loss exponent	2 (rural), 3 (urban) [59]
ς	EH efficiency at each sensor	0.5 [54]
P_C	Cell phone towers' transmission power	500W [80]
E_C	Energy required to wake up and check the capacitor energy level	9.5e-4mJ [78]

E_S	Energy required for sensor to sense data once	3.2e-3mJ [79]
E_{res}	Sensor reserve energy	3.2e-3mJ

6.6.2. Results and Discussion

First, all four algorithms considered – LFNTLRE, ANN-ED, ideal, and constant – are compared in a scenario where a user is walking in the urban environment. There is zero battery outage in all four tested algorithms. This is because in all the tested algorithms, the sensors always waited sufficient amount of time to harvest energy, either by preset or by machine learning methods, before attempting to check energy.

In Figs. 6.6 to 6.8, the LFNTLRE algorithm exhibits the lowest average miss count, highest average hit count, and the highest accuracy percentage. Meanwhile, sensors using a constant polling rate had the highest average miss count, by far the lowest average hit count, and the lowest average accuracy among the four algorithms compared. Sensors using a constant polling rate achieve an average accuracy percentage that is 5.6% below that of an ideal sensor. In comparison, sensors using the LFNTLRE and ANN-ED algorithms are able to attain 99.5% and 95.7% hit count relative to that of ideal sensors, respectively. This is because sensors using a constant polling rate are unable to adaptively increase their data sensing rate, as done in the LFNTLRE and ANN-ED, when the harvested energy increases. Conversely, the sensors with constant polling rate are also unable to adaptively decrease their data sensing rate when harvested energy decreases, contributing to the highest miss count.

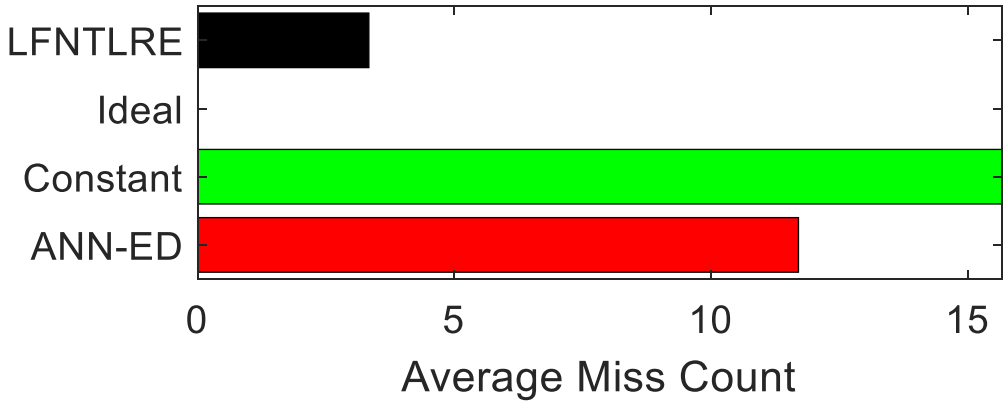

Fig. 6.6. Average miss count – urban walking.

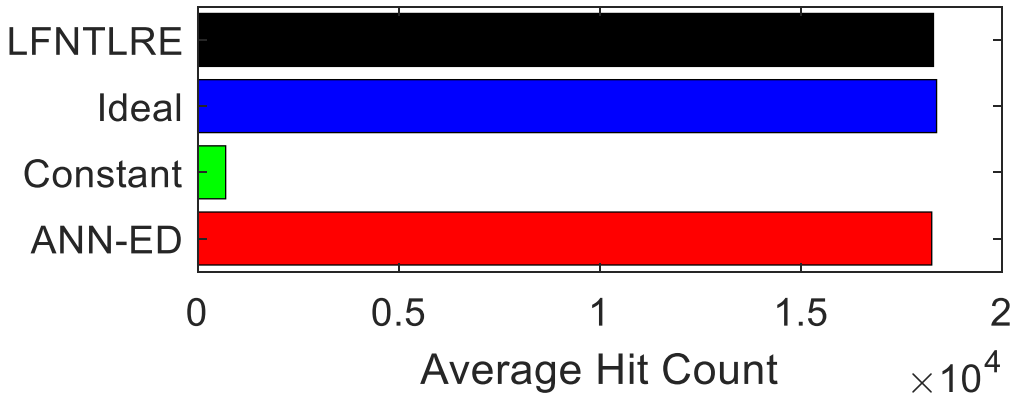

Fig. 6.7. Average hit count – urban walking.

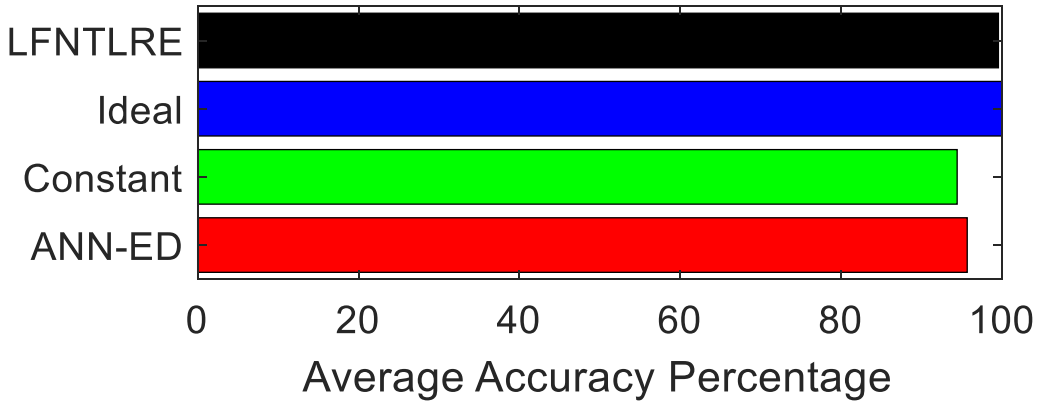

Fig. 6.8. Average accuracy percentage – urban walking.

In Figs. 6.6 to 6.8, the LFNTLRE algorithm performance is slightly better than that of the ANN-ED in all the three performance metrics – average miss count, average hit count, and average

accuracy percentage – because the LFNTLRE algorithm is able to adapt to environmental changes on-the-fly, while the ANN-ED depends on previous training data and operates offline to the environment. However, the performance of the LFNTLRE algorithm and ANN-ED are both very close to that of the ideal sensor in all three performance metrics, meaning both algorithms are working as intended.

Next, the LFNTLRE algorithm and ANN-ED along with the two benchmarks are compared in a scenario where a user is biking in the urban environment.

The results shown in Figs. 6.9 to 6.11 are mostly similar to those in Figs. 6.6 to 6.8 for the reasons previously discussed with the exception of the average miss count. In the urban biking scenario, the sensors with the constant polling rate have a lower average miss count than that of the sensors equipped with the LFNTLRE and ANN-ED. This is because a user biking is moving faster than a user walking. As such, the energy harvesting rate in the urban biking scenario is more unpredictable than in the urban walking scenario due to increased effects of path loss, shadowing, and small-scale fading. This increased energy harvesting unpredictability causes the LFNTLRE and ANN-ED algorithms' predictions to have slightly more misses. However, the increase in misses is mostly inconsequential compared to the average hit count, resulting in 99.8% and 99.0% accuracy percentage for the LFNTLRE and ANN-ED, respectively. Sensors with the LFNTLRE and ANN-ED achieve a hit count that is approximately 1350% higher than that of the sensors with a constant polling rate, because they are able to adaptively increase or decrease their data sensing rates.

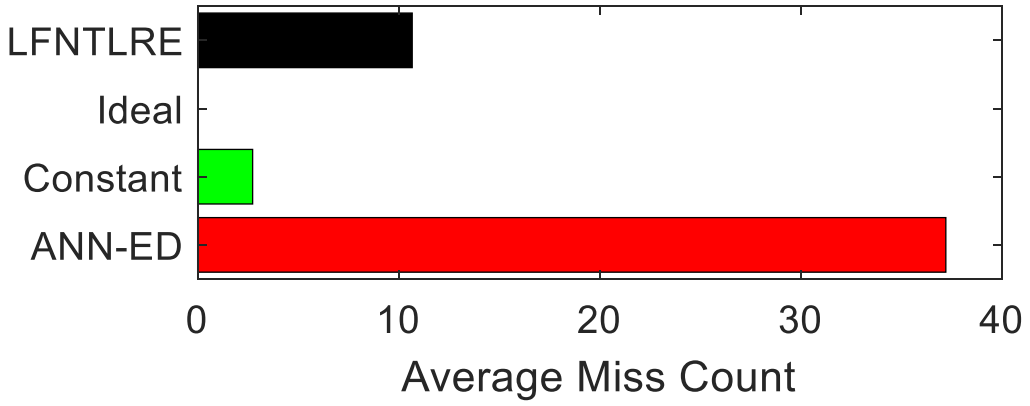

Fig. 6.9. Average miss count – urban biking.

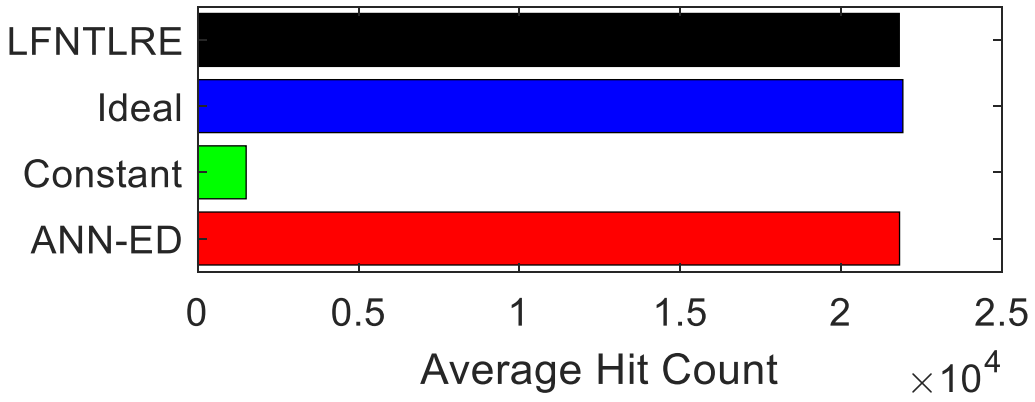

Fig. 6.10. Average hit count – urban biking.

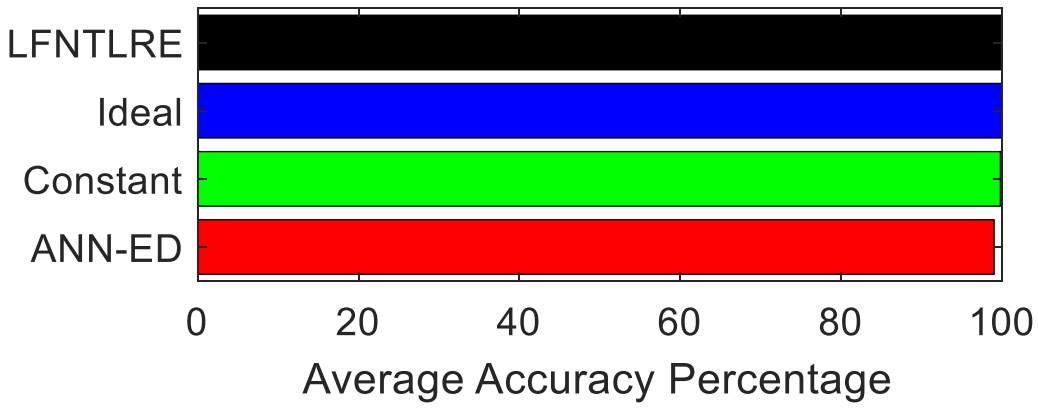

Fig. 6.11. Average accuracy percentage – urban biking.

The next scenario involves a user walking in the rural environment. Both the LFNTLRE and ANN-ED algorithms predict sufficient amount of time for the sensors to harvest enough

energy to check the capacitor energy level, hence there are no battery outages. Sensors using a constant polling rate also have a sufficient delay before starting up, so there is no battery outage as well.

In Fig. 6.12, the LFNTLRE exhibits no misses, ANN-ED has an average of 1 miss, while sensors using a constant polling rate have an average of 22 misses. This is because cell phone tower density is only 0.03056 per km^2 in the rural environment compared to 31.55 per km^2 in the urban environment. In other words, the density of cell phone towers in the urban environment is three orders of magnitude higher. As such, the amount of available harvested energy can vary greatly and setting a constant polling rate will have accuracy percentage that also varies greatly. This resulted in the constant polling rate with an accuracy percentage that ranges from 6.1% to 90.9% with an average of only 33.8% in Fig. 6.14.

In Fig. 6.13, the average hit count for ANN-ED is higher than that of the LFNTLRE because the ANN-ED is more aggressive in attempting to wake up early to sense data. Conversely, the LFNTLRE algorithm is more conservative because it takes time to build its average energy harvesting rate trends of various depths D. Since there is a very limited amount of harvested energy in a rural environment compared to that in the urban environment, there is also less information available to the LFNTLRE algorithm to adjust its capacitor depletion ratio, hence it operates on a more conservative profile by default. The result is that the LFNTLRE has no misses in Fig. 6.12 and with 100% accuracy percentage in Fig. 6.14, which is higher than the 92.7% accuracy percentage achieved by the ANN-ED. Comparing Fig. 6.14 with Fig. 6.8, the reason ANN-ED's accuracy percentage is only 92.7% in the rural walking compared to the 95.6% in the urban walking scenario is because a single miss has a much higher impact proportionally on the accuracy percentage in the rural environment due to the low density of cell phone towers. In Fig. 6.13, the

LFNTLRE also attains an average hit count that is about 7% and 10% less than those of the ANN-ED and ideal sensor, respectively. For reference, ANN-ED exhibits an average hit count that is about 3% less than that of the ideal, while sensors with constant polling rate provide an average hit count that is 36% below that of the ideal. Comparing Fig. 6.13 with Fig. 6.7, the ANN-ED had an average of only 16.9 hits in the rural environment compared to 10,000 or more hits in the urban environment.

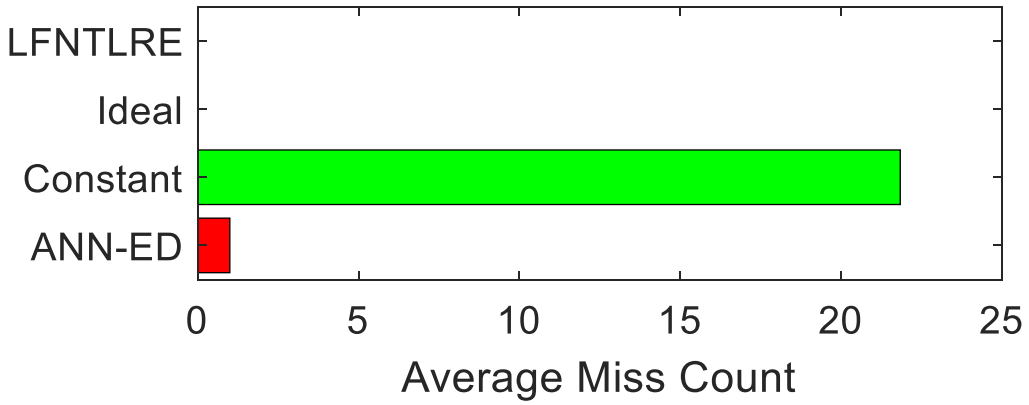

Fig. 6.12. Average miss count – rural walking.

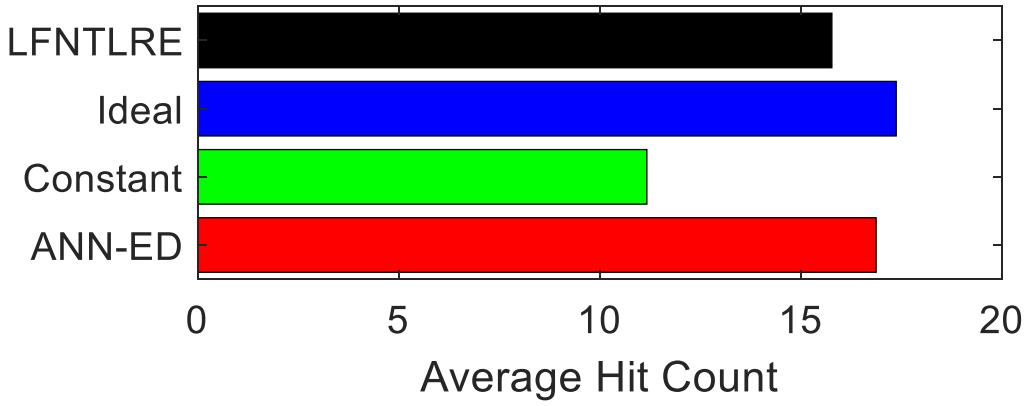

Fig. 6.13. Average hit count – rural walking.

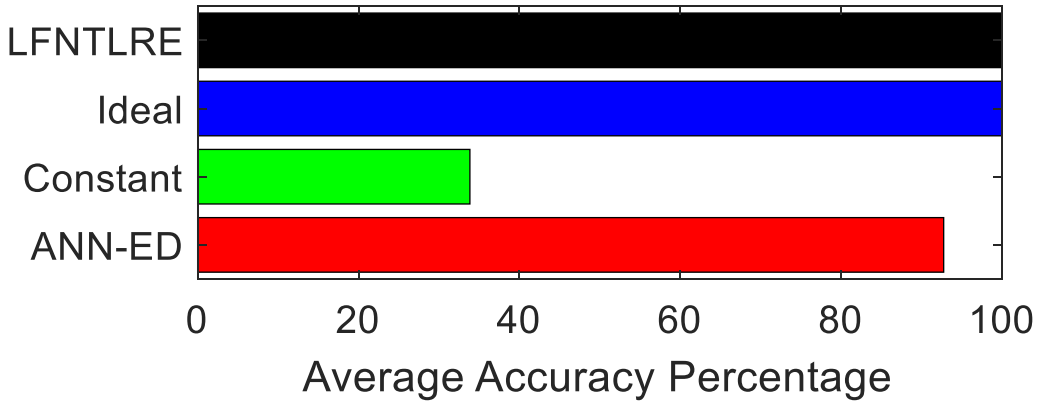

Fig. 6.14. Average accuracy percentage – rural walking.

The last scenario involves a user with 5 on-body sensors biking in the rural environment. Sensors using a constant polling rate and ANN-ED both have some recorded battery outages, as seen in Fig. 6.15. For sensors using a constant polling rate, this is due to an insufficient initial waiting time, hence insufficient energy is harvested by the sensors before attempting to sense data. For sensors using the ANN-ED, the algorithm fails to predict sufficient time for the sensors to harvest enough energy to check the capacitor energy level only once in all trials, hence the battery outage average was 0.2.

The performance of all the algorithms in Figs. 6.16 to 6.18 simulating a user biking in the rural environment is very similar to that shown in Figs. 6.12 to 6.14 for a user walking in the rural environment. While a user biking is moving faster than a user walking and affects the predictability of the energy harvesting rate, the effect is much less pronounced in the rural environment than it is in the urban environment. This is because the user in the rural environment is typically very far away from a cell phone tower given the size of the service area and density of the cell phone towers. As such, when the distance between the sensors and the cell phone towers is very large, channel propagation factors such as path loss, shadowing, and small-scale fading directly contributed by the user's movement is much less significant.

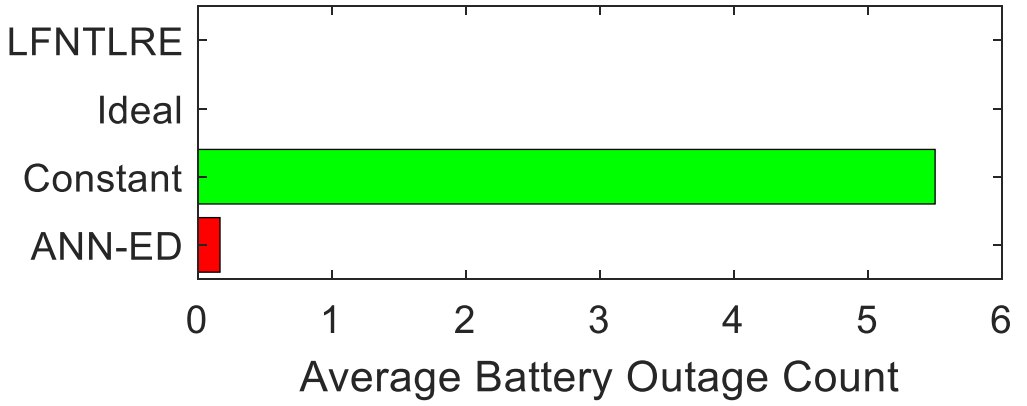

Fig. 6.15. Average battery outage count – rural biking.

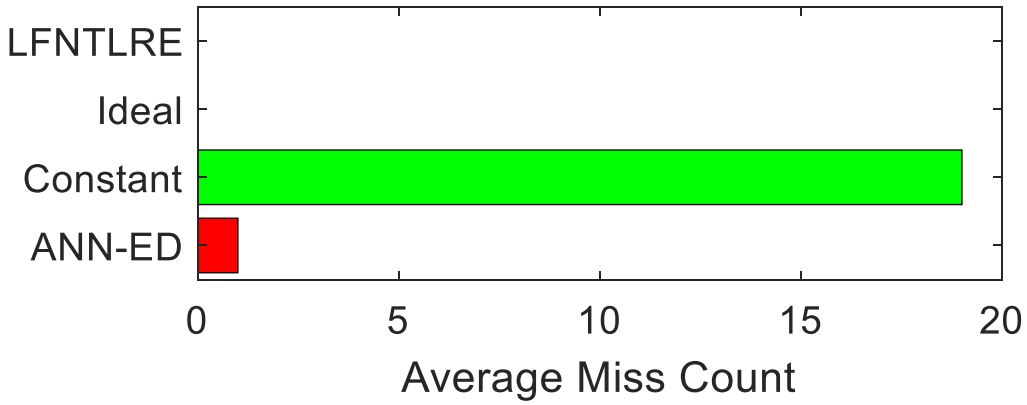

Fig. 6.16. Average miss count – rural biking.

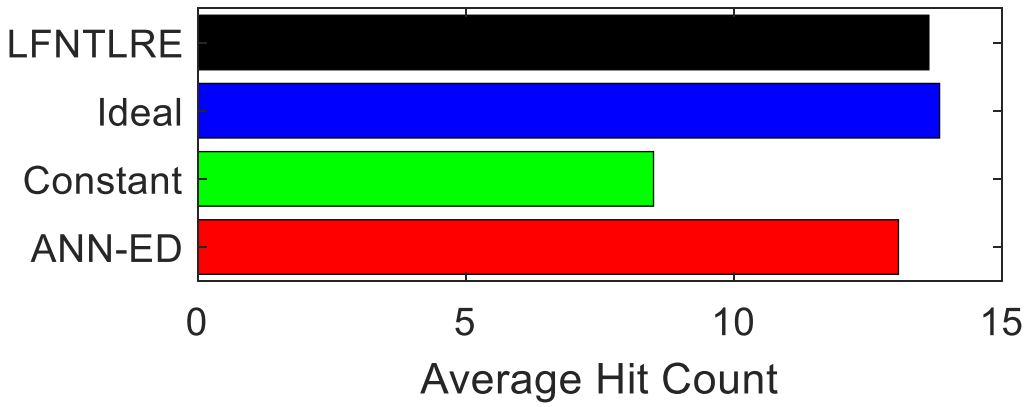

Fig. 6.17. Average hit count – rural biking.

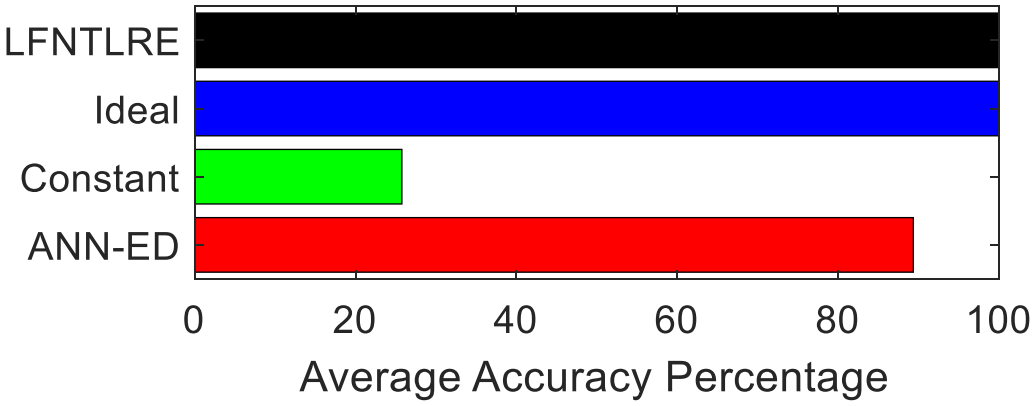

Fig. 6.18. Average accuracy percentage – rural biking.

The biggest difference between the results for a user biking and walking in the rural environment is the magnitude of average miss count, average hit count, and correspondingly, the average accuracy percentage. This is because the starting location and simulated path of the user are random, hence the amount of harvested energy varies. Another difference is that the LFNTLRE outperforms the ANN-ED in all three metrics mainly because the low number of cell phone towers mean any misses will have a significant impact in the results. As such, the conservative nature of sensors using the LFNTLRE algorithm proves advantageous in this case.

Based on the results presented in Figs. 6.6 to 6.18, sensors equipped with the LFNTLRE algorithm or ANN-ED always significantly outperform sensors using a constant polling rate. However, although the LFNTLRE algorithm can operate independently without prior training from the cloud required by the ANN-ED, the LFNTLRE requires more sensor memory – ten times compared to ANN-ED when $D = 10$ – to store a history of live data. With respect to the hit count, sensors using the ANN-ED and LFNTLRE achieve 94.5% to 99.5% and 91.0% to 99.6% hit count relative to that of ideal sensors, respectively, depending on the scenario. Meanwhile, sensors using the ANN-ED and LFNTLRE algorithm have an average accuracy percentage of 89.3% to 99.0% and 99.5% to 100%, respectively, depending on the scenario. These results show the feasibility

and suitability of both the ANN-ED and LFNTLRE algorithm for sensors operating in the ambient mode to harvest energy from unintended sources.

6.7. Summary

This chapter proposes the CA/D RF EH protocol where backscatter-enabled combination sensors are optimized to harvest energy from both the intended sources when in close proximity to the sensors (i.e., dedicated operating mode) and unintended sources when the intended sources are unavailable (i.e., ambient operating mode). For sensors operating in the ambient mode, two new machine learning algorithms are proposed in this chapter for predicting the optimal sensor wake up time. These algorithms include the LFNTLRE algorithm and an artificial neural network with environment detection. Both the ANN-ED and LFNTLRE algorithm exhibit excellent performance, achieving up to 99.5% and 99.6% hit count relative to that of ideal sensors, respectively. Sensors using the ANN-ED and LFNTLRE algorithm are able to achieve an average accuracy percentage of up to 99.0% and 100%, respectively, as well.

CHAPTER 7: CONCLUSIONS AND FUTURE WORK

7.1. Thesis Conclusions

In this thesis, protocols for unintended and intended radio frequency (RF) energy harvesting designed to maximize the wireless network performance and sensor operation ability of an RF energy harvesting (EH) system with multiple RF sources and sensors was investigated. The research performed in the area leads to the following three major conclusions:

1. Based on the results presented in Chapter 3, it is concluded that the combination protocol is most appropriate for wireless powered communication networks (WPCNs) with a large sensor population or when the sensors are very close to the dedicated hybrid access point (H-AP). The time-switching protocol with downlink data decoding should be selected when the WPCN sum-throughput is of a lower priority, the H-AP has limited computational power, and/or having the simplest sensor hardware is a requirement. The hybrid protocol is appropriate when it is required to achieve a good balance in the tradeoff between system sum-throughput and WPCN design complexity.
2. The results in Chapters 4 and 5 can be used for selecting the optimal WPCN protocol based on H-AP transmission power limits, form factor of the H-APs, and the number of H-APs that can be placed in a room. The multi-source, multi-sensor blind adaptive beamforming with combination sensors (MS2-BABF/combo) protocol presents the best tradeoff between sum-throughput and fairness in all the tested scenarios. However, if maximum fairness desired, the MS2-BABF/combo protocol can simply not operate sensors in backscatter mode and hence becomes the multi-source, multi-sensor blind adaptive beamforming with hybrid sensors (MS2-BABF/hybrid) protocol.

3. The results found in Chapters 6 show that the artificial neural network with environment detection (ANN-ED) is preferred for use with sensors in the urban environment. In the urban environment, misses are less significant compared to the rural environment. Furthermore, the ANN-ED performance nearly matches that of the linear forecaster with near-time linear regression-based enhancer (LFNTLRE) algorithm without the need for live data. Meanwhile, the LFNTLRE algorithm is preferred in the rural environment. This is because the number of unintended sources is low in the rural environment and using the most accurate algorithm – the LFNTLRE algorithm – will reduce costly misses.

7.2. Engineering Significance of Thesis Findings

The three proposed protocols – time-switching, hybrid, and combination – in Chapter 3 are important for next generation WPCN systems as they all optimized system timings to maximize the sum-throughput of a WPCN in a dynamic environment.

In Chapter 4, the multi-sensor blind adaptive beamforming with combination sensors (MS-BABF/combo) protocol increases the system achievable data rate and decreasing the sensor dropout rate without increasing the H-AP transmission power, which is important for practical WPCN deployments. Furthermore, compared to MS-BABF with time-switching sensors (MS-BABF/TS), the MS-BABF/combo protocol allows faster and more reliable wireless communication even when the distance between the H-AP and sensors increases.

The MS-BABF with hybrid protocol maximizing the sum-throughput and fairness (MS-BABF/hybrid-STF) proposed in Chapter 4 is significant as it increases the fairness between sensors in a WPCN without resorting to computationally intense sum-throughput and fairness optimization methods for single antenna H-APs. Also, compared to MS-BABF with hybrid protocol maximizing the sum-throughput (MS-BABF/hybrid-ST), the MS-BABF/hybrid-STF protocol

allows fairer throughputs between sensors, thus supporting the transmission of sensors' sensed data with the required quality, in a WPCN even when there are ongoing changes in channel quality.

The adoption of the MS2-BABF/combo protocol proposed in Chapter 5 is important as it prevents destructive interference wireless signals from all H-APs and sensors, because only one H-AP or sensor is transmitting data at any given time by design. At the same time, the MS2-BABF/combo protocol effectively maximized the sum-throughput and fairness of a WPCN in a dynamic environment.

The work in Chapter 6 is significant because the proposed coordinated ambient/dedicated (CA/D) protocol demonstrated that ambient RF EH sensors can operate reliably in all environments, which moves forward the practicality of its implementation in real world applications. The feasibility of using machine learning for sensors to harvest energy from unintended sources is feasible in both urban and rural environments is also realized.

The amalgamation of all the findings in this thesis is significant for future widespread adoption of WPCNs powered by one or more radio RF energy sources by improving wireless network performance and sensor operation ability.

7.3. Suggestions for Future Work

There are six logical extensions identified as future work to the research performed in this thesis:

1. *Hardware implementation of the Coordinated Ambient/Dedicated (CA/D) protocol*

In this thesis, the CA/D protocol was designed in a theoretical manner with its performance validated by simulation only. As such, physically building WPCNs with H-APs and sensors, implementing the CA/D protocol, and measuring the hardware prototypes' performance will be the logical next step to investigate and measure its performance in the real world.

2. Mesh WPCN

This thesis assumes all devices in the WPCN operate only within a small area and only one device can transmit at any given time. Improvements can be made to the MS2-BABF/combo protocol for the WPCN to cover a large area, such as a cross-campus network, by utilizing the mesh network topology. Applications of cell theory to maximize service area and number of users as well as cognitive radio techniques to improve spectrum efficiency can also be investigated.

3. Delay-sensitive applications

This thesis assumes that all data from the sensors in the WPCN are time delay-tolerant. However, in applications where the sensors' data are delay-sensitive, such as the requirement for live bodily vital statistics monitoring from the doctor's office, adding quality of service to all the protocols' optimization problems to minimize the time delay of certain sensors is a future research direction.

4. Wireless interference mitigation

While the adopted MS2-BABF/combo protocol is very effective in increasing the overall performance of the WPCN, if interference can be effectively alleviated when multiple sources are transmitting concurrently, the overall system performance can be further improved. Currently, only one source or sensor can transmit at any given point in time. If one or more H-AP and/or sensor can transmit without interference (i.e. full-duplex operating mode), the EH rate and data throughput of the sensors can be increased. The system will also be able to handle more sensors without decreasing the throughput of each sensor as much. This can be attempted by implementing traditional interference mitigation techniques such as frequency division multiple access and code division multiple access.

5. Combination of multiple energy harvesting methods

This thesis only investigates sensors that can harvest from RF energy sources. For sensors operating in ambient mode, a combination of multiple EH methods can be explored. This can include traditional techniques such as solar, wind, thermal, and kinetic in addition to ambient RF EH from cell phone towers. Further research can look at the feasibility and performance of such a design.

6. Health effects of multiple high-power RF sources in close proximity

Although there is no evidence non-ionizing wireless RF signals have any effect on human health, to the best of the author's knowledge, all current literature only address either low power signals at a close indoor distance (i.e., Wi-Fi routers inside a house) or high power signals at a far outdoor distance (i.e., TV broadcasting stations or cell phone towers). The health effect of having multiple relatively high power 900MHz devices all at a close distance in a small location, such as having five 4W hybrid access points in a $10m^2$ room in our simulation model in Chapter 5, is not known. Further research can be conducted to see if many high-power unlicensed spectrum transmitters within close proximity will have any effect on human health.

APPENDIX A: PROOF OF DIRECT PROPORTIONALITY BETWEEN SUM-THROUGHPUT AND OPTIMAL TIMINGS

For simplicity, start off with assuming a new variable $T_{new} = \alpha T$, where α is any positive real number. Given a solution to problem (P3.3) denoted as $v^* = \left[\tau^*_{EH,UL}\ \tau^*_{UL,1} \cdots \tau^*_{UL,K}\right]$ where $\tau^*_{EH,UL} + \tau^*_{UL} = T$, $\tau^*_{UL} = \sum_{k=1}^{K} \tau^*_{UL,k}$, and $T = 1$ from the constraint (3.13b), then it can be seen that:

$$\alpha\left(\tau^*_{EH,UL} + \tau^*_{UL}\right) = T_{new}. \quad (A.1)$$

Notice $T_{new} \neq 1$ if $\alpha \neq 1$. Using the new notation in a similar manner, we can write:

$$\tau^*_{EH,UL,new} = \alpha\tau^*_{EH,UL}, \quad (A.2)$$

$$\tau^*_{UL,k,new} = \alpha\tau^*_{UL,k}, k = 1 \ldots K. \quad (A.3)$$

Next, modify (3.10) using only $\tau^*_{EH,UL,new}$ and $\tau^*_{UL,k,new}$ values, forming $v^*_{new} = \left[\tau^*_{EH,UL,new}\ \tau^*_{UL,1,new} \cdots \tau^*_{UL,K,new}\right]$. We call the optimum rate for sensor k $R_{UL,k,new}(\tau^*_{EH,UL,new}, \tau^*_{UL,k,new})$ defined as follows:

$$R_{UL,k,new}\left(\tau^*_{EH,UL,new}, \tau^*_{UL,k,new}\right) = \tau^*_{UL,k,new} \log_2\left(1 + \gamma_{UL,k}\frac{\tau^*_{EH,UL,new}}{\tau^*_{UL,k,new}}\right), k = 1 \ldots K. \quad (A.4)$$

Substituting (A.2) and (A.3) back into the logarithmic function of (A.4), (A.4) becomes:

$$R_{UL,k,new}\left(\tau^*_{EH,UL,new}, \tau^*_{UL,k,new}\right) = \tau^*_{UL,k,new} \log_2(1 + \gamma_{UL,k}\frac{\alpha\tau^*_{EH,UL}}{\alpha\tau^*_{UL,k}}), k = 1 \ldots K. \quad (A.5)$$

Notice the α appears on both the denominator and the numerator inside the logarithmic function. Simplifying (A.5) becomes:

$$R_{UL,k,new}\left(\tau^*_{EH,UL,new}, \tau^*_{UL,k,new}\right) = \tau^*_{UL,k,new} \log_2(1 + \gamma_{UL,k}\frac{\tau^*_{EH,UL}}{\tau^*_{UL,k}}), k = 1 \ldots K. \quad (A.6)$$

Rearranging (3.10):

$$\frac{R_{UL,k}\left(\tau^*_{EH,UL},\tau^*_{UL,k}\right)}{\tau^*_{UL,k}} = \log_2(1+\gamma_{UL,k}\frac{\tau^*_{EH,UL}}{\tau^*_{UL,k}}), k = 1 \dots K. \quad (A.7)$$

Plugging (A.7) into (A.6) turns into:

$$R_{UL,k,new}\left(\tau^*_{EH,UL,new},\tau^*_{UL,k,new}\right) = \tau^*_{UL,k,new}\frac{R_{UL,k}\left(\tau^*_{EH,UL},\tau^*_{UL,k}\right)}{\tau^*_{UL,k}}, k = 1 \dots K. \quad (A.8)$$

Substituting (A.3) into (A.8):

$$R_{UL,k,new}\left(\tau^*_{EH,UL,new},\tau^*_{UL,k,new}\right) = \alpha\tau^*_{UL,k}\frac{R_{UL,k}\left(\tau^*_{EH,UL},\tau^*_{UL,k}\right)}{\tau^*_{UL,k}}, k = 1 \dots K. \quad (A.9)$$

Which shows us that:

$$R_{UL,k,new}\left(\tau^*_{EH,UL,new},\tau^*_{UL,k,new}\right) = \alpha R_{UL,k}\left(\tau^*_{EH,UL},\tau^*_{UL,k}\right), k = 1 \dots K. \quad (A.10)$$

As $R_{UL,sum}(v^*) = \sum_{k=1}^{K} R_{UL,k}(\tau^*_{EH,UL},\tau^*_{UL,k})$, then $R_{UL,sum,new}(v^*_{new}) = \alpha R_{UL,sum}(v^*)$.

The above proof is checked using a simple numerical example, where $\tau^*_{EH,UL} = 0.3$, $\tau^*_{UL,k} = 0.7$, and $\gamma_{UL,k} = 1$ using (3.10):

$$R_{UL,k}\left(\tau^*_{EH,UL},\tau^*_{UL,k}\right) = 0.7\log_2\left(1+\frac{0.3}{0.7}\right),$$

$$R_{UL,k}\left(\tau^*_{EH,UL},\tau^*_{UL,k}\right) = 0.36.$$

Assuming $\alpha = 0.5$, (A.2) and (A.3) gives:

$$\tau^*_{EH,UL,new} = 0.5(0.3) = 0.15,$$

$$\tau^*_{UL,k,new} = 0.5(0.7) = 0.35.$$

Calculating the rate using (A.4):

$$R_{UL,k,new}\left(\tau^*_{EH,UL,new},\tau^*_{UL,k,new}\right) = 0.35\log_2\left(1+\frac{0.15}{0.35}\right) = 0.18.$$

The rate can also be calculated directly from (A.10), and should match the solution given by (A.4) above:

$$R_{UL,k,new}\left(\tau^*_{EH,UL,new}, \tau^*_{UL,k,new}\right) = \alpha R_{UL,k}\left(\tau^*_{EH,UL}, \tau^*_{UL,k}\right) = \alpha 0.36$$

$$R_{UL,k,new}\left(\tau^*_{EH,UL,new}, \tau^*_{UL,k,new}\right) = (0.5)0.36 = 0.18.$$

The two solutions are the same. Therefore, the system sum-throughput and optimal timings are directly proportional, i.e., multiplying all the optimal timing values v^* by any positive real number α will also result in a direct proportionality change in the rate $R_{UL,sum}(v^*)$ by the same positive real number. A similar proof applies to the problem (*P*3.2) as it is the same as (*P*3.3) in principle mathematically.

APPENDIX B: PROOF OF CONSTANT OPTIMAL RATIO OF HARVESTED ENERGY TO SUM-THROUGHPUT

First, denote the optimal harvested energy by sensor k on the uplink data transmission phase as $E^*_{UL,k}$ due to optimum timings $\tau^*_{EH,UL}$. From (3.3):

$$E^*_{UL,k} = \varsigma_k P_A h_k \tau^*_{EH,UL}, k = 1 \dots K. \quad (B.1)$$

Similarly, denote the optimal rate for sensor k as $R^*_{UL,k}(\tau^*_{EH,UL}, \tau^*_{UL,k})$ due to optimum timings $\tau^*_{EH,UL}$ and $\tau^*_{UL,k}$. Modified from (3.10):

$$R^*_{UL,k}(\tau^*_{EH,UL}, \tau^*_{UL,k}) = \tau^*_{UL,k} \log_2(1 + \gamma_{UL,k} \frac{\tau^*_{EH,UL}}{\tau^*_{UL,k}}), k = 1 \dots K. \quad (B.2)$$

Creating a ratio from (B.1) and (B.2):

$$\frac{E^*_{UL,k}}{R^*_{UL,k}(\tau^*_{EH,UL}, \tau^*_{UL,k})} = \frac{\varsigma_k P_A h_k \tau^*_{EH,UL}}{\tau^*_{UL,k} \log_2(1 + \gamma_{UL,k} \frac{\tau^*_{EH,UL}}{\tau^*_{UL,k}})}, k = 1 \dots K. \quad (B.3)$$

As done in Appendix A, assume a new variable $T_{new} = \alpha T$, where α is any positive real number. Substituting (A.2) and (A.3) into (B.1) and (B.2) and using the new notation in a similar manner to Appendix A in non-normalized time (i.e., $\alpha \neq 1$ and as such, $T_{new} \neq 1$) will result in the following for energy and rate of sensor k, respectively:

$$E^*_{UL,k,new} = \varsigma_k P_A h_k \tau^*_{EH,UL,new}, k = 1 \dots K, \quad (B.4)$$

$$R^*_{UL,k,new}(\tau^*_{EH,UL,new}, \tau^*_{UL,k,new}) = \tau^*_{UL,k,new} \log_2(1 + \gamma_{UL,k} \frac{\tau^*_{EH,UL,new}}{\tau^*_{UL,k,new}}), k = 1 \dots K. \quad (B.5)$$

Creating a ratio from (B.4) and (B.5):

$$\frac{E^*_{UL,k,new}}{R^*_{UL,k,new}(\tau^*_{EH,UL,new}, \tau^*_{UL,k,new})} = \frac{\varsigma_k P_A h_k \tau^*_{UL,EH,new}}{\tau^*_{UL,k,new} \log_2(1 + \gamma_{UL.k} \frac{\tau^*_{EH,UL,new}}{\tau^*_{UL,k,new}})}, k = 1 \dots K. \quad (B.6)$$

Since $\tau^*_{EH,UL,new} = \alpha \tau^*_{EH,UL}$ and $\tau^*_{UL,k,new} = \alpha \tau^*_{UL,k}, k = 1 \dots K$:

$$\frac{E^*_{UL,k,new}}{R^*_{UL,k,new}\left(\tau^*_{EH,UL,new},\tau^*_{UL,k,new}\right)} = \frac{\varsigma_k P_A h_k \alpha \tau^*_{EH,UL}}{\alpha\tau^*_{UL,k}\log_2(1+\gamma_{UL.k}\frac{\alpha\tau^*_{EH,UL}}{\alpha\tau^*_{UL,k}})}, k = 1 \dots K. \qquad (B.7)$$

Simplifying (B.7):

$$\frac{E^*_{UL,k,new}}{R^*_{UL,k,new}\left(\tau^*_{EH,UL,new},\tau^*_{UL,k,new}\right)} = \frac{\varsigma_k P_A h_k \tau^*_{EH,UL}}{\tau^*_{UL,k}\log_2(1+\gamma_{UL,k}\frac{\tau^*_{EH,UL}}{\tau^*_{UL,k}})}, k = 1 \dots K. \qquad (B.8)$$

The right hand side of (B.8) and (B.3) are the same. Therefore, it can be said that:

$$\frac{E^*_{UL,k}}{R^*_{UL,k}\left(\tau^*_{EH,UL},\tau^*_{UL,k}\right)} = \frac{E^*_{UL,k,new}}{R^*_{UL,k,new}\left(\tau^*_{EH,UL,new},\tau^*_{UL,k,new}\right)} \qquad (B.9)$$

As $R_{UL,sum}(v^*) = \sum_{k=1}^{K} R_{UL,k}(\tau^*_{EH,UL},\tau^*_{UL,k})$, then the following is true:

$$\frac{\sum_{k=1}^{K} E^*_{UL,k}}{R_{UL,sum}(v^*)} = \frac{\sum_{k=1}^{K} E^*_{UL,k,new}}{R_{UL,sum,new}(v^*_{new})} \qquad (B.10)$$

This shows that regardless of the value of α, the ratio of harvested energy to sum-throughput of the network will always remain the same. Since it was shown optimum timings and average sum-throughput are directly proportional in Appendix A, it follows that the solution to problem (*P*3.3) is the normalized optimal ratio between the total harvested energy and average sum-throughput of the sensor uplink data transmission phase in a normalized time block.

A similar mathematical proof applies to the problem (*P*3.2) as it is the same as (*P*3.3) in principle.

APPENDIX C: DOWNLINK HYBRID PROTOCOL SUM-THROUGHPUT MAXIMIZATION PROBLEM PROOF OF CONCAVITY

Considering the constraints given in (3.23b), (3.23c), (3.23d), and (3.23e), substituting (3.22) into (3.24), the Hessian matrix H for $R_{DL,k}(\tau,\lambda)$ is formulated as follows:

$$H = \begin{bmatrix} \frac{\partial^2}{\partial \tau^2} R_{DL,k}(\tau,\lambda) & \frac{\partial^2}{\partial \tau \lambda} R_{DL,k}(\tau,\lambda) \\ \frac{\partial^2}{\partial \tau \lambda} R_{DL,k}(\tau,\lambda) & \frac{\partial^2}{\partial \lambda^2} R_{DL,k}(\tau,\lambda) \end{bmatrix}. \qquad (C.1)$$

Taking the determinant of H, $\det(H)$, will result in the following:

$$\det(H) = -\left(\frac{\frac{-P_A \varsigma_k h_k}{(1-\lambda)\sigma^2 \Gamma}}{\log(2)\left(\frac{\eta_k}{1-\eta_k} - \lambda\right)\left(\frac{(1-\lambda)P_A h_k}{\sigma^2 \Gamma} + 1\right)} + \frac{\varsigma_k \log\left(\frac{(1-\lambda)P_A h_k}{\sigma^2 \Gamma} + 1\right)}{(1-\lambda)^2 \log(2)\left(\frac{\eta_k}{1-\eta_k} - \lambda\right)} + \frac{\varsigma_k \log\left(\frac{(1-\lambda)P_A h_k}{\sigma^2 \Gamma} + 1\right)}{(1-\lambda)\log(2)\left(\frac{\eta_k}{1-\eta_k} - \lambda\right)^2} \right)^2. \qquad (C.2)$$

Clearly, $\det(H)$ is always negative and thus the Hessian matrix is negative semi-definite. Per the second partial derivative test, the downlink power splitting data rate equation given by (3.24) with respect to τ and λ is concave with a global maximum and problem (P3.4) is a convex optimization problem and can be solved using, for example, the Lagrangian method.

REFERENCES

[1] "Energous WattUp - Wireless Charging 2.0 Technology," Energous Corporation, [Online]. Available: https://energous.com. [Accessed 4 May 2020].

[2] "Global Wearable Medical Devices Market - Growth, Trends and Forecasts (2015-2020)," Mordor Intelligence, 2019. [Online]. Available: https://www.mordorintelligence.com/industry-reports/global-wearable-medical-device-market-industry. [Accessed 4 May 2020].

[3] "CC1312R SimpleLink High-Performance Sub-1 GHz Wireless MCU," Texas Instruments Incorporated, [Online]. Available: http://www.ti.com/document-viewer/CC1312R/datasheet/features-swrs1922549#SWRS1922549. [Accessed 4 May 2020].

[4] C. Yuen et al, "Energy harvesting communications: Part 1 [Guest Editorial]," *IEEE Commun. Mag.*, vol. 53, no. 4, pp. 68-69, Apr. 2015.

[5] C. Knight et al, "Energy Options for Wireless Sensor Nodes," *Sensors,* vol. 8, pp. 8037-8066, 2008.

[6] D. Mishra, S. De, S. Jana, S. Basagni, K. Chowdhury and W. Heinzelman, "Smart RF Energy Harvesting Communications: Challenges and Opportunities," *IEEE Commun. Mag,* vol. 53, no. 4, pp. 70-77, Apr. 2015.

[7] A. K. Moghaddam, J. H. Chuah, H. Ramiah, J. Ahmadian, P. I. Mak and R. P. Martins, "A 73.9%-Efficiency CMOS Rectifier Using a Lower DC Feeding (LDCF) Self-Body-Biasing

Technique for Far-Field RF Energy-Harvesting Systems," *IEEE Transactions on Circuits and Systems I: Regular Papers*, vol. 64, no. 4, pp. 992-1002, Apr. 2017.

[8] D. Cavalheiro, F. Moll and S. Valtchev, "A battery-less, self-sustaining RF energy harvesting circuit with TFETs for µW power applications," in *2016 14th IEEE International New Circuits and Systems Conference (NEWCAS)*, Vancouver, BC, 2016.

[9] R. Das and H. Yoo, "A Multiband Antenna Associating Wireless Monitoring and Nonleaky Wireless Power Transfer System for Biomedical Implants," *IEEE Transactions on Microwave Theory and Techniques*, no. 99, pp. 1-11, 2017.

[10] D. K. Ho, I. Kharrat, V. D. Ngo, T. P. Vuong, Q. C. Nguyen and M. T. Le, "Dual-band rectenna for ambient RF energy harvesting at GSM 900 MHz and 1800 MHz," in *2016 IEEE International Conference on Sustainable Energy Technologies (ICSET)*, Hanoi, 2016.

[11] "Powercaster Transmitter," Powercast Corporation, [Online]. Available: https://www.powercastco.com/products/powercaster-transmitter/. [Accessed 4 May 2020].

[12] X. Zhou, R. Zhang and C. K. Ho, "Wireless Information and Power Transfer: Architecture Design and Rate-Energy Tradeoff," *IEEE Trans. Commun.*, vol. 61, no. 11, pp. 4754-4767, Nov. 2013.

[13] H. Ju and R. Zhang, "Throughput Maximization in Wireless Powered Communication Networks," *IEEE Trans. Wireless Commun.*, vol. 13, no. 1, pp. 418-428, Jan. 2014.

[14] J. C. Kwan and A. O. Fapojuwo, "Radio Frequency Energy Harvesting and Data Rate Optimization in Wireless Information and Power Transfer Sensor Networks," *IEEE Sensors Journal*, vol. 17, no. 15, pp. 4862-4874, Aug. 2017.

[15] S. Atapattu and J. Evans, "Optimal Power-Splitting Ratio for Wireless Energy Harvesting in Relay Networks," in *Proc. IEEE 82nd Veh. Technol. Conf.*, Boston, MA, 2015.

[16] S. Atapattu and J. Evans, "Optimal Energy Harvesting Protocols for Wireless Relay Networks," *IEEE Trans. Wirel. Commun.*, vol. 15, no. 8, pp. 5789-5803, Aug. 2016.

[17] K. Han and K. Huang, "Wirelessly Powered Backscatter Communication Networks: Modeling, Coverage, and Capacity," *IEEE Trans. Wirel. Commun.*, vol. 16, no. 4, pp. 2548-2561, Apr. 2017.

[18] J. C. Kwan and A. O. Fapojuwo, "Measurement and analysis of available ambient radio frequency energy for wireless energy harvesting," in *Proc. IEEE 84th Veh. Technol. Conf.*, Montreal, QC, Sep. 2016.

[19] X. Lu, H. Jiang, D. Niyato, D.I. Kim, and Z. Han, "Wireless-Powered Device-to-Device Communications with Ambient Backscattering: Performance Modeling and Analysis," *IEEE Trans. Wirel. Commun.*, vol. 17, no. 3, pp. 1528-1544, Mar. 2018.

[20] S. H. Kim and D. I. Kim, "Hybrid Backscatter Communication for Wireless-Powered Heterogeneous Networks," *IEEE Trans. Wireless Commun.*, vol. 16, no. 10, pp. 6557-6570, Oct. 2017.

[21] B. Lyu, Z. Yang, G. Gui and Y. Feng, "Wireless Powered Communication Networks Assisted by Backscatter Communication," *IEEE Access*, vol. 5, pp. 7254-7262, 2017.

[22] M. K. Sharma, A. Zappone, M. Assaad, M. Debbah and S. Vassilaras, "Distributed Power Control for Large Energy Harvesting Networks: A Multi-Agent Deep Reinforcement Learning Approach," *IEEE Trans. Cogn. Commun. Netw*, vol. 5, no. 4, pp. 1140-1154, Dec. 2019.

[23] M. Chu, H. Li, X. Liao and S. Cui, "Reinforcement Learning-Based Multiaccess Control and Battery Prediction with Energy Harvesting in IoT Systems," *IEEE Internet of Things J*, vol. 6, no. 2, pp. 2009-2020, Apr. 2019.

[24] Z. Zou, A. Gidmark, T. Charalambous and M. Johansson, "Optimal Radio Frequency Energy Harvesting With Limited Energy Arrival Knowledge," *IEEE Journal on Selected Areas in Communications*, vol. 34, no. 12, pp. 3528-3539, Dec. 2016.

[25] S. J. Darak, C. Moy, J. Palicot and Y. Louët, "Smart decision making policy for faster harvesting from ambient RF sources in wireless sensor nodes," in *2016 International Symposium on Wireless Communication Systems (ISWCS)*, Poznan, Poznan.

[26] K. Wu, H. Jiang and C. Tellambura, "Sensing, Probing, and Transmitting Policy for Energy Harvesting Cognitive Radio With Two-Stage After-State Reinforcement Learning," *IEEE Trans. Veh. Technol.*, vol. 68, no. 2, pp. 1616-1630, Feb. 2019.

[27] F. Azmat, Y. Chen and N. Stocks, "Predictive Modelling of RF Energy for Wireless Powered Communications," *IEEE Commun. Lett.*, vol. 20, no. 1, pp. 173-176, Jan. 2016.

[28] H. Yu and M. J. Neely, "Learning-Aided Optimization for Energy-Harvesting Devices with Outdated State Information," *IEEE/ACM Trans. Netw.*, vol. 27, no. 4, pp. 1501-1514, Aug. 2019.

[29] R. Kishore, S. Gurugopinath, P. C. Sofotasios, S. Muhaidat and N. Al-Dhahir, "Opportunistic Ambient Backscatter Communication in RF-Powered Cognitive Radio Networks," *IEEE Trans. Cogn. Commun. Netw.,* vol. 5, no. 2, pp. 413-426, Jun. 2019.

[30] N. Deng, W. Zhou and M. Haenggi, "The Ginibre Point Process as a Model for Wireless Networks With Repulsion," *IEEE Trans. Wirel. Commun.,* vol. 14, no. 1, pp. 107-121, Jan. 2015.

[31] J. C. Kwan and A. O. Fapojuwo, "Sum-Throughput Maximization in Wireless Sensor Networks With Radio Frequency Energy Harvesting and Backscatter Communication," *IEEE Sensors Journal,* vol. 18, no. 17, pp. 7325-7339, Sept. 1, 2018.

[32] J. C. Kwan and A. O. Fapojuwo, "Optimized Wireless Energy Harvesting Sensor Network with Backscatter Communication and Beamforming," in *2019 IEEE 90th Vehicular Technology Conference (VTC2019-Fall)*, Honolulu, HI, 2019.

[33] J. C. Kwan and A. O. Fapojuwo, "Sum-Throughput and Fairness Optimization of a Wireless Energy Harvesting Sensor Network," in *2019 IEEE 90th Vehicular Technology Conference (VTC2019-Fall)*, Honolulu, HI, 2019.

[34] J. C. Kwan and A. O. Fapojuwo, "Performance Optimization of a Multi-Source, Multi-Sensor Beamforming Wireless Powered Communication Network With Backscatter," *IEEE Sensors Journal,* vol. 19, no. 22, pp. 10898-10909, Nov. 15, 2019.

[35] J. C. Kwan, J. M. Chaulk and A. O. Fapojuwo, "A Coordinated Ambient/Dedicated Radio Frequency Energy Harvesting Scheme using Machine Learning," *IEEE Sensors Journal,* no. PP, pp. 1-16, Jun. 2020.

[36] J. C. Kwan, J. M. Chaulk and A. O. Fapojuwo, "Artificial Neural Networks-based Ambient Radio Frequency Energy Harvesting with Environment Detection," to be submitted.

[37] P. D. Diamantoulakis and G. K. Karagiannidis, "Maximizing Proportional Fairness in Wireless Powered Communications," *IEEE Wireless Communications Letters*, vol. 6, no. 2, pp. 202-205, Apr. 2017.

[38] Z. Hadzi-Velkov, I. Nikoloska, H. Chingoska and N. Zlatanov, "Proportional Fair Scheduling in Wireless Networks With RF Energy Harvesting and Processing Cost," *IEEE Communications Letters*, vol. 20, no. 10, pp. 2107-2110, Oct. 2016.

[39] R. K. Jain, D. M. Chiu, and W. R. Hawe, "A Quantitative Measure of Fairness and Discrimination For Resource Allocation in Shared Computer Systems," Technical Report TR-301, DEC Research Report, Sep. 1984.

[40] S. Wu, Y. Shin, J. Y. Kim and D. I. Kim, "Energy outage and achievable throughput in RF energy harvesting cognitive radio networks," in *2016 IEEE 27th Annual International Symposium on Personal, Indoor, and Mobile Radio Communications (PIMRC)*, Valencia, 2016.

[41] M. K. Sharma, A. Zappone, M. Assaad, M. Debbah and S. Vassilaras, "A Multi-Agent Deep Reinforcement Learning Approach," *IEEE Trans. Cogn. Commun. Netw.*, vol. 5, no. 4, pp. 1140-1154, Dec. 2019.

[42] M. Chu, H. Li, X. Liao and S. Cui, "Reinforcement Learning-Based Multiaccess Control and Battery Prediction with Energy Harvesting in IoT System," *IEEE Internet of Things J.*, vol. 6, no. 2, pp. 2009-2020, Apr. 2019.

[43] C. Boyer and S. Roy, "Backscatter communication and RFID: Coding, energy, and MIMO analysis," *IEEE Trans. Commun.*, vol. 62, no. 3, p. 770–785, Mar. 2014.

[44] T. Zeng, G. Wang, Y. Wang, Z. Zhong and C. Tellambura, "Statistical Covariance Based Signal Detection for Ambient Backscatter Communication Systems," in *2016 IEEE 84th Vehicular Technology Conference (VTC-Fall)*, Montreal, 2016.

[45] P. Du, Q. Yang, Z. Shen and K. S. Kwak, "Distortion Minimization in Wireless Sensor Networks With Energy Harvesting," *IEEE Communications Letters*, vol. 21, no. 6, pp. 1393-1396, Jun. 2017.

[46] H. Chamkhia and M. O. Hasna, "Performance analysis of wireless sensor transmission with RF energy harvesting," in *2016 International Wireless Communications and Mobile Computing Conference (IWCMC)*, Paphos, 2016.

[47] X. Yang, M. Sheng, H. Sun, X. Wang and J. Li, "Spatial throughput of energy harvesting cognitive radio networks," in *2016 IEEE 27th Annual International Symposium on Personal, Indoor, and Mobile Radio Communications (PIMRC)*, Valencia, 2016.

[48] T. P. Do, I. Song and Y. H. Kim, "Simultaneous Wireless Transfer of Power and Information in a Decode-and-Forward Two-Way Relaying Network," *IEEE Trans. Wirel. Commun.*, vol. 16, no. 3, pp. 1579-1592, Mar. 2017.

[49] I. Flint, X. Lu, N. Privault, D. Niyato and P. Wang, "Performance Analysis of Ambient RF Energy Harvesting with Repulsive Point Process Modeling," *IEEE Trans. Wirel. Commun.*, vol. 14, no. 10, pp. 5402-5416, Oct. 2015.

[50] J. G. Andrews, F. Baccelli and R. K. Ganti, "A Tractable Approach to Coverage and Rate in Cellular Networks," *IEEE Trans. Commun.*, vol. 59, no. 11, pp. 3122-3134, Nov. 2011.

[51] X. Lu, I. Flint, D. Niyato, N. Privault and P. Wang, "Self-Sustainable Communications With RF Energy Harvesting: Ginibre Point Process Modeling and Analysis," *IEEE Journal on Selected Areas in Communications*, vol. 34, no. 5, pp. 1518-1535, May 2016.

[52] P. S. Yedavalli, T. Riihonen, X. Wang and J. M. Rabaey, "Far-Field RF Wireless Power Transfer with Blind Adaptive Beamforming for Internet of Things Devices," *IEEE Access*, no. 5, pp. 1743-1752, 2017.

[53] T. X. Doan, T. M. Hoang, T. Q. Duong and H. Q. Ngo, "Energy Harvesting-Based D2D Communications in the Presence of Interference and Ambient RF Sources," *IEEE Access*, vol. 5, pp. 5224-5234, 2017.

[54] H. Sun, Y. x. Guo, M. He and Z. Zhong, "Design of a High-Efficiency 2.45-GHz Rectenna for Low-Input-Power Energy Harvesting," *IEEE Antennas and Wireless Propagation Letters*, vol. 11, pp. 929-932, 2012.

[55] L. Zhao and X. Wang, "Massive MIMO Downlink for Wireless Information and Energy Transfer with Energy Harvesting Receivers," *IEEE Trans. Commun.*, vol. 67, no. 5, pp. 3309-3322, May 2019.

[56] "RSS-247—Digital Transmission Systems (DTSs), Frequency Hopping Systems (FHSs) and Licence-Exempt Local Area Network (LE-LAN) Devices," Industry Canada, [Online]. Available: http://www.ic.gc.ca/eic/site/smt-gst.nsf/eng/sf10971.html. [Accessed 2020 5 May].

[57] "15.247 Operation Within the Bands 902–928 MHz, 2400–2483.5 MHz, and 5725–5850 MHz," U.S. Government Publishing Office, [Online]. Available: https://www.gpo.gov/fdsys/pkg/CFR-2013-title47-vol1/pdf/CFR-2013-title47-vol1-sec15-247.pdf. [Accessed 2020 5 May].

[58] E. Khansalee, Y. Zhao and K. Nuanyai, "High frequency rectifier for RF energy harvesting systems," in *7th Int. Conf. Information Technology Electrical Engineering*, Chiang Mai, 2015.

[59] P. Shankar, "Propagation Characteristics of Wireless Channels," in *Introduction to Wireless Systems*, New York, N.Y., Wiley, 2002, pp. 12-21.

[60] "Measuring Bluetooth Low Energy Power," Texas Instruments Incorporated., 13 Apr. 2012. [Online]. Available: https://www.ti.com/lit/an/swra347a/swra347a.pdf. [Accessed 5 May 2020].

[61] F. Mazda, "Source Encoding," in *Telecommunications Engineer's Reference Book*, Oxford, Butterworth-Heinemann College, 1993, p. 4/9.

[62] GS1, "EPC Radio-Frequency Identity Protocols Generation-2 UHF RFID," Nov. 2013. [Online]. Available: https://www.gs1.org/sites/default/files/docs/epc/uhfc1g2_2_0_0_standard_20131101.pdf. [Accessed 3 Sep. 2020].

[63] T. Li, P. Fan and K. Ben Letaief, "Data acquisition with RF-based energy harvesting sensor: From information theory to green system," in *2014 IEEE Global Communications Conference*, Austin, TX, 2014.

[64] M. Mackowiak and L. M. Correia, "Statistical path loss model for dynamic off-body channels," in *2014 IEEE 25th Annu. Int. Symp. Personal, Indoor, and Mobile Radio Communication*, Washington DC, 2014.

[65] E. Reusens, W. Joseph, B. LatrE, B. Braem, G. Vermeeren, E. Tanghe, L. Martens, I. Moerman and C. Blondia, "Characterization of On-Body Communication Channel and Energy Efficient Topology Design for Wireless Body Area Networks," *IEEE Trans. Inf. Technol. Biomed.*, vol. 13, no. 6, pp. 933-945, Nov. 2009.

[66] "Bluetooth Core Specification V5.0," Bluetooth SIG, [Online]. Available: https://www.bluetooth.com/specifications/bluetooth-core-specification/. [Accessed 5 May 2020].

[67] N. K. San Diego and C. C. Wang, "Simple BER Approximations for Generalized Selection Combining (GSC) over Rayleigh Fading Channels and its SNR Gap Properties," in *2006 IEEE Military Communications Conf.*, Washington DC, 2006.

[68] "ISO/IEC/IEEE International Standard - Information technology -- Telecommunications and information exchange between systems -- Local and metropolitan area networks -- Specific requirements -- Part 15-6: Wireless body area network," in *ISO/IEC/IEEE 8802-15-6:2017(E)*, Mar. 2018, pp. 1-274.

[69] M. Nakagami, "The m-Distribution - A General Formula of Intensity Distribution of Rapid Fading," *Statistical Methods in Radio Wave Propagation*, pp. 3-36, 1960.

[70] P. Dharmawansa, N. Rajatheva and K. Ahmed, "On the Distribution of the Sum of Nakagami-m Random Variables," *IEEE Trans. Commun.*, vol. 55, no. 7, pp. 1407-1416, Jul. 2007.

[71] "Intel Core i7-6700K Processor," Intel Corporation, [Online]. Available: https://ark.intel.com/products/88195/Intel-Core-i7-6700K-Processor-8M-Cache-up-to-4-20-GHz-.. [Accessed 6 May 2020].

[72] S. J. Ambroziak et al., "An Off-Body Channel Model for Body Area Networks in Indoor Environments," *IEEE Trans. Antennas Propaga.*, vol. 64, no. 9, pp. 4022-4035, Sept. 2016.

[73] L. Decreusefond, I. Flint, and A. Vergne, "Efficient simulation of the Ginibre point process," *Journal of Applied Probability*, vol. 52, no. 4, pp. 1003-1012, Dec. 2015.

[74] S. J. Miller, The Method of Least Squares, Providence, RI: Brown Univ., 2010.

[75] M. A. Nielsen, Neural Networks and Deep Learning, Determination Press, 2015.

[76] V. Nair and G. E. Hinton, "Rectified linear units improve restricted boltzmann machines," in *Proc. 27th Int. Conf. Machine Learning (ICML'10)*, Madison, WI, 2010.

[77] G. Hinton, "Overview of mini-batch gradient descent," [Online]. Available: https://www.cs.toronto.edu/~tijmen/csc321/slides/lecture_slides_lec6.pdf. [Accessed 26 Nov. 2019].

[78] Texas Instruments Incorporated, "CC1350 Datasheet," Jul. 2018. [Online]. Available: http://www.ti.com/lit/ds/symlink/cc1350.pdf. [Accessed 29 Aug. 2019].

[79] NXP Semiconductors, "MMA8491Q 3-axis Multifunction Digital Accelerometer," Apr. 2016. [Online]. Available: https://www.nxp.com/docs/en/data-sheet/MMA8491Q.pdf. [Accessed 29 Aug. 2019].

[80] Federal Communications Commission, "Human Exposure to Radio Frequency Fields: Guidelines For Cellular and PCS Sites," Oct. 2016. [Online]. Available: https://www.fcc.gov/consumers/guides/human-exposure-radio-frequency-fields-guidelines-cellular-and-pcs-sites. [Accessed 2019 Aug. 29].